UNIVERSIDADE ESTADUAL PAULISTA "JÚLIO DE MESQUITA FILHO"
CAMPUS DE ILHA SOLTEIRA

MALINWO ESTONE AYIKPA

OPTIMAL POWER FLOW ALGORITHMS FOR LARGE-SCALE DISTRIBUTION NETWORKS TO MITIGATE VOLTAGE UNBALANCE AND POWER LOSSES WITH ENERGY RESOURCES

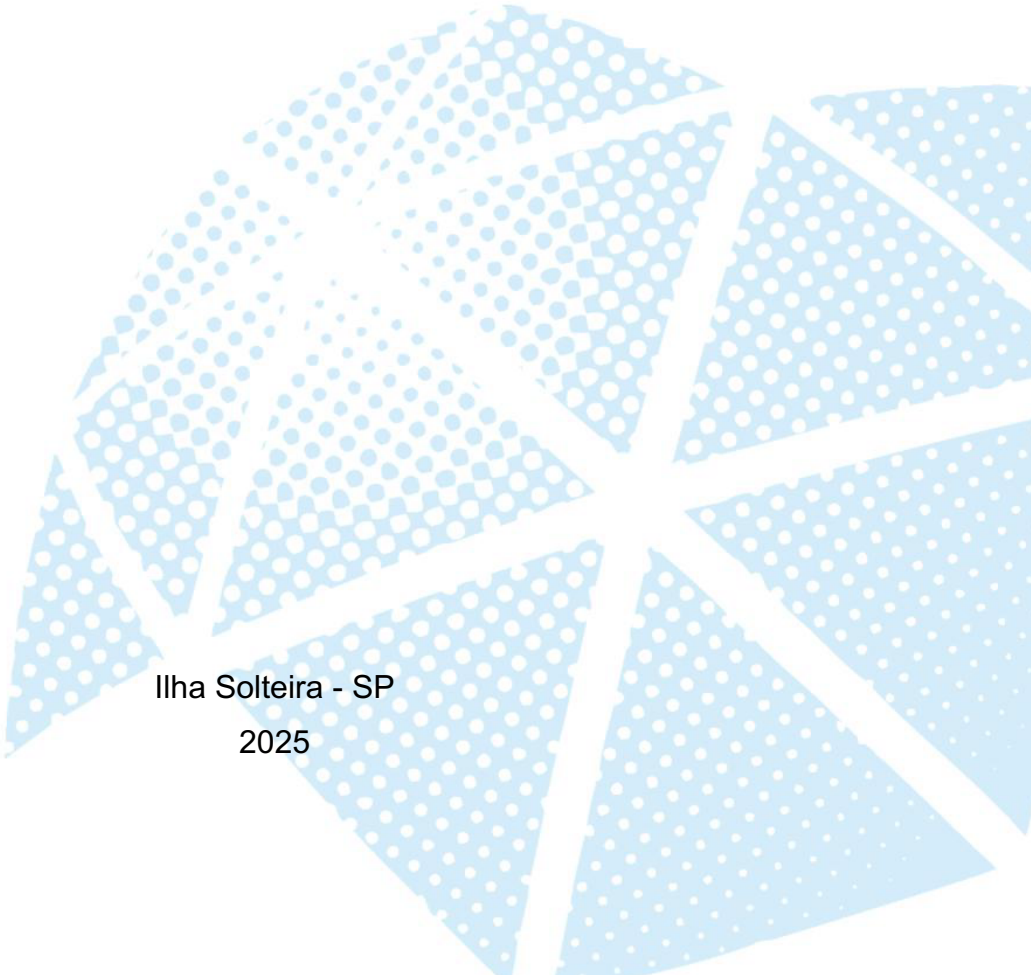

Ilha Solteira - SP
2025

MALINWO ESTONE AYIKPA

Optimal power flow algorithms for large-scale distribution networks to mitigate voltage unbalance and power losses with energy resources

Thesis presented to the Graduate Program of the School of Engineering, São Paulo State University– UNESP, Ilha Solteira, as part of the requirements for obtaining the title of Doctor of Philosophy in Electrical Engineering

Speciality: Automation

Advisor: Prof. Dr. Ruben Augusto Romero Lázaro

Ilha Solteira - SP

2025

FICHA CATALOGRÁFICA
Desenvolvida pela Diretoria Técnica de Biblioteca e Documentação

Ayikpa, Malinwo Estone.
A977o Optimal power flow algorithms for large-scale distribution networks to mitigate voltage unbalance and power losses with energy resources / Malinwo Estone Ayikpa. -- Ilha Solteira: [s.n.], 2025
126 f. : il.

Tese (doutorado) - Universidade Estadual Paulista. Faculdade de Engenharia de Ilha Solteira. Área de conhecimento: Automação, 2025

Orientador: Ruben Augusto Romero Lázaro
Inclui bibliografia

1. Three-phase optimal power flow. 2. Primal-dual interior point method. 3. Photovoltaic power plant. 4. Voltage unbalance. 5. Distribution feeder reconfiguration. 6. Stochastic fractal search.

Elaborada por Raiane da Silva Santos - CRB-8/9999

IMPACTO POTENCIAL DESTA PESQUISA

Neste trabalho apresentam-se metodologias de fluxo de potência ótimo para solucionar problemas de qualidade de energia em redes de distribuição, com a integração de usinas fotovoltaicas, geração distribuída e bancos de capacitores. Como contribuição para o avanço da ciência, esta tese abordou o problema da queda de tensão em redes de distribuição trifásicas desequilibradas de grande escala, com a integração de fontes de geração fotovoltaica operando com fator de potência ajustável. Os impactos positivos na sociedade são evidentes na redução de danos aos equipamentos utilizados em indústrias ou empresas, bem como em motores e máquinas industriais que requerem uma tensão estável e equilibrada para operar em boas condições. Além disso, este trabalho contribui para a reconfiguração simultânea de alimentadores com a alocação e dimensionamento ótimos de geração distribuída e bancos de capacitores na mesma estrutura para sistemas de distribuição de grande escala, o que tem impactos positivos na redução das perdas e na melhoria do perfil de tensão mínima.

POTENTIAL IMPACT OF THIS RESEARCH

This work presents optimal power flow methodologies for solving power quality problems in distribution networks, integrating photovoltaic power plants, distributed generations, and capacitor banks. As a contribution to the advancement of science, this thesis addressed the voltage drop problem in large-scale unbalanced three-phase distribution networks, with the integration of photovoltaic power plants, operating with adjustable power factor. The positive impacts on society are evident in the reduction of damage to equipment used in industries or companies, as well as to industrial motors and machines that require a stable and balanced voltage to operate in good condition. In addition, this work contributes to the simultaneous reconfiguration of feeders with the optimal allocation and sizing of distributed generation and capacitor banks in the same framework for large-scale distribution systems, which has positive impacts on reducing power losses and improving the minimum voltage profile.

UNIVERSIDADE ESTADUAL PAULISTA

Câmpus de Ilha Solteira

CERTIFICADO DE APROVAÇÃO

TÍTULO DA TESE: Optimal power flow algorithms for large-scale distribution networks to mitigate voltage unbalance and power losses with energy resources

AUTOR: MALINWO ESTONE AYIKPA
ORIENTADOR: RUBEN AUGUSTO ROMERO LAZARO

Aprovado como parte das exigências para obtenção do Título de Doutor em Engenharia Elétrica, área: Automação pela Comissão Examinadora:

Prof. Dr. RUBEN AUGUSTO ROMERO LAZARO (Participaçao Presencial)
Departamento de Engenharia Elétrica / UNESP / Câmpus de Ilha Solteira - FEIS

Prof. Dr. LEONARDO HENRIQUE FARIA MACEDO POSSAGNOLO (Participaçao Virtual)
Departamento de Engenharia / UNESP / Câmpus de Rosana - FEC

Prof. Dr. JOSE ROBERTO SANCHES MANTOVANI (Participaçao Presencial)
Departamento de Engenharia Elétrica / UNESP / Câmpus de Ilha Solteira - FEIS

Prof. Dr. CARLOS ROBERTO MENDONÇA DA ROCHA (Participaçao Virtual)
Centro de Engenharias e Ciências Exatas / Universidade Estadual do Oeste do Paraná - UNIOESTE

Prof. Dr. BENVINDO RODRIGUES PEREIRA JÚNIOR (Participaçao Virtual)
Departamento de Engenharia Elétrica / Escola de Engenharia de São Carlos - USP

Ilha Solteira, 10 de dezembro de 2025.

DIDICATION

I dedicate this work to my beloved deceased parents, Célestine Sahossi and Antoine Ayikpa, who were a source of unconditional love and support, the driving force behind this achievement. I also dedicate this work to my brothers and sisters, for their friendship and support during the development of this work.

ACKNOWLEDGEMENTS

I express my gratitude to God, the universe, and my ancestors for their guidance throughout this journey.

I thank Prof. Dr. Ruben Augusto Romero Lázaro for his orientation in this work.

I thank the distinguished members of the examining board for their valuable comments and suggestions, which contributed to the improvement of this work.

I thank the Coordination for the Improvement of Higher Education Personnel – Brazil (CAPES) – Funding Code 001, for their support during the development of this work.

"There is nothing that human beings can create that does not stem from their genius. If you can do that, it means you are in harmony with the essence of humanity" (Malinwo Estone Ayikpa).

ABSTRACT

The integration of solar photovoltaic generation in the distribution system has been largely carried out in small- or medium-scale networks without in-depth analysis. The interaction of PV systems with conventional voltage regulation equipment can cause negative impacts to the grid that need to be studied, especially when PV inverters provide reactive power control to the grid. Moreover, the planning and operation of distribution networks with the integration of distributed generations and capacitor banks was usually done on small-scale and medium-scale systems. The network topology presents a radiality problem with some metaheuristic algorithms that deal with feeder reconfiguration in large-scale distribution systems. Based on the problems mentioned above, this work presents an AC three-phase optimal power flow (TOPF) that minimizes voltage unbalance in large-scale distribution networks, with optimal adjustment of voltage regulator taps and the integration of PV plants operating at maximum power with reactive power control of inverters. The simulations were performed using the IEEE 123 node feeder with three-phase and single-phase PV plants, respectively, and results presented a better understanding of the impacts of distributed PV systems on large-scale distribution networks in terms of power quality. The TOPF developed in this work is based on the current injection method and the optimal solution was achieved using the primal-dual interior point method. Later in this work, we address an optimal power flow based on distribution feeder reconfiguration (DFR), with the integration of distributed generation (DG) and capacitor bank (CB) into large-scale distribution networks to minimize power losses. The stochastic fractal search algorithm (SFS) has been used to solve this problem. The proposed algorithm was tested on the 33-bus, 69-bus, 119-bus, and 136-bus distribution networks. Different simulation cases have been carried out, and the results showed a significant impact on reducing the losses and enhancing the minimum voltage value of the feeder, especially when DGs and CBs are simultaneously addressed in the DFR problem.

Keywords: Three-phase optimal power flow; primal-dual interior point method; photovoltaic power plant; voltage unbalance; distribution feeder reconfiguration; stochastic fractal search.

RESUMO

A integração da geração solar fotovoltaica no sistema de distribuição tem sido realizada principalmente em redes de pequena ou média escala, sem uma análise aprofundada. A interação de sistemas fotovoltaicos com equipamentos convencionais de regulação de tensão pode causar impactos negativos na rede elétrica, os quais precisam ser estudados, especialmente quando os inversores fotovoltaicos fornecem controle de potência reativa à rede. Além disso, o planejamento e a operação de redes de distribuição com a integração de geração distribuída e bancos de capacitores geralmente são realizados em sistemas de pequena e média escala. A topologia da rede apresenta um problema de radialidade com alguns algoritmos meta-heurísticos que lidam com a reconfiguração de alimentadores em sistemas de distribuição de grande escala. Este trabalho apresenta um fluxo de potência ótimo trifásico CA (FPOT) que minimiza o desequilíbrio de tensão em redes de distribuição de grande escala, com ajuste ótimo dos taps do regulador de tensão e a integração de usinas fotovoltaicas operando em potência máxima com o controle de potência reativa dos inversores. As simulações foram realizadas usando o alimentador de nós IEEE 123 com usinas fotovoltaicas trifásicas e monofásicas, respectivamente, e os resultados apresentaram uma melhor compreensão dos impactos dos sistemas fotovoltaicos distribuídos em redes de distribuição de grande escala em termos de qualidade de energia. O FPOT desenvolvido neste trabalho é baseado no método de injeção de corrente e a solução ótima foi alcançada usando o método primal-dual de ponto interior. Posteriormente neste trabalho, abordamos um fluxo de potência ótimo baseado na reconfiguração do alimentador de distribuição (RAD), com a integração de geração distribuída (GD) e banco de capacitores (BC) em redes de distribuição de grande escala para minimizar as perdas de energia. O algoritmo de busca fractal estocástico (BFE) foi utilizado para resolver este problema e testado nos sistemas de 33, 69, 119 e 136 barras e os resultados mostraram um impacto significativo na redução das perdas com a integração simultânea de GDs e CBs nos sistemas.

Palavras-chave: Fluxo de potência ótimo trifásico; método primal-dual de ponto interior; usina fotovoltaica; desequilíbrio de tensão; reconfiguração de rede de distribuição; busca fractal estocástica.

LIST OF FIGURES

LIST OF TABLES

LIST OF ABBREVIATIONS

AC	Alternative Current
ACSA	Ant Colony Search Algorithm
AIS	Artificial Immune System
AMPL	A Mathematical Programming Language
CB	Capacitor Bank
DC	Direct Current
DE	Differential Evaluation
DFR	Distribution Feeder Reconfiguration
DLA	Diffusion Limited Aggregate
DG	Distributed Generation
EWD	Edge Window Decoder
FL	Fundamental Loop
GA	Genetic Algorithm
GWO	Grey Wolf Optimizer
HAS	Harmony Search Algorithm
HS-PABC	Harmonic Search-Particle Artificial Bee Colony
IBER	Inverter-based Energy resources
IEEE	Institute of Electrical and Electronics Engineers
IGBT	Insulated-Gate Bipolar Transistor
IHA	Improved Harmony Algorithm
IWD	Intelligent Water Drop
LSF	Loss Sensitive Factor
MDN	Maximum diffusion number
NEMA	National Electrical Manufactures Association
ONS	National System Operator
OPF	Optimal Power Flow
OF	Objective Function
PV	Photovoltaic
PF	Power Flow
PSO	Particle Swarm Optimization
SA	Simulated Annealing
SDP	Semidefinite Programming

SFS	Stochastic Fractal Search
SVG	Static Var Generator
SW	Tie-switches
TCIM	Three-phase Current Injection Method
TOPF	Three-phase Optimal Power Flow
VSI	Voltage Stability Index
VUF	Voltage Unbalance Factor
WOA	Whale Optimization Algorithm

LIST OF SYMBOLS

V_{max}	Maximum voltage
V_{min}	Minimum voltage
V_{avg}	Average voltage
V_i	Complex voltage
V_{Re-}^2	The square of the real part of the negative sequence component
V_{Im-}^2	The square of the imaginary part of the negative sequence component
V^{abc}	Three-phase complex voltage
$\lvert V^{abc} \rvert$	Three-phase voltage magnitude
V_{Re}^{abc}	Real part of the three-phase voltage
V_{Im}^{abc}	Imaginary part of the three-phase voltage
$V_{Re,ref}^{abc}$	Three-phase voltage on the reference bus
I^{abc}	Three-phase complex current injection
I_{Re}^{abc}	Real part of the three-phase current
I_{Im}^{abc}	Imaginary part of the three-phase current
a^{abc}	Tap position of phase a, b, and c
a_{min}^{abc}	lower bound of the tap per phase
a_{max}^{abc}	upper bound of the tap per phase
$\mathrm{C}^{\mathrm{abc}}$	Capacitive susceptance of the capacitor on phase a, b, and c
Q^{abc}	Nominal reactive power of the capacitor per phase
S_d^{abc}	Three-phase apparent power load
P_d^{abc}	Three-phase active power load
Q_d^{abc}	Three-phase reactive power load
S^{abc}	Three-phase power injection
S_g^{abc}	Three-phase apparent power generation
P_g^{abc}	Three-phase active power generation
Q_g^{abc}	Three-phase reactive power generation
P_{km}^{abc}	Active power flow per phase in the branch km
P_{max}^{abc}	Maximal active power flow capacity of the branch km
S^{abc}	Maximum apparent power of the three-phase PV inverter
$P_{PV\omega}$	Active power generation of a PV plant

$Q_{PV\omega}$	Reactive power generation of a PV inverter
Q_{PV}^{abc}	Reactive power injection of the three-phase PV inverter
Y_{bus}^{abc}	Bus admittance matrix
G^{abc}	Real part of the bus admittance matrix
B^{abc}	Imaginary part of the bus admittance matrix
Z^{abc}	Series impedance of the line
Y^{abc}	Shunt admittance matrix of the line
y_t	Per-unit leakage admittance of the transformer
V_0	Zero sequence voltage
V_+	Positive sequence voltage
V_-	Negative sequence voltage
F_1	Objective function of voltage unbalance
F_2	Objective function of losses
Z_{ii}	Self-impedance of conductor i
Z_{ij}	Mutual impedance between conductors i and j
r_i	Resistance of conductor i
x_i	Reactance of conductor i
I_i	Line current
V_{in}	Line-to-ground voltage
D_{ij}	Distance between conductor i and j
$\mathrm{GMR_i}$	Geometric Mean Radius of conductor i
A_P	Incidence matrix of bus-generators
X	Optimization variables
f(x)	Objective function
g(x)	Equality restrictions
h(x)	Inequality restrictions
$\mathrm{h_{min}}$	Lower bound of inequality constraints
$\mathrm{h_{max}}$	upper bound of inequality constraints
$S_{i,ac}$	Apparent power flow injection
$P_{i,ac}$	Active power flow injection on bus i
$Q_{i,ac}$	Reactive power flow injection on bus i
$P_{k,ac}$	Real part of the accumulated load downstream to node i
$Q_{k.ac}$	Imaginary part of the accumulated load downstream to node i

r_k	Real part of the series impedance of line k
r_k	Imaginary part of the series impedance of line k
P_{DG}	Active power generation from distributed generation
Q_{DG}	Reactive power generation from distributed generation
Q_{CB}	Reactive power of the capacitor bank
$Q_{CB,min}$	Minimum reactive power of the capacitor bank
$Q_{CB,max}$	Maximum reactive power of the capacitor bank
I_{ij}	Current in the branch ij
$I_{ij,max}$	Maximum capacity of the line
X_i	The i^{th} particle in the population
X_{best}	The best particle of the groupe
N_P	Number of particles

SUMMARY

1 INTRODUCTION

Power systems around the world are undergoing significant change with the development of wind and solar power, as well as energy storage technologies. The increased demand from electric vehicles, data centers, and electric heating and cooling systems directly impacts the availability of energy sources. A traditional power system consists of a centralized power generation, transmission, and distribution system. However, the energy needs of modern society have increased significantly in recent years, forcing energy suppliers to adapt their electricity networks to new modernization requirements. Distributed generations, renewable energies, energy storage systems, and power electronic devices are key features that bring smartness and reliability to the grid. Solar photovoltaic (PV) systems are widely used in transmission to provide power backup when the grid is down. According to (Marqusee; Stringer, 2023) PV systems are typically characterized by their size as being residential (< 25 kW), commercial (25 kW to 1,000 kW) and utility (> 1,000 kW) scale. In response to the rapid growth in demand, several countries have implemented policies to encourage the installations of micro and mini-photovoltaic generators for residential and commercial consumption. This gave rise to the concept of net metering, which allows small residential producers to store excess electricity on the grid as credits to offset their own electricity purchases from the utility company. These small producers support the grid by enhancing its reliability, improving the voltage profiles, reducing losses as well as additional expenses for the grid owner. These small producers support the electrical grid by increasing its reliability, improving voltage profiles, reducing losses, and lowering additional costs for the grid owner.

Figure 1 shows the total energy supply by source in Brazil in 2024, where solar PV generation represents 9.3% of total generation, with an electricity production of 70.7 TWh (“Relatório Final_BEN, 2025”). Of this production, distributed micro and mini generation of PV represents 41TWh with 35.89 MW of installed capacity. Despite the great potential of solar energy in Brazil, its widespread adoption still faces significant challenges. Economic, regulatory, and structural barriers limit the sector's growth, hindering access to this technology for lower-income residents, those in regions with lower purchasing power, and small businesses. Although installation costs have decreased, demand for solar systems is still restricted primarily to the wealthier regions of the country, such as the Southeast and South. In addition, Brazil's solar energy

distribution infrastructure still faces limitations. The integration of photovoltaic systems into Brazilian distribution networks is not always efficient, especially in regions further away from urban centers.

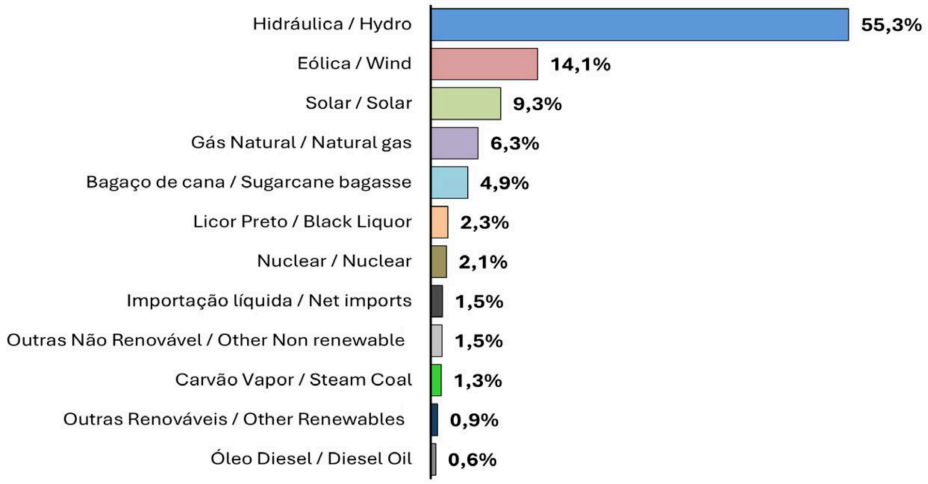

Figure 1 – Total electricity supply in Brazil in 2024 (“Relatório Final_BEN, 2025”)

Considering the challenges of the energy transition faced by Brazil, which are quite similar to those of Benin, and the technical issues related to the large-scale integration of solar PV energy, into existing distribution networks, this thesis proposes an advanced computational tool based on optimal power flow to address this problem. Furthermore, this thesis addresses the distribution feeder reconfiguration (DFR) with the simultaneous integration of distributed generations (DGs) and capacitor banks (CBS) in large-scale distribution systems to reduce power losses and improve the minimum voltage profile of the network. The DFR problem is formulated and solved using the stochastic fractal search (SFS). The next section will present the literature review on the problematics addressed in this work.

1.1 LITERATURE REVIEW ON PV PLANTS INTEGRATION INTO ELECTRIC POWER SYSTEMS

Economic factors and the reduction of greenhouse gas emissions have led policymakers to establish new policies for the development of clean energy resources. Wind and solar PV energies have received considerable attention from government agencies for their large-scale integration. According to the International Renewable

Energy Agency, solar PV energy will reach about 35% of the global world's electricity by 2050 (Varma et al., 2021). However, inverter-based energy resources (IBERs) present challenges regarding their large-scale integration into existing power grids. Some of them are voltage increasing, reverse power flows, voltage unbalance, interaction with conventional voltage regulation equipment, losses, and so on. Furthermore, a heavy reliance on IBERs at the expense of conventional fossil generation can lead to frequency regulation problems and increase power oscillation due to reduced system inertia. To overcome these challenges, the IEEE 1547-2018 standard requires that IBERs provide at least 44% reactive power of the total power generation. Studies carried out in (Dondariya; Sakravdia, 2021), solved the voltage stability problem by increasing the critical loading limit of the network with active and/or reactive power control of PV systems (Liu et al., 2022). Extensive research was devoted to studying the impacts of grid-connected PV systems on power systems. Yu et al. (2024) developed a two-layer reactive power voltage control model to mitigate voltage fluctuation and power losses in the presence of large-scale PV systems. The authors first predicted active power generation at the PV station and grid load demand, then applied a reactive power management strategy to guide the reactive power generation from inverters, capacitor banks, and On-Load Tap Changers. This approach was verified by experiment data to confirm its effectiveness. Yafeng Liu and Bo Zhang (2025) proposed a reactive power optimization model at the grid-connected point of each PV station and a static VAr generator (SVG), to maintain the grid-connected point voltage, reduce the node voltage deviation and the active loss of each collector line. The model also includes the maximum IGBT junction temperature of the PV inverter as an optimization variable to address the operational capacity of the inverters. Power flow (PF) analysis was conducted in (Saw; Navada; Shubhanga, 2022), in which PV generation is modeled as a negative load injection in the PF model and can operate in either PV or PQ mode based on the control strategy applied at the inverter node. Dynamic simulations were performed in (Benny et al., 2024) to evaluate the critical role that active and reactive power control of grid-connected PV inverters can play in the optimization, stability, and efficiency of power systems.

However, most applications of grid-connected PV systems have limited their analyses to small-scale or medium-scale distribution systems, with small-scale PVs or, in some cases to large-scale PV systems (Nzimande; Noro, 2022; Guo et al., 2024). Studies presented in (Araujo et al., 2013) have considered low penetration of PV

systems operating at a unity power factor into a large-scale distribution network. Recent research has focused on mitigating voltage unbalance in large-scale distribution networks with a high penetration of grid-connected PV plants, where PV inverters can inject/absorb reactive power into the grid (Ayikpa, 2025b). The interaction of PV inverters with conventional voltage regulation equipment such as capacitor banks and voltage regulator presents challenges that commercial tools cannot handle.

1.2 LITERATURE REVIEW OF DISTRIBUTION FEEDER RECONFIGURATION WITH THE OPTIMAL PLACEMENT AND SIZING OF DG AND CB

Energy is generally produced by power plants located in areas far from consumers. Its transportation is carried out through transmission and distribution lines, where power losses are often experienced. This phenomenon is more significant in the distribution network, with a high R/X ratio. Modern distribution networks present challenges in the planning and operation of network assets. For example, when a fault occurs in a section of the network, a switching process is necessary to restore energy to the other part of the network. Additionally, for technical purposes, field engineers can transfer the load to another feeder by opening and closing switches during the peak season. This process is usually carried out to minimize the total power loss of the network. Researchers have attempted to mitigate power losses in the distribution system using different approaches. Li *et al*. (2020) proposed a two-stage reactive power optimization strategy for the hybrid AC/DC distribution network that significantly reduced losses compared to the AC network itself. In (Pan et al., 2021), a static VAr compensator was used as a voltage fluctuation regulator to allow reactive power control and loss reduction due to increased penetration of doubly fed wind generators into a distribution network.

Power losses can also be mitigated with the integration of DG into the grid. When DGs are introduced into the distribution network, the power grid may face an overvoltage problem due to inadequate distribution or sizing of them. To avoid this problem, the DG must be optimally sized and placed in the network. In (Rama Prabha et al., 2015), loss-sensitive factor was applied to find the optimal placement of DGs and applied the intelligent water drop (IWD) algorithm to determine their optimal size, in a small-scale distribution network. Antonio José Gil Mena and Juan Andrés Martín García (2015), proposed a mixed integer non-linear model that reduces the search

space of candidate buses for the DG installation and then applies a threshold to find their optimal placement. Subsequently, the sizing of the distributed generators was carried out by solving an optimal power flow problem. Moreover, the integration of capacitor banks (CBs) into the distribution network can also contribute to reducing power losses. In (Ali; Abd Elazim; Abdelaziz, 2016), the loss-sensitive factor and the voltage stability index (VSI) have been used to determine the candidate buses for the placement of the capacitor banks, and an improved harmony algorithm (IHA) to find the optimal size of them. Research carried out in (Devabalaji; Ravi; Kothari, 2015), has also applied the same approach to determine the optimal placement of capacitor banks, but instead used the bacterial foraging optimization algorithm to determine the optimal size of the CBs. However, one of the most effective ways to mitigate power losses in the distribution system is the distribution feeder reconfiguration (DFR). It is a complex combinatorial problem that has been addressed in the literature with exact methods, heuristic, or metaheuristic algorithms. In (Shirmohammadi; Hong, 1989), a heuristic approach was developed for the reconfiguration of the network based on an optimal AC power flow pattern to reduce power losses in the network. Furthermore, Baran and Wu (Baran; Wu, 1989b) proposed a fast radial power flow formulation for branch exchange in a distribution network to reduce resistive losses. Although this approach saved computational time, it should be noted that the branch exchange process was time consuming because of the step-by-step process to accomplish this task.

Research carried out to solve the DFR problem during the last decades was mainly based on metaheuristic algorithms. Simulated annealing (SA) (Carpaneto; Chicco, 2001) and the Genetic Algorithm (GA) (Nara et al., 1992) have been applied to minimize active power losses in the distribution network. Torres *et al*. (2013), developed a GA-based edge window decoder (EWD) encoding strategy for network representation to find the optimal radial topology using DFR. However, in (Young-Jae Jeon; Jae-Chul Kim, 2000), a Tabu Search implementation had been carried out to handle the weakness of SA by preventing revisiting and recycling of the solution already visited. Since interest in the expansion of distributed generations in the planning and operation of the electric power grid has increased, some research studies have considered the optimal placement and sizing of DG in the DFR problem. Then, (Ayodele; Ogunjuyigbe; Akinola, 2015; Ganguly; Samajpati, 2015), introduced DG in the DFR problem using GA. Differential Evaluation (DE) has been used in (Dixit;

Kundu; Jariwala, 2016) to optimally place and size photovoltaic generation using network reconfiguration. To deal with stochastic variables related to uncertainties in PV generation and loads in the mathematical formulation of the DFR problem, Ying-Yi Hong, Faa-Jeng Lin, and Fu-Yuan Hsu (2014) introduced the concept of mean-variance in the particle swarm optimization (PSO) algorithm, to find the optimal configuration of tie switches. Bioinspired Artificial Immune Systems (AIS) (De Oliveira; Seta; De Oliveira, 2016), have been applied to solve the DFR considering uncertainties in load demand and wind-based distributed generation. Drus *et al*. (2023), proposed a Grey Wolf Optimizer (GWO) to solve DFR in the presence of DG, to mitigate active and reactive power losses, as well as voltage deviation in system buses. In most cases where metaheuristics were used to solve the DFR problem, the optimal network configuration presented by the authors is not radial for large-scale distribution systems. The DFR approach presented in (Souza; Romero; Franco, 2015), did not achieve radial configuration for the 119-bus system. Furthermore, research carried out in (Tran The; Vo Ngoc; Tran Anh, 2020; Tran; Truong; Vo, 2020) present non-radial network topologies for both 119-bus and 136-bus systems.

In, (Madeiro et al., 2011) a hybrid GA-based local search strategy was proposed to simultaneously solve the DFR with optimal placement and sizing of CB, where the annual gain due to power losses reduction and the annual gain due to investment in capacitor acquisition are maximized. Regarding the technical benefits that DG alone can provide to the grid, research carried out in (Leghari et al., 2022) showed that the investment cost of DG integration is much higher than that of CB, and the investment-benefit cost ratio of CB is much higher than that of DG. However, most studies on the allocation of DG and CB in distribution network operation are carried out on small- and medium-scale systems. Mahdavi *et al.* (2023b) addressed this problem for small-scale networks considering different load patterns, using the CPLEX solver in AMPL. Only a few extended their analysis to large-scale networks (Biswas et al., 2017; Muthukumar; Jayalalitha, 2016; Tiwari; Dubey; Pandit, 2022). The exploration capabilities of harmonic search combined with the exploitation capabilities of particle artificial bee colony (HS-PABC) were applied to solve the DFR with the allocation and sizing of DGs and CBs considering the 119-bus system, which had a positive impact on the convergence rate algorithm and consequently on the network performance improvement (K.; S., 2017). However, as the network size increases, the search space also increases, and combining DFR with DG and CB allocation and sizing can become

a very complex problem to solve. Recent research developed in (Ayikpa, 2025a) introduced the allocation and sizing of DG and CB simultaneously in the DFR problem for more complex and large-scale distribution network, using the stochastic fractal search algorithm. The proposed tool is capable of simultaneously handling combinatorial variables related to tie-switches, DG, and CB, and providing an optimal solution that challenges the current literature.

1.3 PROBLEMATIC

This work addresses optimal power flow formulations for solving real-world problems in distribution networks. First, we will address the formulation of three-phase optimal power flow with the integration of distributed photovoltaic power plants to solve voltage unbalance problems in large-scale unbalanced distribution systems. Later we will address the optimal power flow formulation using a feeder reconfiguration approach to minimize power losses with the simultaneous integration of distributed generations and capacitor banks into large-scale distribution networks.

The planning and operation of distribution networks with renewable energy sources presents several challenges that are constantly being investigated, and potential solutions brought by researchers around the world to make life better for the population. In previous research carried out in (Ayikpa, 2017), we developed a robust computational tool to mitigate a particular case of voltages unbalances in which the voltage amplitudes present values in modules different from 1.0.pu, however, maintaining the angular phase shift of 120° between phases. This phenomenon is defined as a voltage drop problem and has been extensively studied over the years, receiving numerous proposals to mitigate its effects. The developed tool is a three-phase optimal power flow that integrates constant active power generation and reactive power control from photovoltaic inverters. Simulations have been done with small- and medium-scale unbalanced networks. However, this research proposes an extension of the above-mentioned work to large-scale distribution networks with adjustment of voltage regulator taps.

The heuristic and metaheuristic algorithms proposed in the technical literature to solve the distribution network reconfiguration problem are limited to the allocation of distributed generation or capacitor banks. In some cases where both components were allocated simultaneously, the authors considered small-or medium-scale systems, due

to the difficulty in managing the radiality constraints of large-scale systems. Therefore, this research proposes a robust computational tool based on graph theory to check the radiality of small-, medium-, and large-scale distribution networks and provide only radial topologies while solving the DFR problem with simultaneous allocation of distributed generation and capacitor banks using the stochastic fractal search.

During the development of this research, we faced a challenge in solving the DFR problem due to the basic mathematical model of the SFS, whose diffusion and updating process does not consider the decision variables of the distribution network. To solve this problem, we propose a mathematical model that controls the violation of the tie-switch limits during the optimization process. The mathematical model can be applied to small-, medium- and large-scale systems for the distribution feeder reconfiguration problem.

2 MATHEMATICAL FORMULATION OF THE AC THREE-PHASE OPTIMAL POWER FLOW WITH GRID-CONNECTED PV PLANTS

This chapter presents the mathematical formulation of the three-phase optimal power flow with the integration of photovoltaic plants. It should be noted that the mutual impedances of the lines are disregarded in the construction of the bus admittance matrix to simplify the modeling.

2.1 FUNDAMENTALS OF OPTIMAL POWER FLOW

The optimal power flow was proposed in the early 1960 as an extension of the conventional economic dispatch problem to determine the optimal settings for control variables, respecting physical and operational constraints of the system (Momoh, 2001, p. 339). Unlike a conventional power flow problem in which variables such as voltage magnitudes and active power generations at the PV buses are specified, in the OPF, the optimal power generations are calculated to optimize a system performance criterion. The OPF is used to evaluate numerous performance indexes in large-scale power systems, thus seeking better operating conditions. However, there are several feasible operating points of the system in relation to the evaluated aspects, making some more advantageous than others. A loss minimization process, for example, in which there are no restrictions on power flow in the lines, requires a uniform distribution of generation among the system's generators, whereas, to minimize generation costs, it is advantageous for this distribution to cease being uniform and instead be concentrated among the lowest-cost generators.

In its analytical formulation, the OPF is expressed as a nonlinear optimization problem with equality and inequality constraints. Its objective function represents a system performance index, its equality constraints represent the balance of active and reactive power in the electrical power grid, and the inequality constraints express the physical, operational, and sometimes safety limits of the system. The generic formulation of an OPF problem is as follows.

$$\begin{aligned} &Minimize \;\; f(\mathrm{x}) \\ &s.a \\ &\qquad \mathrm{g}(\mathrm{x}) = 0 \\ &\qquad \mathrm{h}_{\min} \le \mathrm{h}(\mathrm{x}) \le \mathrm{h}_{\max} \end{aligned} \tag{1}$$

Where x is the vector of optimization variables, f(x), the objective function to be optimized, g(x) and h(x), represent respectively the equality and inequality constraints, $\mathrm{h}_{\min}$ and $\mathrm{h}_{\max}$ are the minimum and maximum limits of the inequality constraints.

2.2 THREE-PHASE OPTIMAL POWER FLOW

Power grid analysis tools based on single-phase equivalents may not provide the best operational solutions for three-phase systems, especially when circuits and/or loads are significantly unbalanced (Von Jouanne; Banerjee, 2001). The three-phase representation of the distribution system was first made in power flow programs that use a backward/forward sweep method to obtain the system voltages (Cheng; Shirmohammadi, 1995). Later, many efforts have been concentrated by several authors in the development of power flow tools for distribution networks based on the three-phase representation of the network. In, (Garcia et al., 2000) a three-phase current injection method (TCIM) was proposed resulting in better convergence properties than the backward/forward sweep method. The same formulation was later used in a three-phase optimal power flow (TOPF) which considers the mutual impedances of the lines, the modeling of transformers, and voltage regulators (Araujo et al., 2013). In (Bruno et al., 2011), a TOPF based on quasi-Newton method has been proposed to handle some control variables such as single-phase loads, storages and microgeneration units in a smart grid environment to perform distribution network management. Paudyal; Canizares; Bhattacharya (2011) considered switching operations of load tap changer and capacitors in the TOPF formulation as a mixed-integer nonlinear programming problem. A semidefinite programming (SDP) relaxation technique was developed in (Dall'Anese; Zhu; Giannakis, 2013) to reach the globally optimal solution of the original non-convex TOPF. A TOPF formulation in rectangular coordinates that considers voltage regulator taps and capacitor banks adjustment was carried out in (Baran; Fernandes, 2016) to minimize power losses in distribution

networks. In this work, the TOPF is formulated using three-phase current injections as presented in (Garcia et al., 2000).

2.3 OBJECTIVE FUNCTION

2.3.1 MINIMAL VOLTAGE UNBALANCE

The objective function represents the performance index of the system to be optimized, and in this work the minimum voltage unbalance is studied. According to (Baggini, 2008, p. 163), voltage unbalance in a three-phase electrical system is defined as a condition in which the three phases present different voltage values in module, whether undervoltage or overvoltage, and/or angular phase shift between phases different from 120° at the fundamental frequency of the system. In other words, it refers to the asymmetry of the voltage magnitude or phase angle at the fundamental frequency in a three-phase power system (Seiphetlho; Rens, 2010).

2.3.1.1 Ideal operating conditions for an electrical network

A three-phase electrical system operating in steady state must satisfy the following conditions:

- ✓ Sinusoidal alternating voltages and currents.
- ✓ Constant voltage and current amplitudes equal to nominal values.
- ✓ Constant frequency at the synchronous values.
- ✓ Balanced three-phase voltages and currents.
- ✓ Unit power factors at loads.
- ✓ Zero transmission and distribution losses.

When the system is in an ideal operating condition, that is, free of unbalances, considering phase "a" in the reference and positive phase sequence, the balanced three-phase voltage is expressed as follows.

$$\overline{V_a} = 1,0\angle 0°$$
$$\overline{V_b} = 1,0\angle -120° \quad (2)$$
$$\overline{V_c} = 1,0\angle +120°$$

Equation (2) is no longer valid in unbalanced systems. Figures 2 (a) and 2 (b) show examples of balanced and unbalanced voltages, respectively.

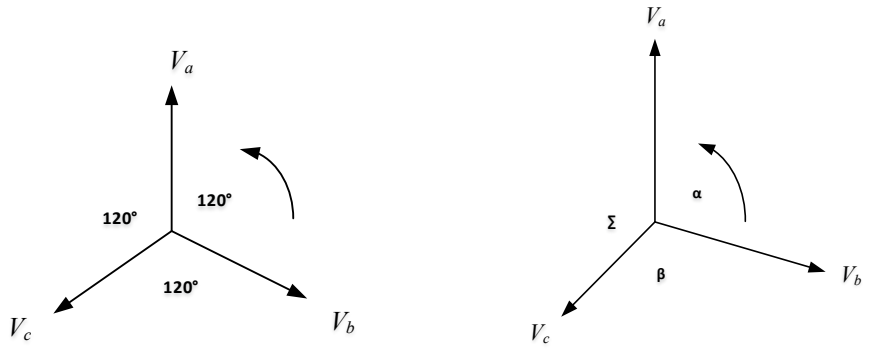

(a) (b)

Figure 2 – (a) Balanced three-phase voltage, (b) Unbalanced three-phase voltage.
Source: Author's elaboration

2.3.1.2 Origins and effects of voltage unbalances

Voltage unbalance mainly affects distribution systems where there is a predominance of poorly distributed single-phase loads, asymmetrical and non-transposed three-phase overhead lines, transformers with open star and delta connections and the presence of two-phase and single-phase lines (Von Jouanne; Banerjee, 2001). Unbalanced voltages can cause adverse effects on the operation of some electrical equipment (three-phase induction motors, single-phase AC-DC static converters and variable speed drives), compromising their performance and useful life. The direct consequence of this on the electrical energy system is excessive losses and increased consumption.

2.3.1.3 Quantification of voltage unbalance

There are several methods for quantifying voltage unbalance. The most popular ones used in the literature are presented as follows.

- National Electrical Manufacturers Association (NEMA) Method

According to (Bonnett; Soukup, 1997) the voltage unbalance factor (VUF) is defined by the National Electrical Manufacturers Association as the ratio between the maximum deviation of the line voltage in relation to their average value, without considering information about the phasor angles.

$$VUF = \frac{\Delta V_{\text{max, line-line}}}{V_{\text{avg, line-line}}} \times 100 \quad (3)$$

Where ΔV_{max} is the maximum deviation of the line-to-line voltage from the average voltage and V_{avg} is the average value of the line-to-line voltages.

- Institute of Electrical and Electronics Engineers (IEEE) Method

The Institute of Electrical and Electronics Engineers defined VUF using two different approaches. The first definition is like that used by NEMA but used phase voltages instead of line-to-line voltage, as described in (4).

$$VUF = \frac{\Delta V_{\text{max, phase}}}{V_{\text{avg, phase}}} \times 100 \quad (4)$$

The second definition uses the ratio of the difference between the highest and lowest phase voltages to their average. It considers the maximum deviation between the voltages and is expressed as follows.

$$VUF = \frac{V_{\text{max}} - V_{\text{min}}}{(V_a + V_b + V_c)/3} \times 100 \quad (5)$$

Where V_a, V_b, and V_c are the magnitudes of the voltages of phases a, b, and c, and V_{max} and V_{min} are the highest and lowest phase voltage values, respectively.

The disadvantage of using the NEMA and the first definition of IEEE methods is the loss of phase angle information, which could result in an error of 13% under extreme conditions (Seiphetlho; Rens, 2010).

– Method of symmetrical components

The symmetrical components method is applied to unbalanced three-phase voltage using the Fortescue transformation (Fortescue, 1918). This method consists of decomposing three unbalanced phasors in the phasor domain into their balanced equivalents in the sequential domain, called positive, negative, and zero sequence symmetric components, through the FORTESCUE transformation. Figure 3 shows the positive, negative, and zero sequence systems of the unbalanced phasor.

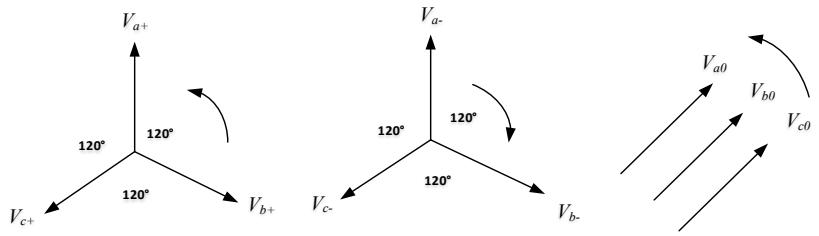

(a) (b) (c)

Figure 3 – (a) Positive Sequence, (b) Negative Sequence, (c) Zero Sequence
Source: Author ‘s elaboration

The application of the FORTESCUE theorem to an unbalanced three-phase voltage is mathematically illustrated by equation (6) where A represents the transformation matrix.

$$A = \begin{pmatrix} 1 & 1 & 1 \\ 1 & a^2 & a \\ 1 & a & a^2 \end{pmatrix}; \quad a = -\frac{1}{2} + j\frac{\sqrt{3}}{2}$$

$$\begin{bmatrix} V_a \\ V_b \\ Vc \end{bmatrix} = A.\begin{bmatrix} V_{a0} \\ V_{a+} \\ V_{a-} \end{bmatrix} \rightarrow \begin{bmatrix} V_{a0} \\ V_{a+} \\ V_{a-} \end{bmatrix} = \frac{1}{3}A^{-1}.\begin{bmatrix} V_a \\ V_b \\ V_c \end{bmatrix} \quad (6)$$

The induction motor can help in the physical interpretation of the effects of symmetrical components on voltage unbalance. The direction of rotation of a three-phase induction motor when subjected to positive-sequence voltages is opposite to the direction of rotation under negative-sequence voltages. When the same motor receives zero-sequence voltages in all three phases, its rotor does not rotate because there is no rotating magnetic field. Based on these observations, voltage unbalance can be quantified by the ratio of the negative-sequence to the positive-sequence component (Seiphetlho; Rens, 2010). The symmetrical components method is known as the most efficient for measuring voltage unbalance between the phases of a system, as it considers the real configuration of the system with the voltage modules and angles in the three phases and is defined as follows.

$$VUF(\%) = \sum_{k\in\Omega_k} \frac{|V_-|}{|V_+|} \times 100 \tag{7}$$

Where *k* indicates the bus index and Ω the set of system bus.

$$V_{a-,k} = V_k^a + a^2 V_k^b + a V_k^c$$

$$V_{a+,k} = V_k^a + a V_k^b + a^2 V_k^c$$

$$a = 1\angle 120°$$

Based on (7), the objective function used in this work to represent voltage imbalance in electrical power systems is expressed by (8).

$$OF_1 = \min \sum_{k\in\Omega_k} \sum_{i\in I} \left(V_{\mathrm{Re},k,-}^{i^2} + V_{\mathrm{Im},k-}^{i^2} \right) \tag{8}$$

Where, $V_{\mathrm{Re},k-}^2$ and $V_{\mathrm{Im},k-}^2$, are respectively the square of the real part and the imaginary part of the negative sequence component of the voltages. Ω_k represents the set of network buses and *I*, the set of phases (a,b,c).

2.4 LINES MODELING

The three-phase lines can be represented by the equivalent circuit in Figure 4, where the self and mutual impedances are calculated by (9).

$$Z_{ii} = r_i + 0.09530 + j0.1234\left(\ln\frac{1}{\mathrm{GMR}_i} + 7.93402\right)\ \Omega/\mathrm{mile}$$
$$Z_{ij} = 0.09530 + j0.12134\left(\ln\frac{1}{D_{ij}} + 7.93402\right)\ \Omega/\mathrm{mile} \quad (9)$$

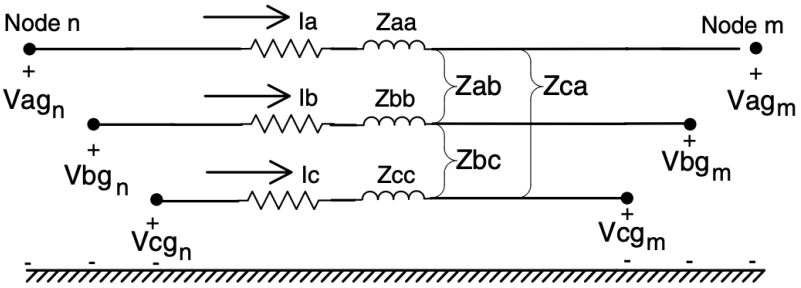

Figure 4 – Three-phase model of a line segment (Kersting, 2002, p. 88)

Z_{ii} and Z_{ij} are the line's self-impedance and the mutual impedance between conductor i and j, r_i is the resistance of conductor i and j. V_{in} e I_i are the line-to-ground voltage and line current, respectively. For the TOPF studies, the lines are represented by their π-equivalent circuit, as shown in Figure 5.

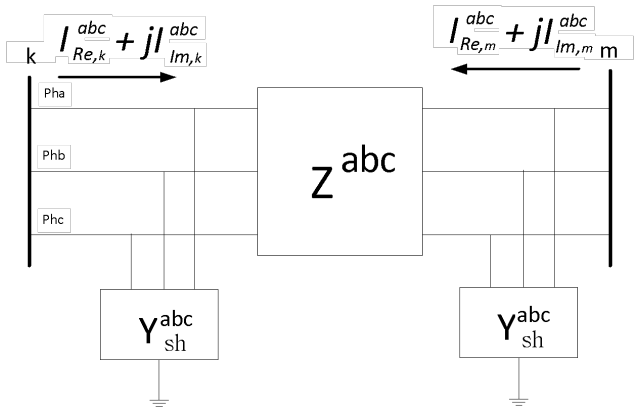

Figure 5 – Circuit π-equivalent of a three-phase line
Source: Author 's elaboration

The matrices of the equivalent circuit elements are expressed as follows.

$$Z^{abc} = \begin{bmatrix} z^{aa} & z^{ab} & z^{ac} \\ z^{ba} & z^{bb} & z^{bc} \\ z^{ca} & z^{cb} & z^{cc} \end{bmatrix} = \begin{bmatrix} r^{aa} & r^{ab} & r^{ac} \\ r^{ba} & r^{bb} & r^{bc} \\ r^{ca} & r^{cb} & r^{cc} \end{bmatrix} + j \begin{bmatrix} x^{aa} & x^{ab} & x^{ac} \\ x^{ba} & x^{bb} & x^{bc} \\ x^{ca} & x^{cb} & x^{cc} \end{bmatrix} \quad (10)$$

$$Y^{bc} = j \begin{bmatrix} b^{aa} & b^{ab} & b^{ac} \\ b^{ba} & b^{bb} & b^{bc} \\ b^{ca} & b^{cb} & b^{cc} \end{bmatrix} \quad (11)$$

Single-phase and two-phase lines are common in distribution system, the series impedance of missing phases is assumed to be infinite and replaced in practice by a large number, usually 10^{10}. The mutual impedance and the capacitive susceptance of the missing phases is set to zero. The contributions of the lines to the current injections are given by (12).

$$\begin{bmatrix} I^{abc}_{\mathrm{Re},k} \\ I^{abc}_{\mathrm{Im},k} \\ \vdots \\ I_{\mathrm{Re},m} \\ I^{abc}_{\mathrm{Im},m} \end{bmatrix} = \begin{bmatrix} G^{abc} & -\left(B^{abc}\right)^t & \cdots & -G^{abc} & B^{abc} \\ \left(B^{abc}\right)^t & G^{abc} & \cdots & -B^{abc} & -G^{abc} \\ \vdots & \vdots & \ddots & \vdots & \vdots \\ -G^{abc} & B^{abc} & \cdots & G^{abc} & -\left(B^{abc}\right)^t \\ -B^{abc} & -G^{abc} & \cdots & \left(B^{abc}\right)^t & G^{abc} \end{bmatrix} \cdot \begin{bmatrix} V^{abc}_{\mathrm{Re},k} \\ V^{abc}_{\mathrm{Im},k} \\ \vdots \\ V^{abc}_{\mathrm{Re},m} \\ V^{abc}_{\mathrm{Im},m} \end{bmatrix} \quad (12)$$

In (12), G^{abc} and B^{abc} are the real and imaginary parts of the admittance matrix elements and *t* indicates the transposed matrix. It should be noted that the mutual impedances of the lines are disregarded in the construction of the bus admittance matrix to simplify the modeling.

2.5 TRANSFORMER MODELING

The transformers are represented in this work by the π-equivalent circuit, while the voltage regulators are modeled as autotransformers using the same equivalent circuit as shown in Figure 5.

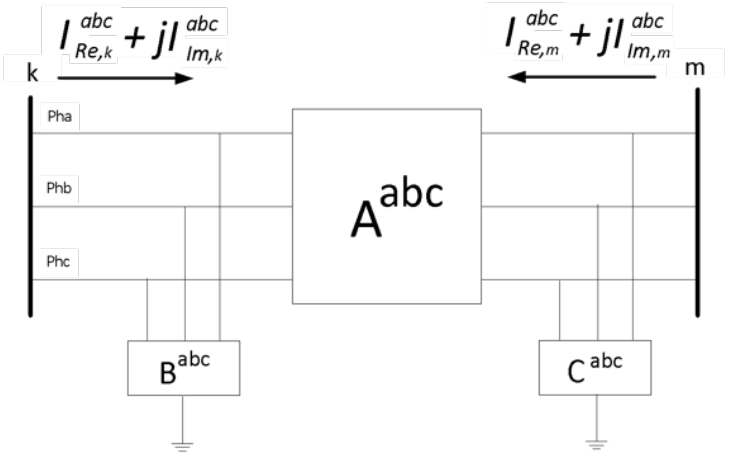

Figure 6 – Circuit π-equivalent of a three-phase transformer

Source: Author ‘s elaboration

$$
\begin{aligned}
\mathrm{A}^{\mathrm{abc}} &= \alpha^{abc} y_t \\
\mathrm{B}^{\mathrm{abc}} &= \alpha^{abc}\left(\alpha^{abc} - 1\right) y_t \\
\mathrm{C}^{\mathrm{abc}} &= \left(1 - \alpha^{abc}\right) y_t \\
\alpha^{abc}_{\min} &\le \alpha^{abc} \le \alpha^{abc}_{\max}
\end{aligned}
\tag{13}
$$

α^{abc}: represent the tap positions for phases *a, b* and *c*.

y_t : is the per-unit leakage admittance of the transformer or autotransformer.

The contributions to the transformer or autotransformer current injections at buses *k* and *m* can be expressed as follows.

$$
\begin{aligned}
I^{abc}_k &= A^{abc}\left(V^{abc}_k - V^{abc}_m\right) + B^{abc} V^{abc}_k \\
I^{abc}_m &= A^{abc}\left(V^{abc}_m - V^{abc}_k\right) + C^{abc} V^{abc}_m
\end{aligned}
\tag{14}
$$

2.6 CAPACITOR MODELING

Capacitors are modeled with constant susceptance and can be connected in delta, isolated star, or grounded star when they are three-phase. In the case of two-phase or single-phase connection, the currents for the missing phases are fixed at zero. Capacitor banks are modeled in this work by (15).

$$C_k^{abc} = \frac{Q_k^{abc}}{\left|V_k^{abc}\right|^2} \tag{15}$$

C_k^{abc} : is the capacitive susceptance of the capacitor connected to bus k.

Q_k^{abc} : is the nominal reactive power of the capacitor per phase on bus *k*.

$\left|V_k^{abc}\right|$: is the voltage magnitude per phase on bus *k.*

2.7 MODELING OF LOADS

In a distribution system, loads are specified by the complex power consumed. It can be specified as kVA and power factor, kW and power factor, or active power and reactive power, and can be single-phase, two-phase, or three-phase. Loads can be connected to specific buses (spot load) or uniformly distributed along a line (distributed load). When three-phase, they can be connected in a star or delta configuration and represented by the ZIP model: constant power (P), constant current (I), constant impedance (Z), or any combination of the above-mentioned configurations.

2.7.1 WYE-CONNECTED LOADS

Figure 7 shows the wye-connected load. The ZIP model of the load is expressed by (16).

$$\begin{aligned} P_{d,k}^{abc} &= P_{d,0}^{abc}\left(\alpha_0 + \alpha_1 \frac{\left|V_k^{abc}\right|}{\left|V_0\right|} + \alpha_2 \left(\frac{\left|V_k^{abc}\right|}{\left|V_0\right|}\right)^2\right) \\ Q_{d,k}^{abc} &= Q_{d,0}^{abc}\left(\beta_0 + \beta_1 \frac{\left|V_k^{abc}\right|}{\left|V_0\right|} + \beta_2 \left(\frac{\left|V_k^{abc}\right|}{\left|V_0\right|}\right)^2\right) \end{aligned} \tag{16}$$

$P_{d,0}^{abc}$ e $Q_{d,0}^{abc}$ are the nominal values of active and reactive power at the nominal voltage value V_o.

$P_{d_k}^{abc}$ and $Q_{d_k}^{abc}$ are the active and reactive powers of the load at bus k.

α_i, β_i, are the weights that define the proportions of each component in the ZIP model, $\sum_{i=0}^{2}\alpha_i = 1$ and $\sum_{i=0}^{2}\beta_i = 1$.

The current injections of the wye-connected load are given by (17).

$$I_{y,k}^{a} = \frac{S_{sc}^{a*}}{V_k^{a*}} + \frac{V_k^a S_{ic}^{a*}}{\left|V_k^a\right|} + V_k^a S_{zc}^{a*}$$
$$I_{y,k}^{b} = \frac{S_{sc}^{b*}}{V_k^{b*}} + \frac{V_k^b S_{ic}^{b*}}{\left|V_k^b\right|} + V_k^b S_{zc}^{b*} \quad (17)$$
$$I_{y,k}^{c} = \frac{S_{sc}^{c*}}{V_k^{c*}} + \frac{V_k^c S_{ic}^{c*}}{\left|V_k^c\right|} + V_k^c S_{zc}^{c*}$$

$$S_{sc}^{abc^*} = \alpha_0 P_{d,0}^{abc} - j\beta_0 Q_{d,0}^{abc}$$

$$S_{ic}^{abc^*} = \alpha_1 P_{d,0}^{abc} - j\beta_1 Q_{d,0}^{abc}$$

$$S_{zc}^{abc^*} = \alpha_2 P_{d,0}^{abc} - j\beta_2 Q_{d,0}^{abc}$$

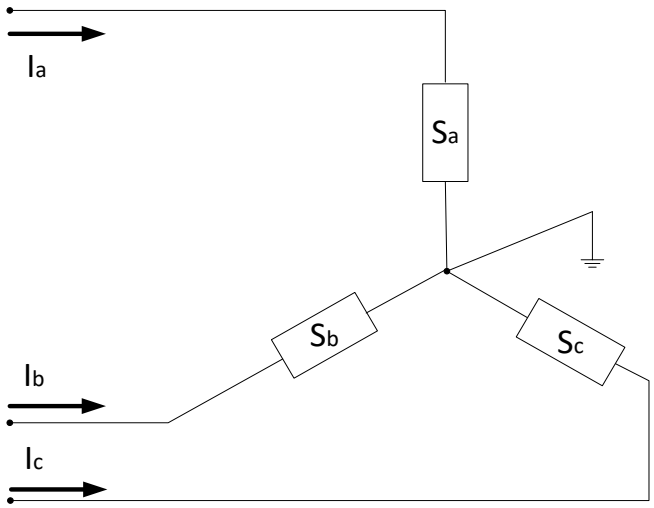

Figure 7 – Wye-connected load

Source: Author's elaboration.

2.7.2 DELTA-CONNECTED LOADS

The delta-connected load is represented by Figure 8. Based on the ZIP model, the current injection of the load is represented by (18).

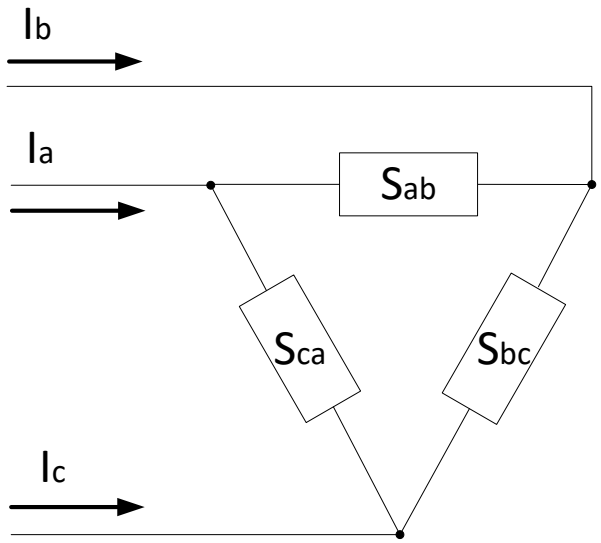

Figure 8 – Wye-connected load

Source: Author's elaboration.

$$
\begin{aligned}
I_{\Delta,k}^{ab} &= \frac{S_{sc}^{ab*}}{V_k^{a*} - V_k^{b*}} + \frac{\left(V_k^a - V_k^b\right) S_{ic}^{ab*}}{\left|V_k^a - V_k^b\right|} + \left(V_k^a - V_k^b\right) S_{zc}^{ab*} \\
I_{\Delta,k}^{bc} &= \frac{S_{sc}^{bc*}}{V_k^{b*} - V_k^{c*}} + \frac{\left(V_k^b - V_k^c\right) S_{ic}^{bc*}}{\left|V_k^b - V_k^c\right|} + \left(V_k^b - V_k^c\right) S_{zc}^{bc*} \\
I_{\Delta,k}^{ca} &= \frac{S_{sc}^{ca*}}{V_k^{c*} - V_k^{a*}} + \frac{\left(V_k^c - V_k^a\right) S_{ic}^{ca*}}{\left|V_k^c - V_k^a\right|} + \left(V_k^c - V_k^a\right) S_{zc}^{ca*}
\end{aligned}
\tag{18}
$$

The line current in a delta-connected load is determined by applying Kirchhoff's current law at each node of the delta connection and is given in matrix form by (19).

$$
\begin{bmatrix} I_{\Delta,k}^{a} \\ I_{\Delta,k}^{b} \\ I_{\Delta,k}^{c} \end{bmatrix} = \begin{bmatrix} 1 & 0 & -1 \\ -1 & 1 & 0 \\ 0 & -1 & 1 \end{bmatrix} . \begin{bmatrix} I_{\Delta,k}^{ab} \\ I_{\Delta,k}^{bc} \\ I_{\Delta,k}^{ca} \end{bmatrix} \tag{19}
$$

This thesis represents the system loads as constant power and connected in a grounded wye. Based on this assumption, the current injection equations are given by (20).

$$I_{y,k}^{a} = I_{Re,k}^{a} + jI_{Im,k}^{a} = \left(\frac{P_{d,k}^{a} + jQ_{d,k}^{a}}{V_{k}^{a}} \right)^{*}$$
$$I_{y,k}^{b} = I_{Re,k}^{b} + jI_{Im,k}^{b} = \left(\frac{P_{d,k}^{b} + jQ_{d,k}^{b}}{V_{k}^{b}} \right)^{*} \quad (20)$$
$$I_{y,k}^{c} = I_{Re,k}^{c} + jI_{Im,k}^{c} = \left(\frac{P_{d,k}^{c} + jQ_{d,k}^{c}}{V_{k}^{c}} \right)^{*}$$

2.8 MODELING OF GENERATORS

In static studies such as power flow or optimal power flow, generators are modeled as constant active and reactive power sources or as a constant active power source and an ideal voltage controller. The complex power supplied by the three phases generator is given by the expression (21), where the variables $\mathrm{P_g}$ and $\mathrm{Q_g}$ can be unknown or fixed, depending on the procedure adopted.

$$S_{g,k}^{abc} = V_{k}^{abc} I_{g,k}^{*abc} = P_{g,k}^{abc} + jQ_{g,k}^{abc} \quad (21)$$

The contribution in current injections of the generators can be expressed as follows.

$$I_{g,k}^{abc} = I_{\mathrm{Re},g,k}^{abc} + jI_{\mathrm{Im},g,k}^{abc} = \left(\frac{P_{g,k}^{abc} + jQ_{g,k}^{abc}}{V_{k}^{abc}} \right)^{*} \quad (22)$$

2.9 VOLTAGE REGULATOR MODELING

In the distribution system, the load behavior is very unstable, and this instability is responsible for voltage collapse. The regulation of voltages is an important function that maintains load voltages within an acceptable range and is carried out in this work with step voltage regulators. The step-voltage regulator can be modeled as an autotransformer with adjustable taps. Figure 9 represents the π-equivalent circuit of the autotransformer used in this work.

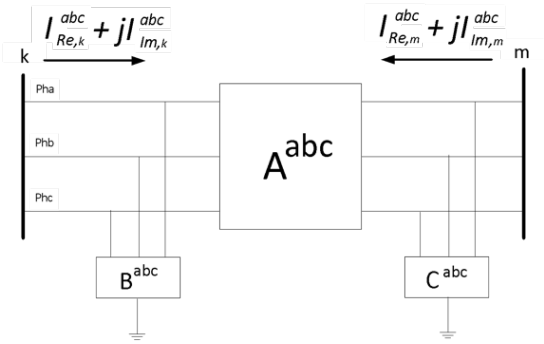

Figure 9 – Circuit π-equivalent of an autotransformer

Source: Author ‘s elaboration

$$
\begin{aligned}
\mathrm{A}^{\mathrm{abc}} &= \alpha^{abc} y_t \\
\mathrm{B}^{\mathrm{abc}} &= \alpha^{abc}\left(\alpha^{abc}-1\right) y_t \\
\mathrm{C}^{\mathrm{abc}} &= \left(1-\alpha^{abc}\right) y_t \\
\alpha_{\min}^{abc} &\le \alpha^{abc} \le \alpha_{\max}^{abc}
\end{aligned}
\tag{23}
$$

α^{abc}: represent the tap positions for phases *a, b* and *c*.

y_t : is the per-unit leakage admittance of the autotransformer.

The contributions to the transformer or autotransformer current injections at buses *k* and *m* can be expressed as:

$$
\begin{aligned}
I_k^{abc} &= A^{abc}\left(V_k^{abc} - V_m^{abc}\right) + B^{abc} V_k^{abc} \\
I_m^{abc} &= A^{abc}\left(V_m^{abc} - V_k^{abc}\right) + C^{abc} V_m^{abc}
\end{aligned}
\tag{24}
$$

2.10 EQUALITY RESTRICTION

The current balance equations at a bus k of the system are obtained by adding the current injections per phase of the elements connected to that bus. The current injection equations at the buses are established as follows.

$$
S^{abc} = V^{abc}\left(I^{abc}\right)^{*} \longrightarrow I^{abc} = \left(\frac{S^{abc}}{V^{abc}}\right)^{*} \tag{25}
$$

Equation (26) can be expressed in another form.

$$I^{abc} = \left(Y_{bus}^{abc}\right) V^{abc} \tag{26}$$

Where I^{abc} is the vector of current injections at buses; Y_{bus}^{abc} is the bus admittance matrix; V^{abc} is the bus voltage vector and S^{abc} is the vector of power injections into the buses and is expressed by (27).

$$S^{abc} = \left(P_{\mathrm{g}}^{abc} + jQ_{\mathrm{g}}^{abc}\right) - \left(P_{\mathrm{d}}^{abc} + jQ_{\mathrm{d}}^{abc}\right) \tag{27}$$

From equations (26) and (27) the current balance equation is established by (28).

$$I^{abc} = \left(\frac{S^{abc}}{V^{abc}}\right)^{*} = Y_{bus}^{abc} V^{abc} \tag{28}$$

By developing expression (28) we obtain the current injection equations for all buses of the system as presented in (29).

$$\left(\frac{P_g^{abc} + jQ_g^{abc}}{V_{\mathrm{Re}}^{abc} + jV_{\mathrm{Im}}^{abc}}\right)^{*} - \left(\frac{P_d^{abc} + jQ_d^{abc}}{V_{\mathrm{Re}}^{abc} + jV_{\mathrm{Im}}^{abc}}\right)^{*} - \left(G^{abc} + jB^{abc}\right)\left(V_{\mathrm{Re}}^{abc} + jV_{\mathrm{Im}}^{abc}\right) = 0 \tag{29}$$

Equation (29) can be written in simplified form for a given bus *k* as:

$$I_{g,k}^{abc} - I_{d,k}^{abc} - I_k^{abc} = 0 \tag{30}$$

Where, $I_{g,k}^{abc}$ are the contribution of generators, $I_{d,k}^{abc}$ the contribution of loads and I_k^{abc}, the contribution of lines, transformers, voltage regulators and other equipment of the grid. Separating the real and imaginary parts of equation (30), we obtain the current balance equations of the TOPF.

$$\begin{aligned} I_{\mathrm{Re},g,k}^{abc} - I_{\mathrm{Re},d,k}^{abc} - I_{\mathrm{Re},k}^{abc} &= 0 \\ I_{\mathrm{Im},g,k}^{abc} - I_{\mathrm{Im},d,k}^{abc} - I_{\mathrm{Im},k}^{abc} &= 0 \end{aligned} \tag{31}$$

For the voltages on the reference bus to be 120° out of phase, the equations described in (32) are imposed.

$$\begin{aligned} &V^{a}_{\mathrm{Im},ref} = 0 \\ &V^{b}_{\mathrm{Im},ref} - V^{b}_{\mathrm{Re},ref}\tan(\,{}^{-2\pi}\!/_{3}\,)=0 \\ &V^{c}_{\mathrm{Im},ref} - V^{c}_{\mathrm{Re},ref}\tan(\,{}^{2\pi}\!/_{3}\,)=0 \end{aligned} \tag{32}$$

When modeling substations, it is crucial that the voltage magnitudes in the three phases of the reference bus are equal. The equations that represent this constraint in TOPF are defined as follows.

$$\begin{aligned} &\left(V^{a}_{\mathrm{Re},ref}\right)^{2} + \left(V^{a}_{\mathrm{Im},ref}\right)^{2} - \left(V^{b}_{\mathrm{Re},ref}\right)^{2} - \left(V^{b}_{\mathrm{Im},ref}\right)^{2} = 0 \\ &\left(V^{a}_{\mathrm{Re},ref}\right)^{2} + \left(V^{a}_{\mathrm{Im},ref}\right)^{2} - \left(V^{c}_{\mathrm{Re},ref}\right)^{2} - \left(V^{c}_{\mathrm{Im},ref}\right)^{2} = 0 \end{aligned} \tag{33}$$

In this work, PV plants are modeled as dispatchable generators, and to represent the reactive power control performed by these plants, it is necessary to assume that they inject equal amounts of reactive power into the three phases, which characterizes the operating principle of inverters. Therefore, for the power plant connected to bus k, the reactive power injection from the PV inverters on the three phases of a given bus k must satisfy the restriction (34).

$$\begin{aligned} &Q^{a}_{PV,k} = Q^{b}_{PV,k} \\ &Q^{a}_{PV,k} = Q^{c}_{PV,k} \end{aligned} \tag{34}$$

2.11 INEQUALITY CONSTRAINTS

The inequality constraints represent the limits on the bus voltage amplitudes, active and reactive powers of generators, transformers and voltages taps, active power flows as presented in (35).

$$
\begin{aligned}
V_{\min,k}^{abc^2} \leq V_{\mathrm{Re},k}^{abc^2} + V_{\mathrm{Im},k}^{abc^2} \leq V_{\max,k}^{abc^2} \\
P_{\mathrm{g}_{\min,k}}^{abc} \leq P_{\mathrm{g}_k}^{abc} \leq P_{\mathrm{g}_{\max,k}}^{abc} \\
Q_{\mathrm{g}_{\min,k}}^{abc} \leq Q_{\mathrm{g}_k}^{abc} \leq Q_{\mathrm{g}_{\max,k}}^{abc} \\
a_{\min}^{abc} \leq a^{abc} \leq a_{\max}^{abc} \\
-P_{\max}^{abc} \leq P_{km}^{abc} \leq P_{\max}^{abc}
\end{aligned}
\tag{35}
$$

The active power flow constraints in (35) ensure that at the optimal operating point, no circuit will have its thermal line violated. P_{km}^{abc}: is the active power flow in the line *km* and is given by (36).

$$
P_{km}^{abc} = \Re\left(V_k^{abc} I_{km}^{abc^*}\right) \tag{36}
$$

The reactive power generation of PV inverters is performed using (37), where $S_{PV}^{\max}$ and P_{PV_ω} are the maximum apparent power and active power generation of the PV plant at a given solar time ω. As the active power generation of the PV plant fluctuates throughout the day, Q_{PV_ω} also keep changing during the day. Furthermore, based on the available reactive power capacity of the inverters, reactive power can be injected/absorbed within the range defined by (38).

$$
Q_{PV_\omega} = \sqrt{S^{max^2} - P_{PV_\omega}^2} \tag{37}
$$

$$
-Q_{PV_{max}} \leq Q_{PV_\omega} \leq Q_{PV_{max}} \tag{38}
$$

The next section presents the formulation of the TOPF problem, based on the established network equations.

2.12 FORMULATION OF THE THREE-PHASE OPTIMAL POWER FLOW IN RECTANGULAR COORDINATES

The generic formulation of the three-phase optimal power flow problem in rectangular coordinates with the insertion of photovoltaic plants is presented as follows.

- The real and imaginary parts of the voltages are defined by vectors V_{Re}^{abc} and V_{Im}^{abc} of dimension $(3 \times n,\ 3 \times n)$, where *n* is the number of buses in the system under study.
- In addition, we define the incidence matrices A_P and A_q with dimension (*n, np*) and (*n, nq*) where *np* is the number of synchronous generators and PV plants supplying active power and *nq*, the number of synchronous generators and PV plants injecting reactive power into the grid.

The problem is formulated to minimize negative sequence voltages in unbalanced distribution networks.

$$\min \sum_{k\in\Omega_k} \sum_{i\in I} \left(V_{\mathrm{Re},k-}^{i^2} + V_{\mathrm{Im},k-}^{i^2} \right) \tag{39}$$

Subject to

$$\begin{aligned} &diag\left(A_P P_g^{abc} - P_d^{abc} \right) V_{\mathrm{Re}}^{abc} + diag\left(A_q Q_g^{abc} - Q_d^{abc} \right) V_{\mathrm{Im}}^{abc} \\ &-diag\left(\left(V_{\mathrm{Re}}^{abc} \right)^2 + \left(V_{\mathrm{Im}}^{abc} \right)^2 \right) \left(G^{abc} V_{\mathrm{Re}}^{abc} - B^{abc} V_{\mathrm{Im}}^{abc} \right) = 0 \end{aligned} \tag{40}$$

$$\begin{aligned} &-diag\left(A_P Q_g^{abc} - Q_d^{abc} \right) V_{\mathrm{Re}}^{abc} + diag\left(A_p P_g^{abc} - P_d^{abc} \right) V_{\mathrm{Im}}^{abc} \\ &-diag\left(\left(V_{\mathrm{Re}}^{abc} \right)^2 + \left(V_{\mathrm{Im}}^{abc} \right)^2 \right) \left(G^{abc} V_{\mathrm{Im}}^{abc} + B^{abc} V_{\mathrm{Re}}^{abc} \right) = 0 \end{aligned} \tag{41}$$

$$\begin{aligned} &V_{\mathrm{Im},ref}^{a} = 0 \\ &V_{\mathrm{Im},ref}^{b} - V_{\mathrm{Re},ref}^{b} \tan\left({}^{-2\pi}\!/_{3} \right) = 0 \\ &V_{\mathrm{Im},ref}^{c} - V_{\mathrm{Re},ref}^{c} \tan\left({}^{2\pi}\!/_{3} \right) = 0 \end{aligned} \tag{42}$$

$$\begin{aligned} &\left(V_{\mathrm{Re},ref}^{a} \right)^2 + \left(V_{\mathrm{Im},ref}^{a} \right)^2 - \left(V_{\mathrm{Re},ref}^{b} \right)^2 - \left(V_{\mathrm{Im},ref}^{b} \right)^2 = 0 \\ &\left(V_{\mathrm{Re},ref}^{a} \right)^2 + \left(V_{\mathrm{Im},ref}^{a} \right)^2 - \left(V_{\mathrm{Re},ref}^{c} \right)^2 - \left(V_{\mathrm{Im},ref}^{c} \right)^2 = 0 \end{aligned} \tag{43}$$

$$\begin{aligned} &Q_{PV,k}^{a} = Q_{PV,k}^{b} \\ &Q_{PV,k}^{a} = Q_{PV,k}^{c} \end{aligned} \tag{44}$$

$$
\begin{aligned}
V_{\min,k}^{abc^2} \le V_{\mathrm{Re},k}^{abc^2} + V_{\mathrm{Im},k}^{abc^2} \le V_{\max,k}^{abc^2} \\
P_{\mathrm{g}_{\min,k}}^{abc} \le P_{\mathrm{g}_k}^{abc} \le P_{\mathrm{g}_{\max,k}}^{abc} \\
Q_{\mathrm{g}_{\min,k}}^{abc} \le Q_{\mathrm{g}_k}^{abc} \le Q_{\mathrm{g}_{\max,k}}^{abc} \\
a_{\min}^{abc} \le a^{abc} \le a_{\max}^{abc} \\
-P_{\max}^{abc} \le P_{km}^{abc} \le P_{\max}^{abc}
\end{aligned}
\tag{45}
$$

$$
-Q_{PV_{max}} \le Q_{PV} \le Q_{PV_{max}}
$$

$$
P_{km}^{abc} = \Re\left(V_k^{abc} I_{km}^{abc^*}\right) \tag{46}
$$

In this work we define the voltage limits as $V_{min}^{abc} = 0.95\ p.u$ and $V_{max}^{abc} = 1.05\ p.u$. The problem defined above is solved using the Prima-dual Interior Point method as described in Appendix C. The current injection equations of the network elements in the buses are given by (47).

$$
I_g^{abc} - I_d^{abc} - I^{abc} = 0 \tag{47}
$$

Where, I_{g}^{abc} is the contribution in current injection of the generators.

$$
I_g^{abc} = \frac{P_g^{abc} V_{\mathrm{Re}}^{abc} + Q_g^{abc} V_{\mathrm{Im}}^{abc}}{\left(V_{\mathrm{Re}}^{abc}\right)^2 + \left(V_{\mathrm{Im}}^{abc}\right)^2} + j\frac{P_d^{abc} V_{\mathrm{Im}}^{abc} - Q_g^{abc} V_{\mathrm{Re}}^{abc}}{\left(V_{\mathrm{Re}}^{abc}\right)^2 + \left(V_{\mathrm{Im}}^{abc}\right)^2} \tag{48}
$$

I_{d}^{abc}, is the contribution in current injection of the loads, given by (49).

$$
I_d^{abc} = \frac{P_d^{abc} V_{\mathrm{Re}}^{abc} + Q_d^{abc} V_{\mathrm{Im}}^{abc}}{\left(V_{\mathrm{Re}}^{abc}\right)^2 + \left(V_{\mathrm{Im}}^{abc}\right)^2} - j\frac{P_d^{abc} V_{\mathrm{Im}}^{abc} - Q_d^{abc} V_{\mathrm{Re}}^{abc}}{\left(V_{\mathrm{Re}}^{abc}\right)^2 + \left(V_{\mathrm{Im}}^{abc}\right)^2} \tag{49}
$$

I^{abc}, is the contribution in current injection of lines, transformers, voltage regulators, and capacitors, and defined by (50).

$$
I^{abc} = \left(G^{abc} + jB^{abc}\right)\left(V_{\mathrm{Re}}^{abc} + jV_{\mathrm{Im}}^{abc}\right) \tag{50}
$$

In this work we address the formulation of optimal power flow to solve the distribution feeder reconfiguration problem in which power losses are minimized. The purpose of this implementation is to propose an alternative formulation of the OPF for

large-scale networks using single-phase representation of the network to achieve the nominal voltage profile. The next chapter will present the mathematical formulation of the distribution feeder reconfiguration with simultaneous integration of distributed generations and capacitor banks in large-scale distribution networks.

3 MATHEMATICAL FORMULATION OF THE OPTIMAL POWER FLOW USING FEEDER RECONFIGURATION

In this chapter, we will present the most important topics for the distribution network reconfiguration. In the first section we will present the backward-forward sweep power flow model used to calculate the load flow in the MATPOWER environment. Then, we will present in section 2 the optimization constraints relative to the distribution feeder reconfiguration problem, including the distributed generation and capacitors bank modeling. Section 3 presents the fundamental loops concept, while section 4 presents the loss sensitive factor calculation. Finally, we will present the stochastic fractal search algorithm with its different steps for solving the DFR problem.

3.1 BACKWARD-FORWARD SWEEP POWER FLOW

In the DFR resolution process, we must evaluate each configuration of tie-switches found as a candidate solution to determine if it represents the best solution that optimizes the objective function. As is known, the backward-forward power flow calculation method is suitable for power flow analyses in radial distribution networks. Therefore, the power summation approach presented in the MATPOWER package was used in this work to evaluate the objective function.

Consider a generic representation of the radial distribution network represented by Figure 10. The power flow injected into bus i through branch i, $S_{i,ac} = P_{i,ac} + jQ_{i,ac}$, supplies the load and losses downstream of the line i, and is expressed by (51), where K_i represents the set of buses immediately downstream of the bus i.

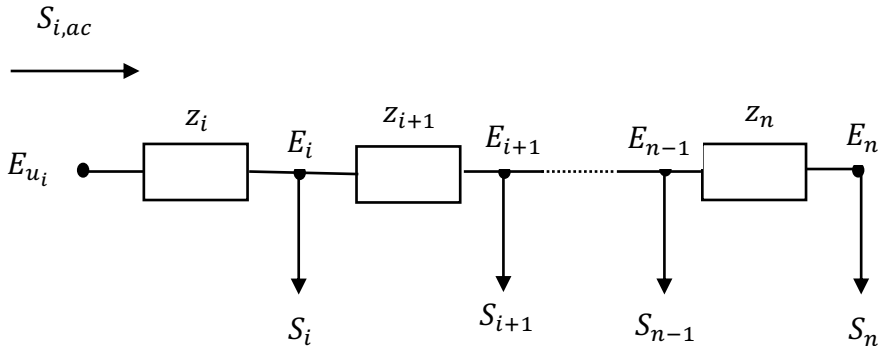

Figure 10 – Generic representation of the radial distribution network

$$S_{i,ac} = S_i + \sum_{k \in K_i} S_{k,ac} + \sum_{k \in K_i} z_k \left(\frac{S_{k,ac}}{V_k} \right)^2 \tag{51}$$

Separating (51) into its real and imaginary parts, we obtain (52) and (53) that represent the active and reactive powers flowing out of bus i, respectively. These equations are known as the first law of Kirchhoff. $P_{k,ac}$ and $Q_{k,ac}$ represent the active and reactive loads accumulated on the bus $k \in K_i$.

$$P_{i,ac} = P_i + \sum_{k \in K_i} \left[P_{k,ac} + r_k \left(\frac{P_{k,ac}^2 + Q_{k,ac}^2}{V_k} \right) \right] \tag{52}$$

$$Q_{i,ac} = Q_i + \sum_{k \in K_i} \left[Q_{k,ac} + x_k \left(\frac{P_{k,ac}^2 + Q_{k,ac}^2}{V_k} \right) \right] \tag{53}$$

Applying Kirchhoff's second law to a simple network circuit, we obtain the restriction (54). A detail about this expression can be found in Appendix A.

$$\left| V_{u_i} \right|^2 = |V_i|^2 + 2 \left(r_i P_{i,ac} + x_i Q_{i,ac} \right) + \left(r_i^2 + x_i^2 \right) \frac{\left(P_{i,ac}^2 + Q_{i,ac}^2 \right)}{|V_i|^2} \tag{54}$$

3.2 MATHEMATICAL FORMULATION OF THE SIMULTANEOUS DFR AND OPTIMAL PLACEMENT AND SIZING OF DG AND CB USING THE SFS

The objective function of the DFR-DG-CB problem is to minimize the total power losses of the feeder, expressed in (55).

$$OF_2 = \min \sum_{k \in K_i} r_k \left(\frac{P_{k,ac}^2 + Q_{k,ac}^2}{V_k^2} \right) \tag{55}$$

Since we will be using a metaheuristic to solve this problem, we will not present the mathematical model of the DFR problem. However, we present the equations for the radial load flow model and the radiality constraint of the problem.

$$P_{i,ac} = P_i - P_{DG,i} + \sum_{k \in K_i} \left[P_{k,ac} + r_k \left(\frac{P_{k,ac}^2 + Q_{k,ac}^2}{V_k} \right) \right] \tag{56}$$

$$Q_{i,ac} = Q_i - Q_{DG,i} - Q_{CB,i} + \sum_{k \in K_i} \left[Q_{k,ac} + x_k \left(\frac{P_{k,ac}^2 + Q_{k,ac}^2}{V_k} \right) \right] \tag{57}$$

$$\left| V_{u_i} \right|^2 = |V_i|^2 + 2 \left(r_i P_{i,ac} + x_i Q_{i,ac} \right) + (r_i^2 + x_i^2) \frac{\left(P_{i,ac}^2 + Q_{i,ac}^2 \right)}{|V_i|^2} \tag{58}$$

The voltage magnitude at all buses must satisfy their lower and upper bounds, as described in (59).

$$V_{i,min} \leq V_i \leq V_{i,max} \tag{59}$$

Additionally, the current flowing through the branches must not exceed the thermal capacity of the line as shown in (60).

$$\left| I_{ij} \right| \leq I_{ij,max} \tag{60}$$

The active power of distributed generation must lie between the minimum and maximum range as follows.

$$P_{DG,min} \leq P_{DG} \leq P_{DG,max} \tag{61}$$

The reactive power compensation of the capacitor banks is presented as a discrete value varying in 100 kVAr steps and must lie between a minimum and a maximum range as follows.

$$Q_{CB,min} \leq Q_{,CB} \leq Q_{CB,max} \quad (62)$$

The distribution network configuration must be radial, and this test is carried out in this study by checking the determinant of the incidence matrix A of each network topology.

$$\det(A) = \pm 1 \quad (63)$$

3.3 FUNDAMENTAL LOOPS AND RADIALITY CHECKING

From graph theory, a tree is a connected acyclic subgraph with *n* nodes and (*n* -1) arcs that contains all nodes of a graph without containing any loops. This can be applied to check the radiality condition of the generated distribution network topology to solve the DFR problem. The process of opening and closing switches in distribution feeder reconfiguration may generate network topologies that violate radiality constraints. Thus, the fundamental loops (FLs) are performed in this work to avoid this problem, using graph theory. An illustration of the formation of fundamental loops is shown in Appendix B with a 14-bus system. After computing the FLs, the radiality check helps to discard the network configurations that are not a tree (radial). According to (Nguyen; Truong; Phung, 2016), for each network configuration, the incidence matrix A is calculated and the first column corresponding to the reference node is removed. The rows of matrix A corresponding to the tie-switches are also removed. If the rest of matrix A is a square matrix and its determinant is 1 or -1, the network configuration is a radial topology.

3.4 LOSS-SENSITIVE FACTOR

The candidates buses for the DG or CB allocation are determined using the loss-sensitive factor method (Mohamed Imran A; Kowsalya M, 2014). In this study, we consider the LSF approach to reduce the search space of candidate nodes for the allocation of DG or CB, in the initialization process, and later in the diffusion and update processes of the SFS to correct the violation of the bounds from the placement of DG and CB.

The loss-sensitive factor is calculated considering a single-line distribution network with an impedance $R_k + jX_k$ and a load $P_L + jQ_L$ connecting between two nodes *p* and *q* as shown in Figure 11. Equation (64) represents the active power losses on the k^{th} line.

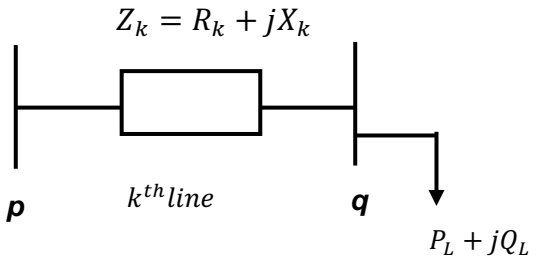

Figure 11 – Generic representation of the radial distribution network

$$P_{loss,p\Leftrightarrow q} = \frac{\left(P_L^2[q] + Q_L^2[q]\right) \times R_k}{\left(V[q]\right)^2} \tag{64}$$

From (64), the LSF for DG placement are calculated using (65), while (66) is used to determine those for CB allocation.

$$\frac{\partial P_{loss,p\Leftrightarrow q}}{\partial P_L} = \frac{2P_L[q] \times R_k}{\left(V[q]\right)^2} \tag{65}$$

$$\frac{\partial P_{loss,P_{p\Leftrightarrow q}}}{\partial Q_L} = \frac{2Q_L[q] \times R_k}{\left(V[q]\right)^2} \tag{66}$$

Based on the power flow results, LSFs are calculated and arranged in descending order. Nodes with high LSF have priority for DG or CB installation. According to (Prakash; Sydulu, 2007), the voltage amplitudes of the candidate nodes are normalized (*norm* V[i] = V[i] /0.95). For the i^{th} node, if the value norm V[i] is greater than 1.01, this node does not need the DG or CB allocation and therefore must be removed from the list. The remaining buses are affected by the installation of DG or CB.

3.5 STOCHASTIC FRACTAL SEARCH

Metaheuristics are designed to solve a wide range of optimization problems. They are specially used to solve complex optimization problems by exploring a large search space. Based on three main purposes: solving problems faster, solving large-scale problems, and obtaining a robust algorithm, metaheuristics can provide a variety of local solutions for the same decision variables, which makes them non-deterministic. During the optimization process, metaheuristics uses two important feathers: intensification (or exploitation), which consists of searching around the current best solutions and selecting the best solution; and diversification (or exploration), which investigates the efficiency of the algorithm in exploring the search space.

Stochastic fractal search is the improved version of fractal search algorithm that inspires random fractals grown by the diffusion limited aggregate (DLA) concept and can solve complex problems and provide a good solution compared to a global optimum solution in a reasonable computational time. The SFS is carried out using two statistical methods: the diffusion process (intensification), which is similar to the fractal search algorithm in which each particle imitates the branching property of a dielectric breakdown as search tool for solving global optimization problems, and the updating process (diversification), which explores the problem space efficiently using some stochastic rules (Salimi, 2015). The SFS uses a static diffusion process in which only the best particle generated at each generation is considered and the remaining particles are discarded.

3.5.1 DIFFUSION PROCESS

In this process, each particle diffuses around its current position to explore the search space, increasing the chance of finding global minima. Static diffusion is used in the SFS algorithm, allowing only the best particle generated from this process to form the new population in the next stage of the optimization process (Salimi, 2015). The generation of new particles is done using the Gaussian walk, as shown in (67) and (68).

$$X_{i,new1} = Gaussian\left(\mu_{X_{best}}, \sigma\right) + \left(\varepsilon \times X_{best} - \varepsilon' \times X_i\right) \tag{67}$$

$$X_{i,new2} = Gaussian\,(\mu_X, \sigma) \tag{68}$$

where,

$$\begin{cases} \mu_{X_{best}} = & X_{best}, \quad \mu_X = X_i \\ \sigma = & \left| \frac{log\,(iter)}{iter} \times (X_i - X_{best}) \right| \end{cases} \tag{69}$$

The ratio $\frac{log(iter)}{iter}$ is implemented to reduce the size of the Gaussian jumps over each iteration, ε and ε' are normal distributed random numbers between [0,1]. X_{best} and X_i are respectively the best point and the i^{th}point in the group. σ and $\mu_{X_{best}}$ represent the standard deviation and mean of the Gaussian distribution.

3.5.2 UPDATING PROCESS

This process is carried out using two statistical procedures to explore the search space accurately. The first statistical procedure is performed on each individual vector index, while the second is applied to all points. During the first statistical method, all points are ranked according to their fitness values, and then a probability value $P_{a,i}$ is calculated for each point as described in (70).

$$P_{a,i} = \frac{rank(X_i)}{N_p} \tag{70}$$

where, $rank(X_i)$ is the rank of point X_i in the group. Equation (70) states that the higher the probability, the better the point. It helps increase the chance of changing the position of points with a poor fitness function in the next generation. For each point X_i in the group, if $P_{a,i} < \varepsilon$, the *j-th* component of X_i is updated based on (71). Otherwise, there is no need to change the position of the point.

$$X_i^{'}\,(j) = X_r\,(j) - \varepsilon \times (X_t\,(j) - X_i\,(j)) \tag{71}$$

X_r and X_t are random selected points in the group and ε, a random number selected between [0,1].

For the second statistical procedure, all points obtained from the first statistical procedure are ranked according to (70). As in the first procedure, if $P'_{a,i} < \varepsilon'$, the position of X'_i is updated according to (72). Otherwise, X'_i maintains his components.

$$\begin{cases} X''_i = & X'_i - \varepsilon' \times (X'_t - X_{best}) \ \text{ if } \varepsilon \leqslant 0.5 \\ X''_i & X'_i - \varepsilon' \times (X'_t - X'_r) \quad \text{if } \varepsilon > 0.5 \end{cases} \tag{72}$$

The new point X''_i is replaced by that of X'_i if its fitness function is better than X'_i.

3.6 DFR PROBLEM USING THE SFS ALGORITHM

3.6.1 INITIALIZATION

Similarly, in many metaheuristics, the implementation of the SFS to solve the DFR starts by defining an initial population. In this study, X_i $(i = 1, \dots., N_p)$ represents a vector of N_p components classified in five parts represented by tie-switches (SW_i), candidate buses to DGs installation $(X_{DG,i})$, the sizes of DG units $(P_{DG,i})$, candidate buses to capacitor banks installation $(X_{CB,i})$, and the sizes of CB units $(Q_{CB,i})$. The structure of the solution vector is represented as follows.

$$X_i = \begin{bmatrix} SW_1, \dots, SW_{NT_{Tie}}, X_{DG,1}, \dots, X_{DG,N_{DG}}, P_{DG,1}, \dots, P_{DG,N_{DG}}, \dots \\ X_{CB,1}, \dots, X_{CB,N_{CB}}, Q_{CB,1}, \dots, Q_{CB,N_{CB}} \end{bmatrix} \tag{73}$$

Before starting the optimization process, each point is randomly initialized according to the parameters of the variables. For the DFR problem addressed in this study, the components of the tie-switches are initialized by first calculating the index of the tie-switches in each FL vector. This is done using (74). Then, the tie-switch corresponding to the position of the index in the *i-th* FL is chosen as the *j-th* initial component of the tie-switches vector (SW).

$$Tie_{index,i} = round\left[SW_{min,i} + rand \times \left(SW_{max,i} - SW_{min,i}\right)\right] \tag{74}$$

where, $SW_{min,i} = 1$ and $SW_{miax,i}$ is equal to the length of the ith FL vector, $i = 1, \dots, N_{FL}$.

The candidates' buses for the installation of DG and CB are initialized within the search space defined by the LSF method. Thus, the components of X_i representing DG and CB locations are defined based on (75) and (76) respectively.

$$X_{DG,i} = round\left[X_{DGmin,i} + rand \times \left(X_{DGmax,i} - X_{DGmin,i}\right)\right] \quad (75)$$

$$X_{CB,i} = round\left[X_{CBmin,i} + rand \times \left(X_{CBmax,i} - X_{CBmin,i}\right)\right] \quad (76)$$

where $X_{DGmin,i} = X_{CBmin,i} = 2$;

$X_{DGmax,i} = X_{CBmax,i} = N_b$ (Number of buses of the system), $i = 1, \dots, N_{DG} = N_{CB} = 3$.

The size of the DG units is initialized using (77).

$$P_{DG,i} = round\left[P_{DGmin,i} + rand \times \left(P_{DGmax,i} - P_{DGmin,i}\right)\right] \quad (77)$$

where,

$$\begin{cases} P_{DG,min,k} = \dfrac{1}{10}\sum P_{D_i} \\ P_{DG,max,k} = \dfrac{6}{10}\sum P_{D_i} \end{cases} \quad (78)$$

The initialization of capacitor banks' size is down by first determining the index of each capacitor bank in the component vector of CBs using (79), where $Index_{CB,i}$ represents the position of the discrete value of CB in the CBs vector, initially defined within the bounds of (80) with 100 kVAr steps. $Index_{min} = 1$, and $Index_{max}$ is the length of CBs vector. The size of each capacitor bank is then initialized by choosing the CB size corresponding to the index in the CBs vector. The minimum and maximum discrete values of the CBs vector are defined based on (79).

$$Index_{CB,i} = round\left[Index_{min} + rand \times \left(Index_{max} - Index_{min}\right)\right] \quad (79)$$

$$\begin{cases} Q_{CB,min,k} = & \frac{2}{100}\sum Q_{D_i} \\ Q_{CB,max,k} = & \frac{8}{100}\sum Q_{Di} \end{cases} \quad (80)$$

where Q_{D_i} is the reactive load value at bus i, $Q_{CB,min,k}$ and $Q_{CB,max,k}$, the minimum and maximum limits of capacitor banks.

Furthermore, after generating new points from the diffusion and updating process, if a tie-switch violates his bound, a repair action is performed using (81) and (82).

$$FL_{Tie} = \{FL_1, ..., FL_{NTie}\} \quad (81)$$

Equation (81) is the set of all the fundamental loops of the system.

$$Tie_{new} = round\,[min(FL_{Tie}) + rand \times (max(FL_{Tie}) - min(FL_{Tie})] \quad (82)$$

In the same way, if the DG or CB location bound is violated, a repair strategy is carried out using (75) or (76), respectively. Also, for the DG and CB sizes, if their bounds are violated, a repair action is set up using (77) and (79), respectively.

The main steps for solving the DFR problem are presented in the next section, where variable bounds are checked in the diffusion and updating process of the SFS algorithm to make sure that none of them has violated his limit.

3.6.2 THE MAIN STEP OF THE DFR PROBLEM USING SFS ALGORITHM

To solve the DFR problem, we started by implementing an algorithm that determines the fundamental loops of the network under analysis and then determining the loss sensitive factors. Next, we developed algorithms to initialize the combinatorial optimization variables. After this stage, we implemented the stochastic fractal search algorithm step by step to solve the distribution network reconfiguration problem. During this stage, we performed several simulations to test the consistency of the SFS algorithm. A mathematical model was proposed to address the infeasibility problem of combinatorial variables related to the tie-switches limits in the diffusion and update processes of the SFS algorithm. Then, distributed generations were added to the initial

SFS model to simultaneously solve the DFR problem with DG integration. A summary of the different steps to solve the DFR problem using the SFS algorithm is given below.

1) Set the optimization parameters such as number of population (N_p), the maximum diffusion number (MDN), the maximum number of iteration ($Iter_{max}$) and the Gaussian walk parameter.

2) Determine the fundamental loops (FLs) and set the lower and upper bounds of the variables.

3) Create random initial solutions using (74) - (80).

4) Check the radiality condition of network with the new switches' configuration.

5) Calculate the load flow and identify the best point (X_{best}), using (55).

6) Set the iteration to 1 ($iter = 1$).

7) Generate new points via the diffusion process using (67)-(68), and set the bounds violated using (75)-(77), (79) and (81)-(82).

8) Check the radiality conditions and constraints.

9) Calculate the load flow and identify the best point (X_{best}), (55).

10) Generate new points via the updating process using (70)-(72), and set the bounds violated using (75)-(77), (79) and (81)-(82).

11) Check the radiality conditions and constraints.

12) Evaluate the fitness function and identify the best point (X_{best}), (55).

13) Repeat step 7 to step 12 until reaching $iter_{max}$.

Figure 12 shows the flowchart of the stochastic fractal search, where in diffusion and updating process, equations (81)-(82) are applied to check and set the violation of tie-switches bounds.

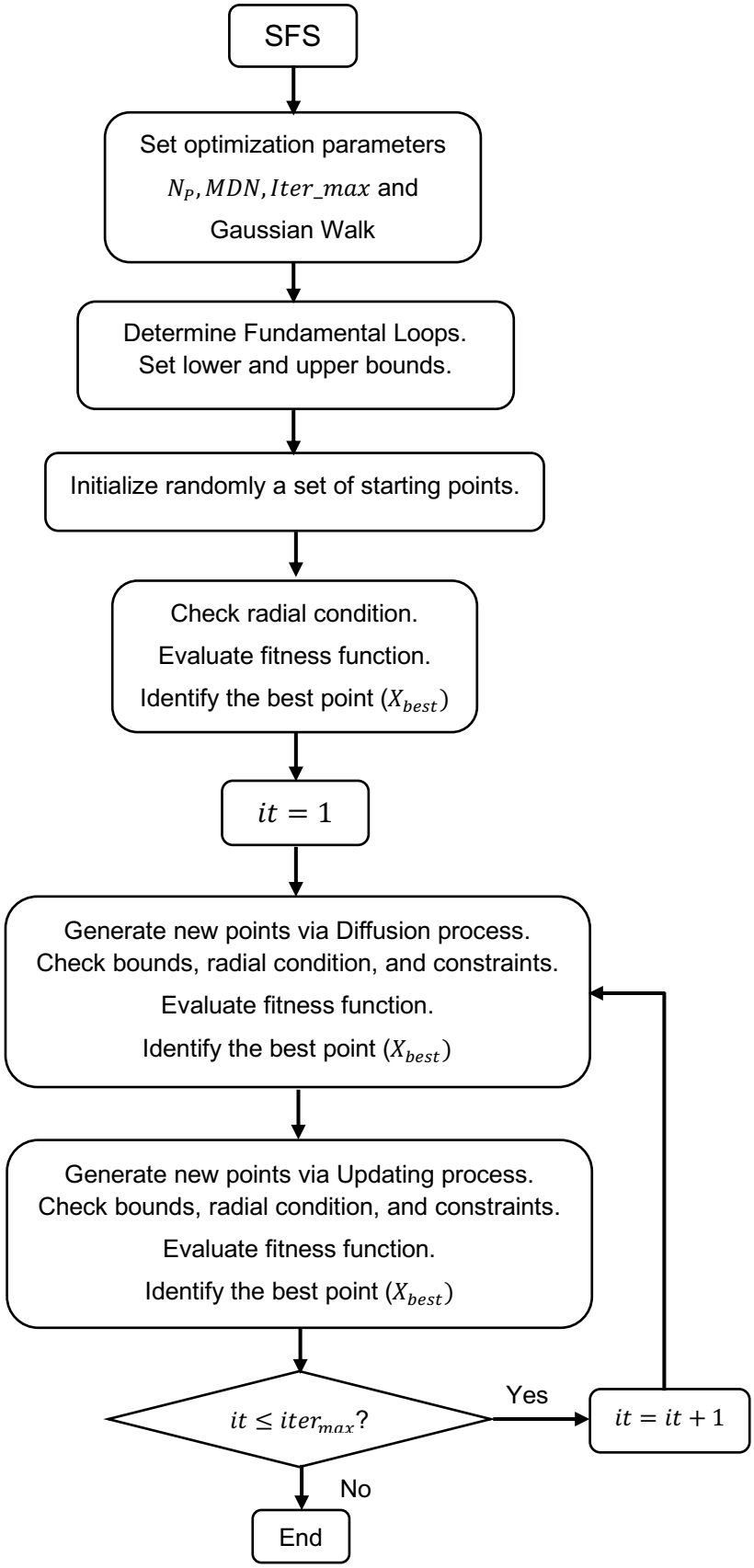

Figure 12 – Flowchart of the stochastic fractal search

Source: Author's elaboration

4 RESULTS AND DISCUSSIONS

This chapter presents the results of the computational experiments conducted in this work. In the first section, we will present simulation results carried out using the three-phase optimal power flow (TOPF) with PV plants integration to mitigate voltage unbalance in large-scale unbalanced distribution networks. The next section will present results of the application of stochastic fractal search (SFS) to solve the distribution network reconfiguration with distributed generation and capacitor bank integration. TOPF and SFS were coded in MATLAB R2022b and run on an Apple M1 Pro 8-core CPU silicon Apple M1 Pro.

4.1 RESULTS OF THE THREE-PHASE OPTIMAL POWER FLOW WITH PV PLANTS INTEGRATION TO MITIGATE VOLTAGE UNBALANCE IN THE GRID

This section presents analyses of the impact of photovoltaic generation on unbalanced distribution systems, considering its single-phase and three-phase modeling. The studies were performed on the IEEE 123 node test feeder (“IEEE PES Test Feeder”, 2025). It is an unbalanced network with active and reactive power loads distributed between the three phases as follows: 1440 kW, 785 kVAr on phase A; 915 kW, 525 kVAr on phase B and 1155 kW, 630 kVAr on phase C. It operates at a nominal voltage of 4.16 kV and includes voltage regulators, capacitors banks, and multiple switches. The total active power losses of the system are 95.61 kW. Figure 13 presents the network topology, where the substation is located at bus 150.

Three simulation cases were analyzed to show the impacts of PV plants on voltage unbalance and power losses.

1) Case 1: TOPF is performed without PV plants.

2) Case 2: TOPF was carried out with three (03) three-phase PV plants located at buses 13, 60, and 67, operating at maximum power generation, with adjustable power factor (PF~=1).

3) Case 3: TOPF was performed with thirty (30) single-phase PV plants distributed in ten (10) per phase along the grid as described in Table 4

and operating at maximum power generation, with adjustable power factor (PF~=1).

It is worth mentioning that the PV plants data used in this work are taken from previous work carried out in (Malinwo E. Ayikpa; Katia C. De Almeida; Guilherme C. Danielski, 2017).

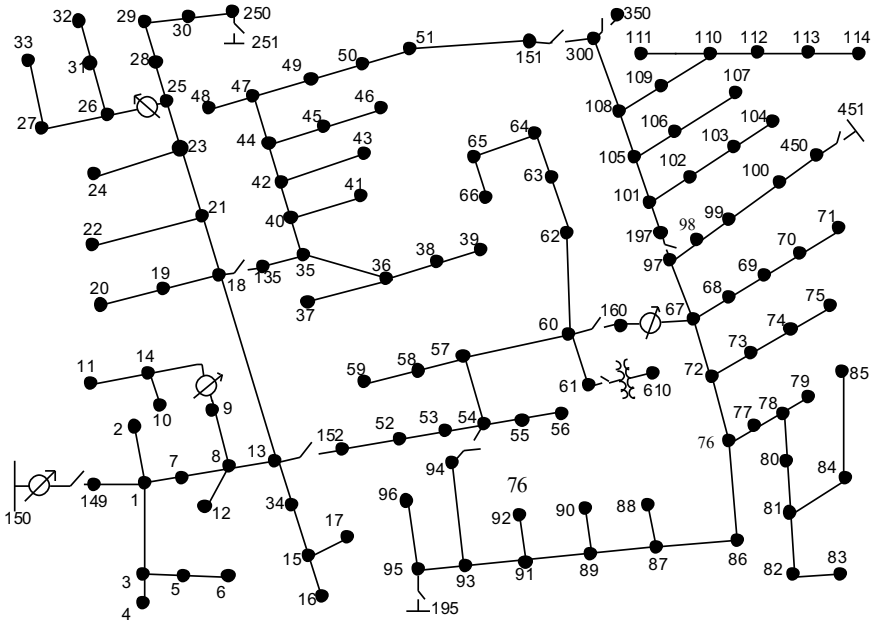

Figure 13 – IEEE 123 node test feeder (“IEEE PES Test Feeder”, 2025).

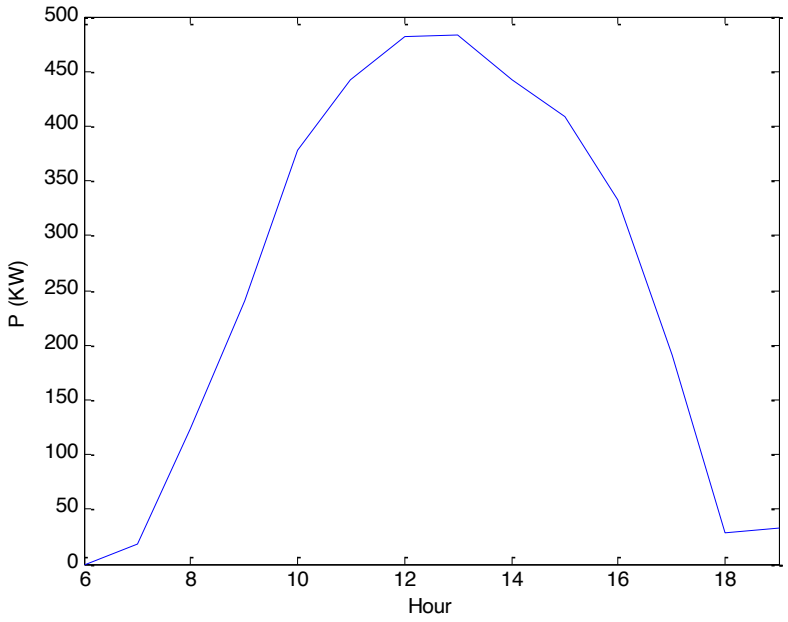

Figure 14 – 500 kW PV plant generation in a daytime period

Source: Author’s elaboration

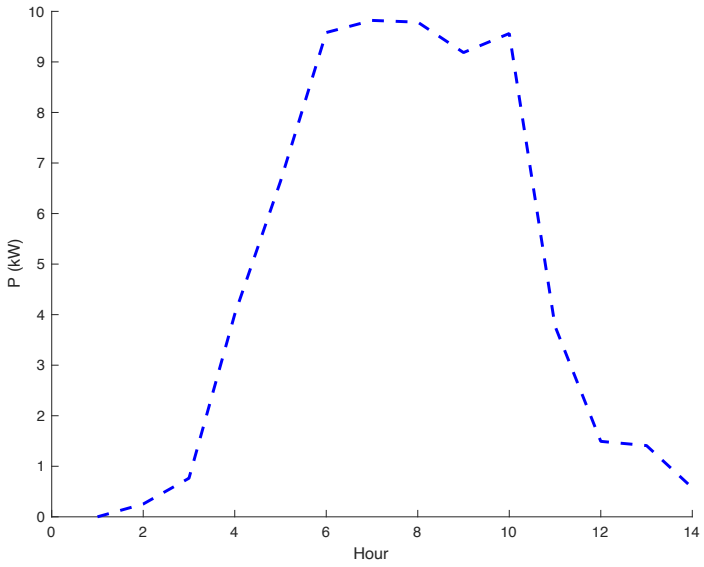

Figure 15 – 12 kW PV plant generation in a daytime period

Source: Author's elaboration.

Figures 14 and 15 show the PV generation output in a daytime period for both three-phase and single-phase PV, respectively. The single-phase PV has a capacity of 12 kW and the three-phase PV a capacity of 500 kW.

Table 1 – Results with and without PV plants

IEEE 123	Cases		
	TOPF without PV	TOPF with Three-phase PV plants	TOPF with only single-phase PV plants
OF_1	$\mathbf{7.90 \times 10^{-03}}$	$\mathbf{4.05 \times 10^{-03}}$	$\mathbf{3.41 \times 10^{-03}}$
VUF (%)	30.80	15.35	14.03
Losses (kW)	90.20	93.40	83.07

Figure 16 shows the grid voltage profile based on the IEEE power flow data in ("Resources – IEEE PES Test Feeder", 2025). From these data, the actual voltage unbalance of the network is calculated using (7), and Figure 17 presents the overview of the VUF on all buses. Most buses present high voltage unbalance. The maximum VUF value in percentage is 100%. This means that the voltages on these buses have the same values of positive and negative sequence components. The total VUF of the network calculated with the IEEE power flow data is 5862%.

Table 1 presents the optimal operating state of the network without PV plants. The objective function (7.90×10^{-03}) and the total voltage unbalance factor (30.80%)

present higher values in case 1 when compared to case 2 with the integration of three-phase PV plants which dropped to 4.05×10^{-03} and 15.35%, respectively. However, we observed a slight difference in losses in both cases. When only single-phase PV plants are introduced into the grid, the losses decrease to 83.07 kW and the total VUF of the system reaches 14.03%. The negative sequence component of the voltages is also minimized in this case with OF_1 equal to 3.41×10^{-03}.

Table 2 – Active power generation (kW)

IEEE 123	P (kW)		
	TOPF without PV	TOP with Three-phase PV plants	TOPF with only single-phase PV plants
Subst.	3600	2190	3300
PVs	-	1413	294.60

The active power generation of the substation decreases with higher penetration of PV plants to keep the losses close to the optimal value obtained in case 1, as shown in Table 2, case 2. Moreover, the substation increased its reactive power generation to better contribute to voltage unbalance control. As is known, when a PV plant operates at its maximum active power generation, the inverter's capacity to supply reactive power to the grid is reduced. The active power control capability of smart inverters can solve this problem by reducing the active power of PV plants, especially during the peak periods when PV plants are generating their maximum power.

Table 3 – Reactive Power Generation (kVAr)

IEEE 123	Q (kVAr)		
	TOPF without PV	TOP with Three-phase PV plants	TOPF with only single-phase PV plants
Subst.	1588	2334	1496
PVs	-	127.12	40.82

Table 3 showed that when single-phase PV plants are distributed along the grid, the active and reactive power generations at the substation decrease. The voltage unbalance and power losses are well mitigated in the network, as shown in Table 1, case 3.

Table 4 – Candidate buses for single-phase PV Plant Installation

IEEE 123	Phase A		Phase B		Phase C	
Buses	5	74	6	40	18	78
	17	80	15	51	29	99
	26	92	20	61	47	106
	34	105	27	98	60	115
	57	122	33	111	70	121

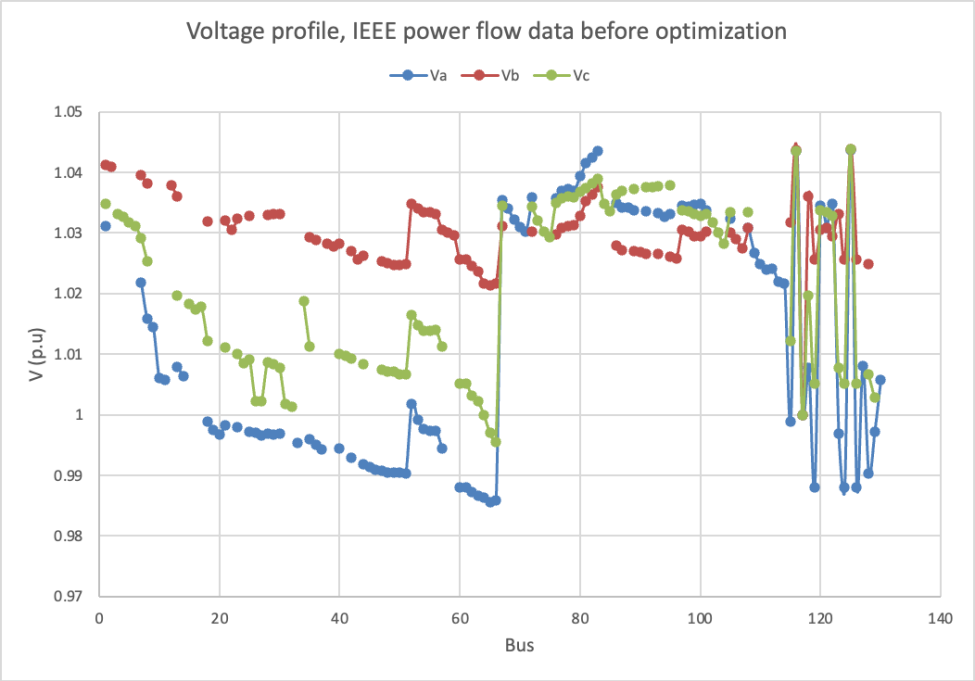

Figure 16 – Voltage profile of the network before optimization

Source: Author's elaboration.

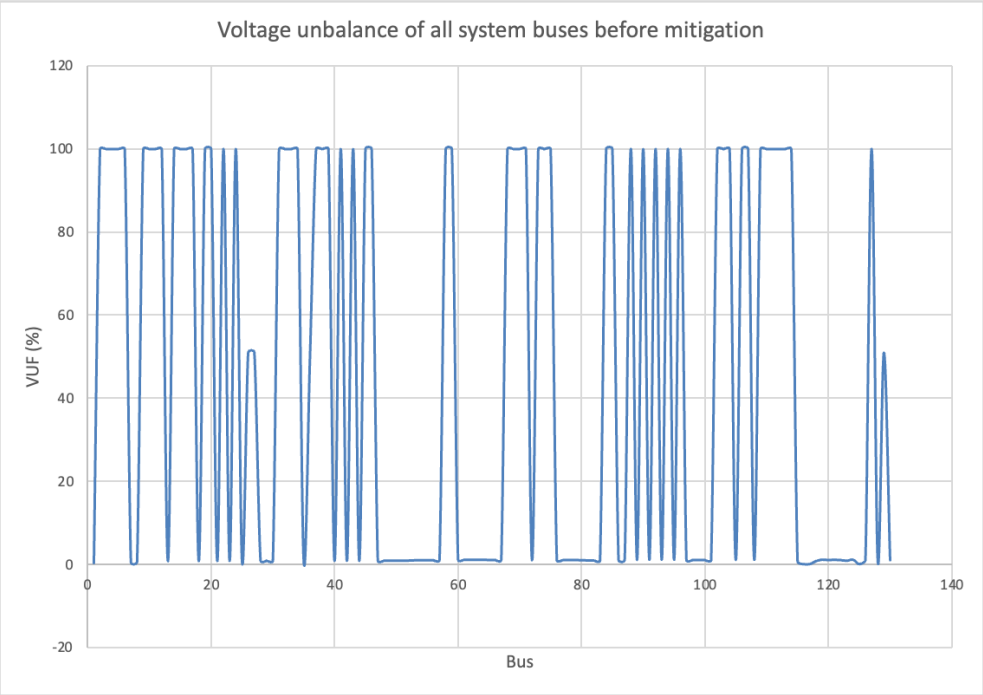

Figure 17 – Voltage unbalance at all network buses before optimization

Source: Author's elaboration.

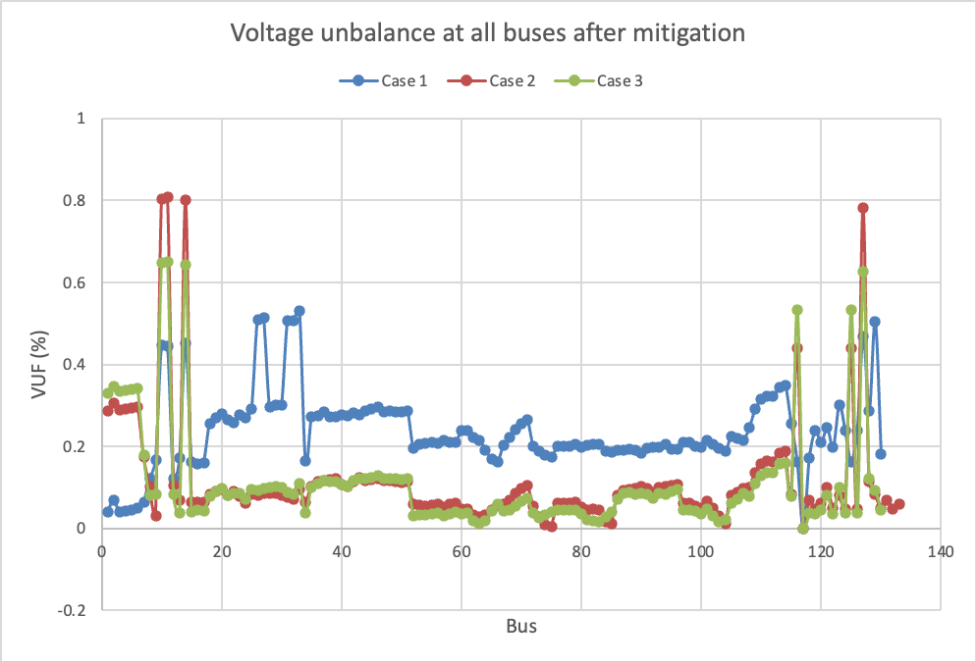

Figure 18 – Voltage unbalance profiles of the network

Source: Author's elaboration.

Figure 18 shows the voltage unbalance profiles across all system buses. We observed that the voltage unbalance is lower in almost all buses when we perform

TOPF with the integration of PVs plants. However, we noticed some VUF peaks around 0.8% at buses 10, 11, 14, and 127 when three-phase PV plants are connected to the grid, compared to the base case when TOPF is performed alone. An optimal positioning of three-phase PV plants in the network can help mitigate this problem. When single-phase PV plants are distributed along the three phases of the network, the UVF of the same buses drops to 0.6%. The simulation carried out in case 2 with three-phase PV plants was done without the network capacitor banks, to allow the inverters to better control reactive power in the grid.

Table 4 presents the phase configuration of candidate buses for single-phase PV plants installation. The single-phase PV plants are distributed along the network at a rate of 10 PV plants per phase. The allocation of single-phase PV plants was made based on the distribution of loads in the network.

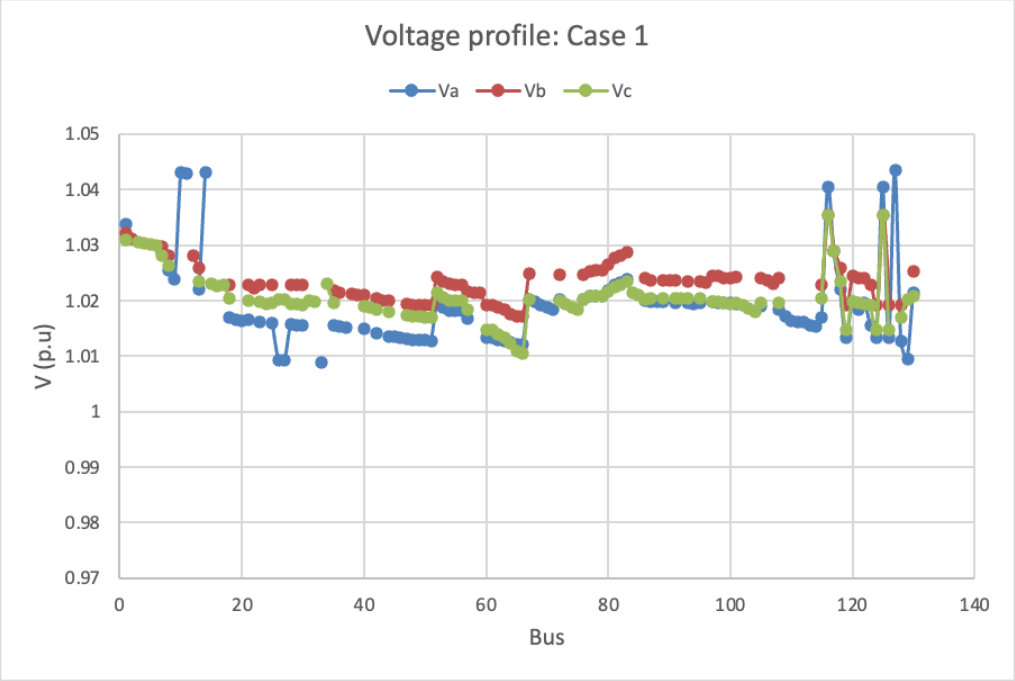

Figure 19 – Voltage profile in case 1: TOPF without PV plants.

Source: Author's elaboration.

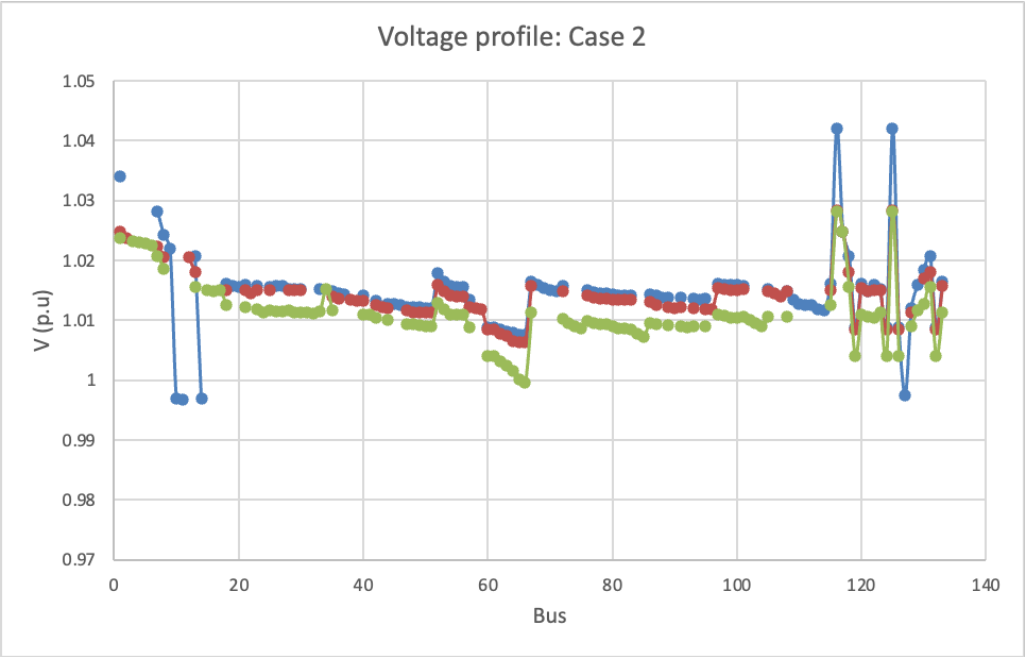

Figure 20 – Voltage profile in case 2 TOPF with three-phase PV plants.

Source: Author's elaboration.

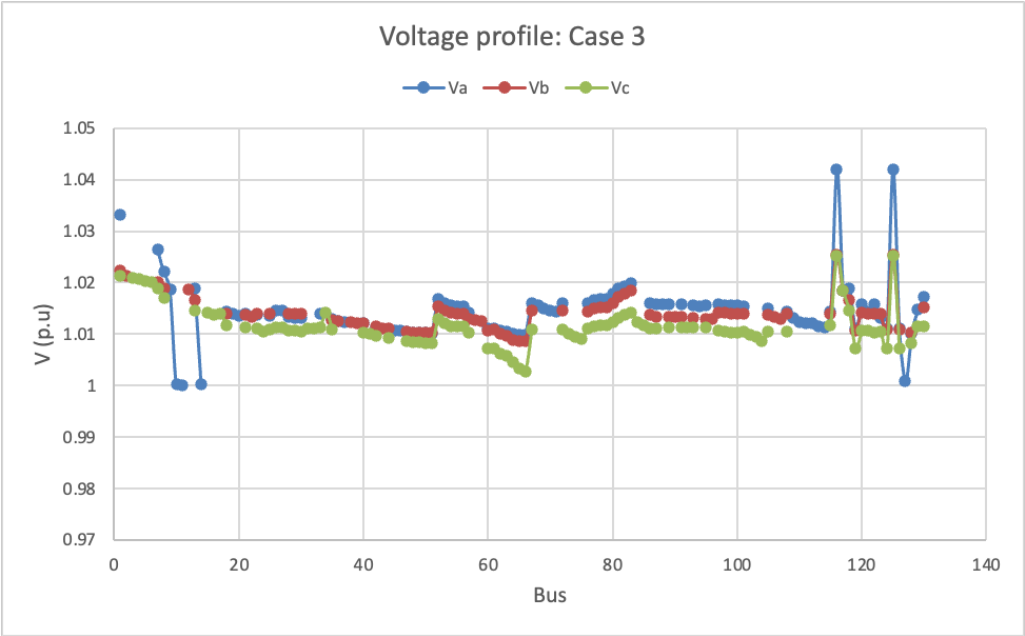

Figure 21 – Voltage profile TOPF with single-phase PV plants.

Source: Author's elaboration.

Figure 20 shows the grid voltage profiles when we perform the three-phase optimal power flow alone. It is important to highlight that phase A of the IEEE 123 feeder is more loaded than the others and, therefore, is subject to voltage unbalance

problems in the network. The base case without PV presents voltage unbalance in all three phases, but even worse in phase A. This problem was mitigated when PV plants injected both active and reactive power into the grid, making the voltage profiles closer to the nominal value, as shown respectively in Figures 20 and 21.

4.2 RESULTS OF THE OPTIMAL PLACEMENT AND SIZING OF DISTRIBUTED GENERATIONS AND CAPACITOR BANKS IN LARGE-SCALE DISTRIBUTION NETWORK USING FEEDER RECONFIGURATION

This section presents the results of distribution network reconfiguration with distributed generations and capacitor bank, using the stochastic fractal search. In the first sub-section we will present the DFR with optimal placement and sizing of DG and then the second sub-section will only focus on the simultaneous feeder reconfiguration with the optimal placement and sizing of DG and CB in large-scale systems. The backward-forward sweep power summation algorithm of MATPOWER 8.0b1 package was used to perform power flow analysis.

4.2.1 DISTRIBUTION FEEDER RECONFIGURATION WITH THE OPTIMAL PLACEMENT AND SIZING OF DISTRIBUTED GENERATION USING THE STOCHASTIC FRACTAL SEARCH

The distribution feeder reconfiguration was performed on the 33-bus, 69-bus, 119-bus system, and 136-bus systems from Matpower 8.0b1. Five simulation cases were analyzed.

1) Case 1: Original configuration of tie-switches without DFR and DG.
2) Case 2: The DFR is performed alone.
3) Case 3: Optimal placement and sizing of DG.
4) Case 4: The DFR is performed after optimal placement and sizing of the DGs using the results of Case 3.
5) Case 5: The DFR and optimal placement and sizing of the DGs are performed simultaneously.

Table 5 presents the optimization parameters of the SFS algorithm and the limits of the state variables to solve the DNR problem. Five features, such as open switches, total power loss, minimum voltage profile, percentage of loss reduction, and optimal location and size of the DG are considered for the evaluation of the network performance for all simulation cases performed in this section.

Table 5 – Simulations parameters

System	N_p	$Iter_{max}$	MDN	Gaussian walk	V_{min}	V_{max}
33-bus	30	500	5	0.75	0.9	1.0
69-bus	30	500	5	0.75	0.9	1.0
119-bus	100	1000	5	0.70	0.9	1.0
136-bus	100	3000	5	0.70	0.9	1.0

Source: Author's elaboration

4.2.1.1 Fundamental loop

Tables 6 – 9 present the fundamental loops of the 33-bus, 69-bus, 119-bus, and 136-bus systems analyzed in this work, where the components of each fundamental loop are potential candidates to generate a radial network topology.

Table 6 – Fundamental loops of the 33-bus system

FL	Switches	n Ties
1	2, 3, 4, 5, 6, 7, 18, 19, 20, 33	10
2	9, 10, 11, 12, 13, 14, 34	7
3	2, 3, 4, 5, 6, 7, 8, 9, 10, 11, 18, 19, 20, 21, 35	15
4	6, 7 8, 9, 10, 11, 12, 13, 14, 15, 16, 17, 25, 26, 27, 28, 29, 30, 31, 32, 36	21
5	3, 4, 5, 22, 23, 24, 25, 26, 27, 28, 37	11

Source: Author's elaboration

Table 7 – Fundamental loops of the 69-bus system

FL	Switches	n Ties
1	3, 4, 5, 6, 7, 8, 9, 10, 35, 36, 37, 38, 39, 40, 41, 42, 69	17
2	13, 14, 15, 16, 17, 18, 19, 20, 70	
3	3, 4, 5, 6, 7, 8, 9, 10, 11, 12, 13, 14, 35, 36, 37, 38, 39, 40, 41, 42, 43, 44, 45, 71	9 24
4	4, 5, 6, 7 8, 46, 47, 48, 49, 52, 53, 54, 55, 56, 57, 58, 72	17
5	9, 10, 11, 12, 13, 14, 15, 16, 17, 18, 19, 20, 21, 22, 23, 24, 25, 26, 52, 53, 54, 55, 56, 57, 58, 59, 60, 61, 62, 63, 64, 73	32

Source: Author's elaboration

Table 8 – Fundamental loops of the 119-bus system

FL	Switches	n Ties
1	3, 9, 10, 17, 18, 19, 20, 21, 22, 23, 24, 25, 26, 27, 28, 37, 38, 39, 40, 41, 42, 43, 44, 45, 118	25
2	11, 12, 13, 14, 15, 16, 17, 18, 19, 20, 21, 22, 23, 24, 25, 26, 119	17
3	3, 4, 5, 6, 7, 9, 10, 17, 18, 19, 20, 21, 22, 23, 120	
4	29, 30, 31, 32, 33, 34, 37, 38, 39, 40, 41, 42, 46, 47, 48, 49, 50, 51, 52, 53, 121	15 21
5	29, 30, 31, 32, 33, 34, 46, 47, 48, 54, 55, 56, 57, 58, 59, 60, 61, 122	18
6	29, 35, 36, 54, 55, 56, 57, 58, 59, 60, 61, 123	12
7	4, 5, 6, 7, 8, 27, 28, 37, 38, 39, 124	11
8	1, 3, 27, 28, 54, 55, 56, 57, 62, 63, 64, 88, 89, 90, 95, 125	16
9	65, 66, 67, 68, 69, 70, 71, 72, 88, 89, 90, 126	12
10	64, 65, 66, 67, 68, 69, 70, 71, 72, 73, 74, 77, 78, 85, 86, 87, 127	17
11	65, 66, 67, 68, 69, 70, 71, 72, 73, 74, 75, 76, 88, 89, 90, 95, 96, 97, 98, 128	20
12	62, 63, 77, 78, 79, 80, 81, 82, 99, 100, 101, 102, 103, 104, 105, 106, 107, 129	18
13	62, 63, 77, 78, 85, 99, 100, 101, 102, 103, 104, 130	12

14	100, 101, 102, 103, 104, 105, 106, 107, 108, 109, 113, 114, 115, 116, 117, 131	16
15	3, 9, 10, 17, 18, 19, 20, 21, 22, 23, 24, 27, 28, 29, 30, 31, 32, 33, 34, 132	20

Source: Author's elaboration

Table 9 – Fundamental loops of the 136-bus system

FL	Switches	n Ties
1	1, 2, 3, 4, 5, 6, 7, 63, 64, 65, 66, 67, 68, 70, 73, 136	16
2	1, 2, 3, 4, 5, 6, 8, 9, 17, 18, 19, 20, 22, 24, 137	15
3	1, 2, 3, 4, 5, 6, 8, 10, 13, 15, 75, 76, 77, 78, 79, 80, 81, 83, 138	19
4	17, 18, 19, 20, 22, 24, 25, 26, 27, 28, 31, 35, 38, 121, 122, 123, 125, 127, 129, 130, 131, 132, 133, 134, 135, 139	26
5	17, 18, 19, 20, 22, 24, 25, 39, 40, 42, 43, 45, 46, 47, 48, 51, 140	17
6	39, 40, 42, 43, 45, 46, 47, 48, 49, 50, 85, 86, 88, 89, 90, 91, 92, 93, 94, 95, 96, 141	22
7	39, 40, 42, 43, 45, 46, 47, 48, 51, 52, 53, 54, 55, 85, 86, 88, 89, 90, 91, 92, 93, 97, 98, 142	24
8	39, 40, 42, 43, 45, 46, 47, 62, 99, 100, 101, 103, 104, 118, 119, 120, 143	17
9	63, 64, 65, 66, 75, 76, 77, 78, 79, 144	10
10	75, 76, 77, 78, 79, 121, 122, 123, 125, 127, 129, 130, 131, 145	14
11	75, 76, 77, 78, 79, 80, 81, 83, 84, 121, 122, 123, 125, 127, 129, 130, 131, 132, 133, 134, 135, 146	22
12	85, 86, 88, 89, 90, 91, 99, 100, 101, 103, 104, 147	12
13	85, 86, 88, 89, 90, 121, 122, 123, 125, 127, 129, 148	12
14	85, 86, 88, 89, 90, 99, 100, 101, 103, 149	10
15	85, 86, 88, 89, 90, 91, 92, 99, 100, 101, 103, 104, 150	13
16	85, 86, 88, 89, 90, 91, 92, 121, 122, 123, 125, 127, 129, 130, 131, 132, 151	17
17	85, 86, 88, 89, 90, 91, 92, 93, 94, 95, 96, 99, 100, 101, 103, 104, 118, 119, 120, 152	20
18	39, 40, 42, 43, 45, 46, 47, 99, 100, 101, 103, 104, 105, 106, 107, 110, 153	17
19	75, 76, 121, 122, 123, 125, 126, 154	8
20	75, 76, 77, 121, 122, 123, 125, 127, 128, 155	10
21	85, 86, 88, 89, 90, 91, 92, 93, 97, 98, 121, 122, 123, 125, 127, 129, 130, 131, 132, 133, 134, 135, 156	23

Source: Author's elaboration

4.2.1.2 Results for the 33-bus system with DG allocation

The 33-bus system has 37 branches, 32 sectionalizing switches, and 5 tie-switches. The initial configuration of the tie-switches is 33-34-35-36-37, as shown in Figure 22. The total active and reactive load of this system is respectively 3.72 MW and 2.3 MVAr. The base case of this system presents an active power loss of 202.68 kW and 0.913.p.u as the worst voltage profile (Baran; Wu, 1989b). The results obtained by the SFS were compared with other metaheuristics such as ACSA (Nguyen; Truong; Phung, 2016), HSA (Rao et al., 2013) and WOA (Mahdavi et al., 2023a). For both 33-bus and 69-bus systems, in case 3 the optimal DG placement was carried out using the buses index from LSF in priority order, and the optimal DG sizing was performed using the SFS, considering the base case tie-switches configuration.

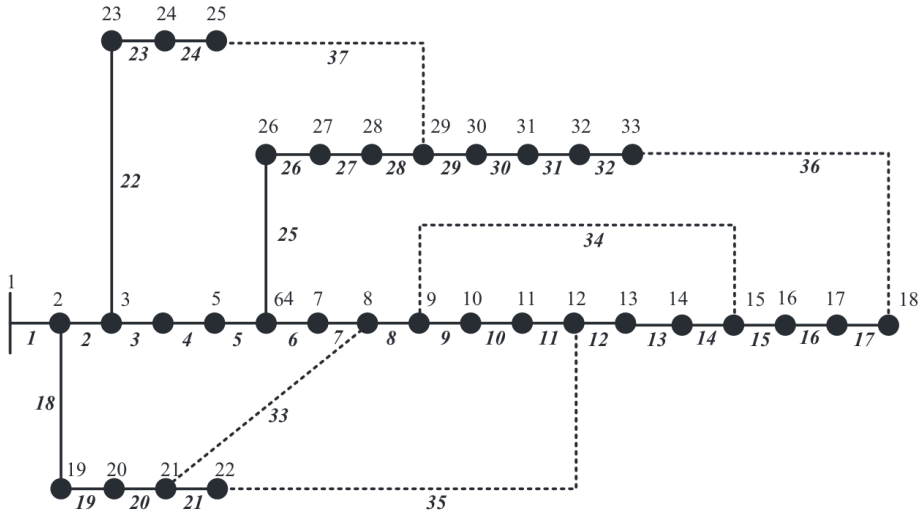

Figure 22 – 33-bus system (Nguyen; Truong; Phung, 2016).

Table 10 – Comparison of simulation results for Case 2: 33-bus system

Case	Item	ACSA	HSA	WOA	SFS
2	Opened Switches	7-14-9-32-28	7-14-9-32-37	7-9-14-32-37	7-9-14-32-37
	P_{loss} (kW)	139.98	138.06	139.55	139.55
	V_{min} (p.u.)	0.9413	0.9342	0.9378	0.938
	Loss reduction (%)	30.93	31.88	31.15	31.15

Source: Author's elaboration

Table 10 presents results of simulation performed in case 2. The best configuration of tie-switches is 7-9-14-32-37, and the power loss is 139.55 kW. This configuration was found in HAS and WOA. The minimum voltage profile of the network has been improved from 0.913.p.u to 0.938.p.u. In Case 2, HAS, WOA and SFS present the same configuration of tie-switches, but the power loss found with the HAS is different from others. This can be justified by the tolerance in the power flow calculation.

Table 11 – Comparison of simulation results for Case 3, 33-bus system

Case	Item	ACSA	HSA	WOA	SFS
3	Opened Switches	33-34-35-36-37	33-34-35-36-37	-	33-34-35-36-37
	P_{loss} (kW)	74.26	96.76	-	30.36
	V_{min} (p.u.)	0.9778	0.9670	-	0.9735
	Loss reduction (%)	63.26	52.26	-	85.02
	P_{DG} (MW)/(Node)	0.7798 (14)	0.1070 (18)	-	0.4172 (31)
		1.1251 (24)	0.5724 (17)	-	1.3584 (8)
		1.3496 (30)	1.0462 (33)	-	0.4834 (30)
	Total DG size (MW)	3.2545	1.7256	-	2.26

Source: Author's elaboration

When adding 3 DGs to the grid, the SFS performed with a minimum loss equal to 30.36 kW against 74.26 kW in ACSA and 96.76 kW in HAS, as shown in Table 11. However, the total active power generated by ACSA is 3.25 MW, which is higher than that obtained by the SFS, 2.26 MW. It can be inferred that the SFS controls better the power generation from DG, while reducing the total active power losses of the network. This is a good behavior that we can expect from the grid when addressing an optimal DG placement and sizing problem in the distribution network.

Table 12 – Comparison of simulation results for Case 4, 33-bus system

Case	Item	ACSA	HSA	WOA	SFS
4	Opened Switches	33-9-8-36-27	-	-	37-11-4-28-13
	P_{loss} (kW)	62.98	-	-	23.08

	V_{min} (p.u.)	0.9826	-	-	0.9810
	Loss reduction (%)	68.93	-	-	88.61
	P_{DG} (MW)/(Node)	0.7798 (14)	-	-	0.4172 (31)
		1.1251 (24)	-	-	1.3584 (8)
		1.3496 (30)	-	-	0.4834 (30)
	Total DG size (MW)	3.2545	-	-	2.26

Source: Author's elaboration

Results presented in Table 12 show a reduction in power losses and an improvement of the minimum voltage profile when performing the DFR after optimal placement and sizing of DGs. Power losses dropped to 23.08 kW and the minimum voltage was increased to 0.981.p.u. These results are better than those found with ACSA.

Table 13 – Comparison of simulation results for Case 5, 33-bus system

Case	Item	ACSA	HSA	WOA	SFS
5	Opened Switches	33-34-11-31-28	7-14-10-32-28	7-8-9-27-36	20-13-35-26-23
	P_{loss} (kW)	53.21	73.05	31.17	8.81
	V_{min} (p.u.)	0.9806	0.9700	0.9804	0.9931
	Loss reduction (%)	73.75	63.95	84.62	95.65
	P_{DG} (MW)/(Node)	0.8968 (18)	0.5258 (32)	0.614 (13)	0.7943 (32)
		1.4381 (25)	0.5586 (31)	0.610 (29)	1.1234 (8)
		0.9646 (7)	0.5840 (33)	0.613 (32)	1.1854 (25)
	Total DG size (MW)	3.2995	1.6684	1.837	3.1031

Source: Author's elaboration

In Case 5, Table 13, the same behavior is observed with ACSA for the simultaneous DFR and optimal DG placement and sizing; but compared to WOA, the SFS performs better than results obtained from WOA in terms of minimum losses and minimum voltage profile (8.8074 kW & 0.9932.p.u from SFS) and (31.17 kW & 0.9804.p.u. from WOA).

Figure 23 presents the convergence characteristics of the SFS, of the 33-bus system. We noticed that Case 2 and Case 4 reached their convergence around the 100th iteration. In Case 3 the convergence rate is faster and occurred around the 10th iteration. Case 5 reached its convergence around the 200th iteration. This can be explained by the fact that SFS performs a deep search to find the global minimum. Figure 24 shows the voltage profile for the 33-bus system. We observe that in cases 5, the voltage profiles are better than in other cases, mainly when compared to Case 1 (base case without any improvement).

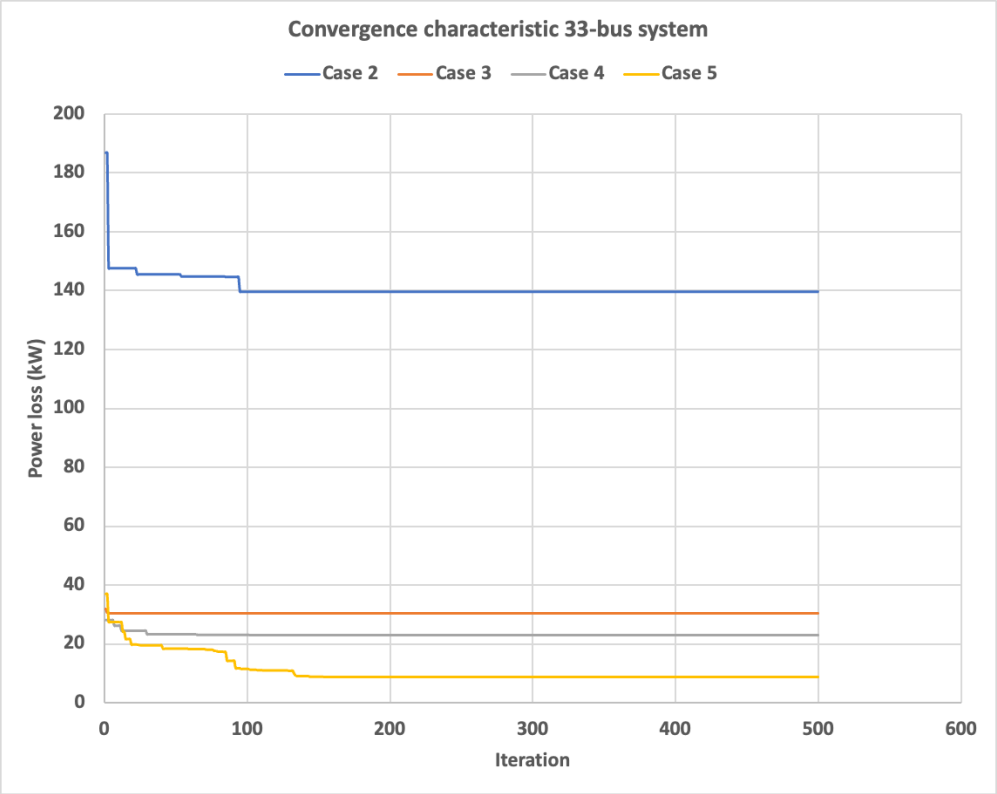

Figure 23 – Convergence rate of the 33-bus system

Source: Author's elaboration.

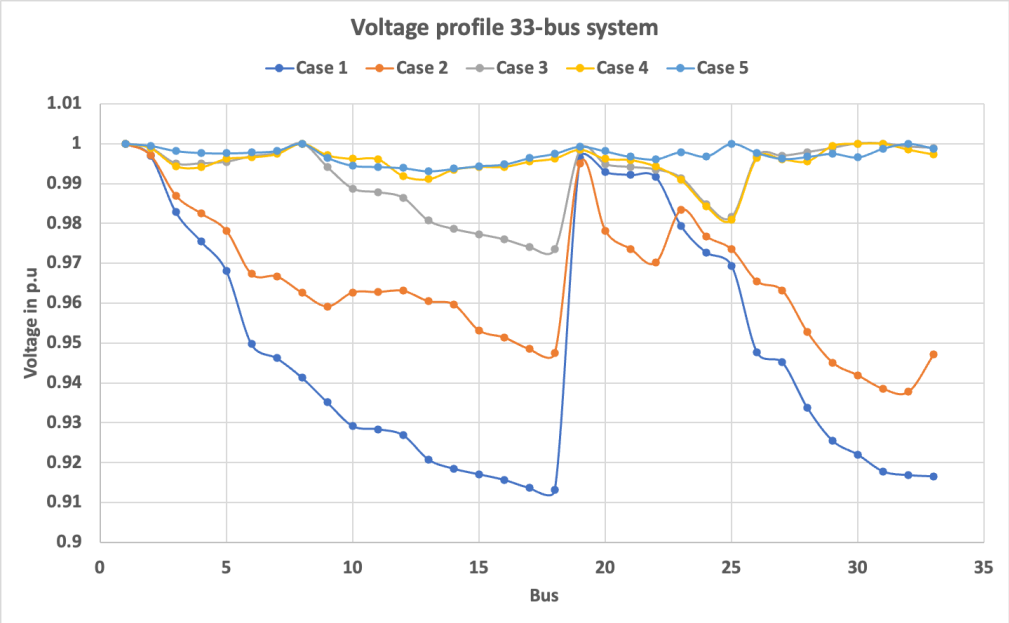

Figure 24 – Voltage profile of the 33-bus system

Source: Author's elaboration.

4.2.1.3 Results for the 69-bus system with DG allocation

The base case of the 69-bus system gives a power loss estimated at 225 kW with a minimum voltage profile equal to 0.9092.p.u (Baran; Wu, 1989a). This system is a medium voltage feeder that presents 68 sectionalizing switches and 5 tie-switches as shown in Figure 25. Its active and reactive loads are 3.802 MW and 2.696 MVAr, respectively.

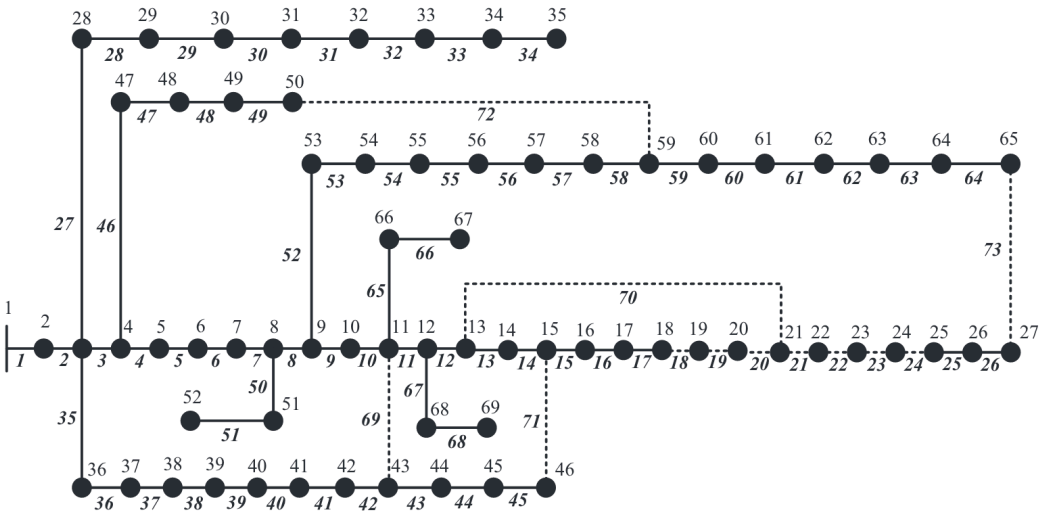

Figure 25 – 69-bus system

Source:(Nguyen; Truong; Phung, 2016)

Table 14 – Comparison of simulation results for Case 2, 69-bus system

Case	Item	ACSA	HSA	WOA	SFS
2	Opened Switches	69-70-14-57-61	69-18-13-56-61	12-57-61-69-70	14-57-70-61-69
	P_{loss} (kW)	98.59	99.35	99.80	99.62
	V_{min} (p.u.)	0.9495	0.9428	0.9427	0.9428
	Loss reduction (%)	56.16	55.85	55.64	55.72

Source: Author's elaboration

The DFR was performed alone in Case 2, Table 14, and the SFS found the optimal tie-switches configuration 14-57-61-69-70, the same in ACSA. Power loss decreased from 225 kW to 99.62 kW, and the minimum voltage profile was improved to 0.9428.p.u.

Table 15 – Comparison of simulation results for Case 3, 69-bus system

Case	Item	ACSA	HSA	WOA	SFS
3	Opened Switches	69-70-71-72-73	69-70-71-72-73	-	69-70-71-72-73
	P_{loss} (kW)	72.44	86.77	-	31.84
	V_{min} (p.u.)	0.9890	0.9677	-	0.9726
	Loss reduction (%)	67.79	61.43	-	85.85
	P_{DG} (MW)/(Node)	0.6022 (11)	0.1018 (65)	-	1.0835 (61)
		0.3804 (18)	0.3690 (64)	-	0.3802 (64)
		2.0000 (61)	1.3024 (63)	-	0.3802 (65)
	Total DG size (MW)	2.9826	1.7732	-	1.8439

Source: Author's elaboration

In Case 3, the optimal placement and sizing of DG, performed by the SFS resulted in active power losses of 31.84 kW and a minimum voltage profile of 0.9726.p.u.

Table 16 – Comparison of simulation results for Case 4, 69-bus system

Case	Item	ACSA	HSA	WOA	SFS
4	Opened Switches	69-70-12-58-61	-	-	10-17-12-55-60
	P_{loss} (kW)	41.13	-	-	11.86

	V_{min} (p.u.)	0.9828	-	-	0.9891
	Loss reduction (%)	81.71	-	-	94.73
	P_{DG} (MW)/(Node)	0.6022 (11)	-	-	1.0835 (61)
		0.3804 (18)	-	-	0.3802 (64)
		2.0000 (61)	-	-	0.3802 (65)
	Total DG size (MW)	2.9826	-	-	1.8439

Source: Author's elaboration

In Case 4, Table 16, when DFR is carried out after optimal DG placement and sizing, the SFS presents 11.86 kW, 0.9891.p.u & 1.8439 MW, respectively, as minimum losses, worst voltage profile, and total active power generation from DGs; while ACSA presents, respectively, 41.13 kW, 0.9828.p.u & 2.9826 MW. We concluded that SFS outperforms ACSA in this case. These results were highlighted in Case 5, Table 17, when performing the simultaneous DFR and optimal placement and sizing of DG. The SFS presents a power loss and a minimum voltage profile equal to 4.16 kW & 0.9950.p.u, better than those obtained with other metaheuristics analyzed in this case.

Table 17 – Comparison of simulation results for Case 5, 69-bus system

Case	Item	ACSA	HSA	WOA	SFS
5	Opened Switches	69-70-14-58-61	69-17-13-58-61	10-12-20-21-58	44-13-10-54-24
	P_{loss} (kW)	37.02	40.30	19.49	4.16
	V_{min} (p.u.)	0.9869	0.9736	0.9820	0.9950
	Loss reduction (%)	83.54	82.08	91.34	98.15
	P_{DG} (MW)/(Node)	0.5413 (11)	1.0666 (61)	0.6337 (62)	0.8041 (32)
		1.7240 (61)	0.3525 (60)	0.496 (63)	1.7022 (49)
		0.5336 (65)	0.4227 (62)	0.607 (64)	0.5855 (22)
	Total DG size (MW)	2.8189	1.8718	1.7367	3.0918

Source: Author's elaboration

The convergence characteristic for the 69-bus system is shown in Figure 26. Case 2 reached a first convergence rate around the 60th iteration and later improved the objective function around the 430th iteration. This demonstrates SFS's ability to

reach a global minimum as the number of iterations increases. In Cases 3 and 4, the convergence rate was reached in the 10th and 40th iterations, respectively. However, the best solution was achieved in Case 5, around the 200th iteration. Figure 27 shows the voltage profiles of the system in all cases. In Case 5, the voltage profiles are better than in the other cases, especially when compared to the base case.

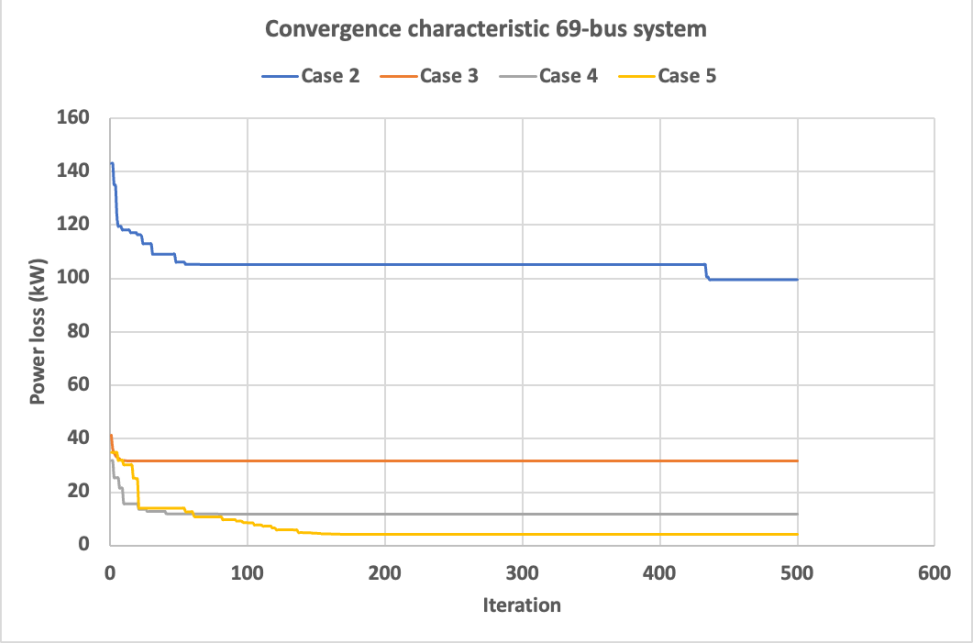

Figure 26 – Convergence characteristic of the 69-bus system

Source: Author's elaboration.

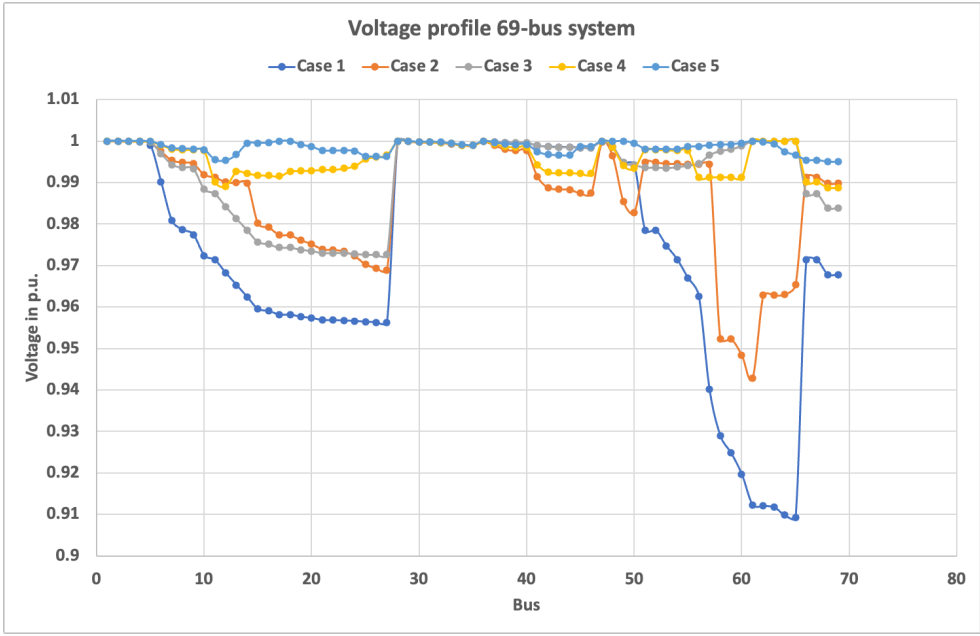

Figure 27 – Voltage profile of the 69-bus system

Source: Author's elaboration.

4.2.1.4 Results for the 119-bus system with DG allocation

The 119-bus system is a large-scale 11 kV distribution network with 118 sectionalizing switches and 15 tie-switches. Total active and reactive power loads are 22709.7 kW and 17041.1 kVAr, respectively (Nguyen; Truong; Phung, 2016). The tie-switches of this feeder test are shown in Figure 28 and represented by the interconnections 118-119-120-121-122-123-124-125-126-127-128-129-130-131-132. The system presents for this initial configuration 1298.1 kW as power losses and 0.8688 p.u. as a minimum voltage profile.

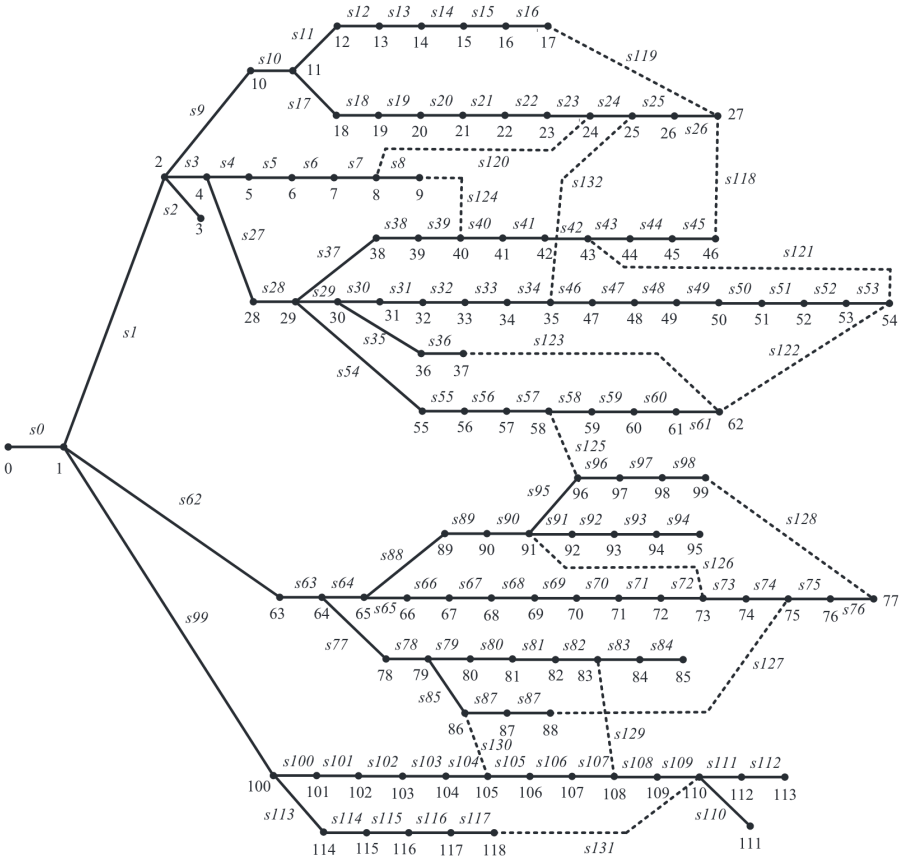

Figure 28 – Topology of the 119-bus system
Source:(Nguyen; Truong; Phung, 2016).

Table 18 – Simulation results for Case 2: 119-bus system

Case	Item	SFS
2	Opened Switches	42-26-23-51-122-58-39-95-71-74-97-129-130-109-34
	P_{loss} (kW)	869.73

	V_{min} (p.u.)	0.9323
	Loss reduction (%)	33

Source: Author's elaboration

In Case 2, Table 18, the total power losses from the network are 869,73 kW with a minimum voltage equal to 0.9323.p.u. These results were improved in Case 3, Table 19, with the optimal placement and sizing of DGs, where power losses dropped to 344.73 kW and the worst voltage of the system increased to 0.9606.p.u.

Table 19 – Simulation results for Case 3: 119-bus system

Case	Item	SFS
3	Opened Switches	118-119-120-121-122-123-124-125-126-127-128-129-130-131-132
	P_{loss} (kW)	344.73
	V_{min} (p.u.)	0.9606
	Loss reduction (%)	73.44
	P_{DG} (MW)/(Node)	2.9050 (50)
		2.9986 (71)
		2.8736 (110)

Source: Author's elaboration

Table 20 – Simulation results for Case 4: 119-bus system

Case	Item	SFS
4	Opened Switches	42-26-21-121-46-123-39-57-68-87-76-81-130-107-34
	P_{loss} (kW)	278.67
	V_{min} (p.u.)	0.9728
	Loss reduction (%)	78.53
	P_{DG} (MW)/(Node)	2.9050 (50)
		2.9986 (71)
		2.8736 (110)

Source: Author's elaboration

In case 4, Table 20, when the DFR is performed after DGs allocation, the power losses and minimum voltage (278.67 kW, 0.9728.p.u). This results in power losses reductions equivalent to 78%, when compared to the base case.

Table 21 – Simulation results for Case 5: 119-bus system

Case	Item	SFS
5	Opened Switches	45-24-21-57-42-119-36-85-69-76-127-104-90-116-8
	P_{loss} (kW)	224.92
	V_{min} (p.u.)	0.9819
	Loss reduction (%)	82.67
	P_{DG} (MW)/(Node)	4.3357 (49)
		4.3746 (109)
		3.6945 (73)

Source: Author's elaboration

The simultaneous DFR and DG placement and sizing has been performed in Case 5, Table 21, which presents better results than those previously analyzed. In fact, the total power losses and the minimum voltage profile carried out in this case are respectively 224.92 kW and 0.9819.p.u, which leads to a power reduction rate equal to 82.67%. Furthermore, the total active power generation in this case is 12.40 MW versus 8.78 MW in Case 3. This confirms the SFS's ability to efficiently perform the DFR simultaneously with the optimal allocation and sizing of DGs.

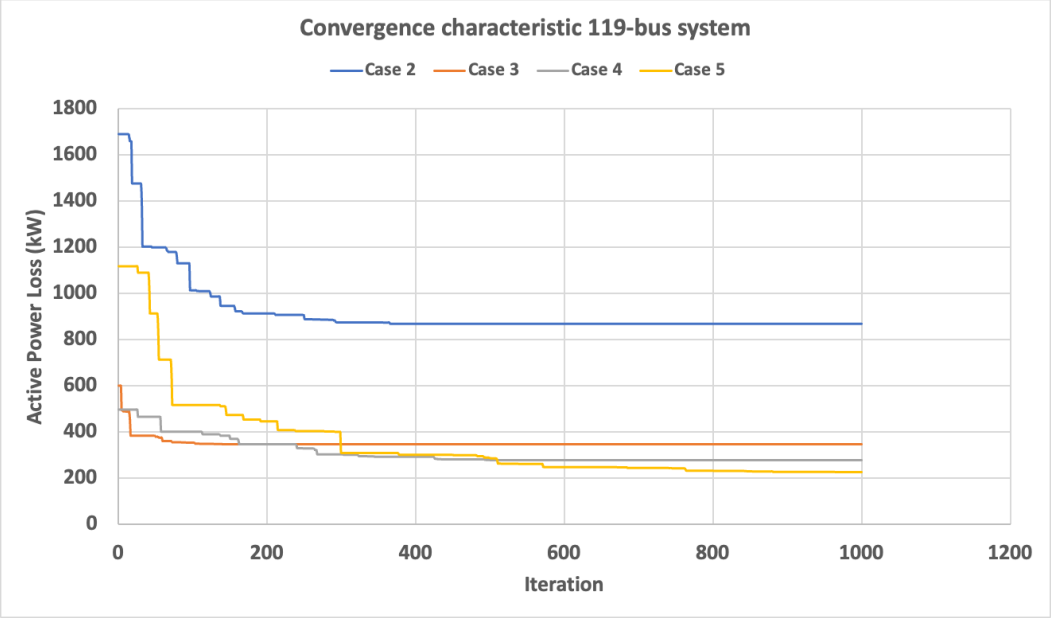

Figure 29 – Convergence characteristic of the 119-bus system

Source: Author's elaboration.

Figure 29 presents the convergence characteristic of the 119-bus system. In Case 2 the convergence was reached around the 400th iteration, while in Case 3 this occurred around the 200th iteration. Case 4 and Case 5 reached their convergence, respectively, around the 500th and the 900th iteration. These results demonstrate the ability of SFS to perform a deep search and find a better solution that satisfies all constraints. The voltage profiles are presented in Figure 30 for the same feeder test, where the integration of DGs has significantly improved the overall voltage profile of the network, mainly in Case 5 when the DFR is performed simultaneously with DGs allocation.

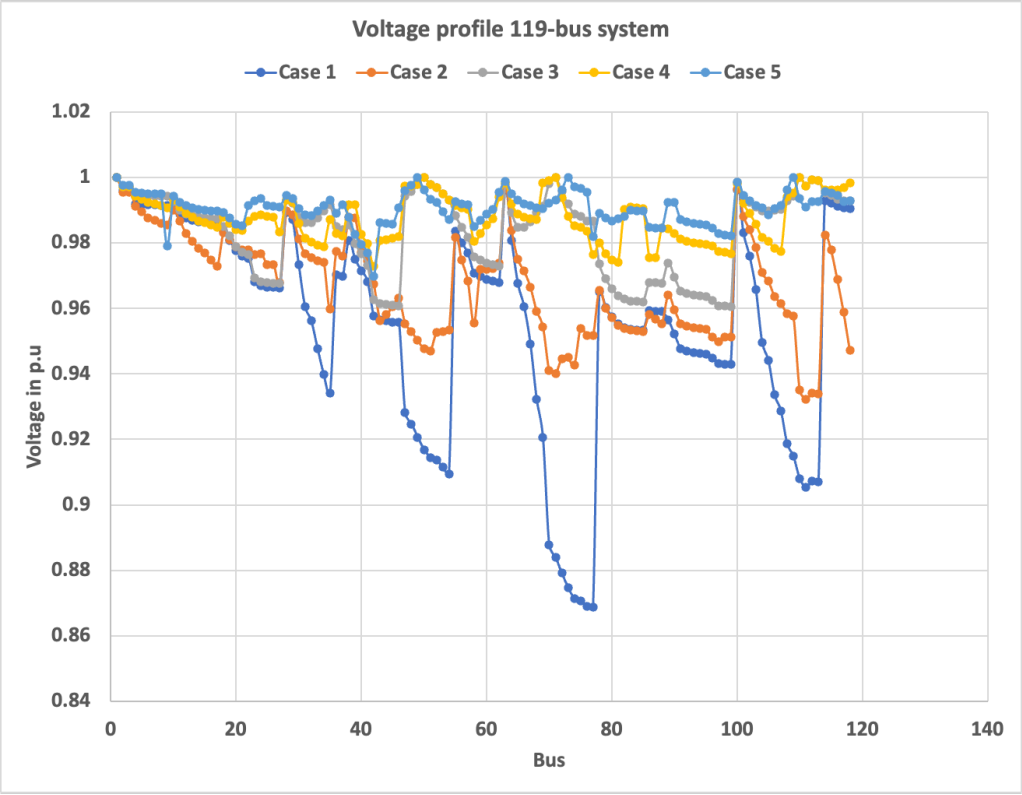

Figure 30 – Voltage profile of the 119-bus system

Source: Author's elaboration

4.2.1.5 Results for the 136-bus system with DG allocation

The 136-bus system is a large-scale 13.8 kV distribution network with 156 feeders. It presents respectively 18313.81 kW and 7932.534 kVAr as total active and reactive power loads. The total active power losses are 320 kW, and the minimum voltage profile is 0.9307.p.u. Figure 31 shows the topology of the system, where the

tie-switches are represented by the interconnection 136-137-138-139-140-141-142-143-144-145-146-147-148-149-150-151-152-153-154-155-156.

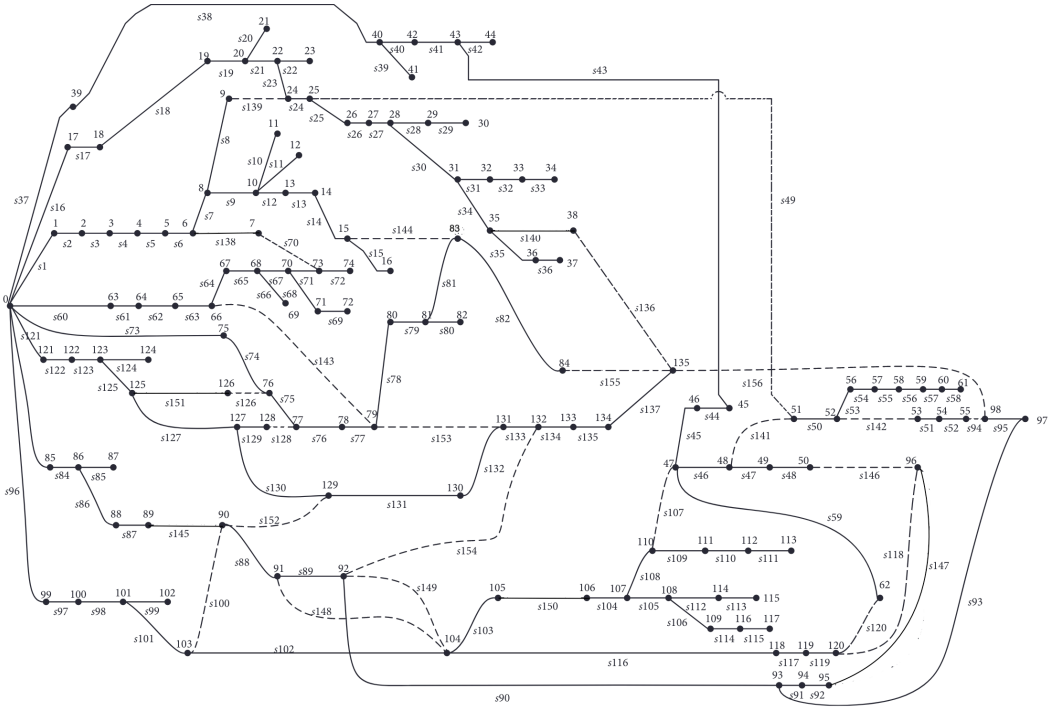

Figure 31 – Topology of the 136-bus system

Source: Author's elaboration

Table 22 – Simulation results for Case 2: 136-bus system

Case	Item	SFS
2	Opened Switches	7-137-83-38-51-141-53-119-144-145-84-147-148-150-90-151-96-106-128-154-156
	P_{loss} (kW)	284.13
	V_{min} (p.u.)	0.9594
	Loss reduction (%)	11.31

Source: Author's elaboration

The total power losses from the network in Case 2 is 284.13 kW and the minimum voltage profile is 0.9594.p.u. These results were improved in Case 3 with an optimal placement and sizing of DGs and in Case 4 when the DFR is performed after DGs allocation.

Table 23 – Simulation results for Case 3: 136-bus system

Case	Item	SFS
3	Opened Switches	136-137-138-139-140-141-142-143-144-145-146-147-148-149-150-151-152-153-154-155-156
	P_{loss} (kW)	142.12
	V_{min} (p.u.)	0.9711
	Loss reduction (%)	55.64
	P_{DG} (MW)/(Node)	2.0680 (29)
		2.3347 (11)
		2.8240 (106)

Source: Author's elaboration

In Case 3 the optimal placement and sizing of DGs was performed and results presented in Table 23 show a reduction on power losses and an improvement on the minimum voltage profile, 142.12 kW and 0.9711.p.u.

Table 24 – Simulation results for Case 4, 136-bus system

Case	Item	SFS
4	Opened Switches	73-8-81-134-51-96-142-143-144-145-84-104-148-89-147-132-152-110-126-155-156
	P_{loss} (kW)	94.86
	V_{min} (p.u.)	0.9819
	Loss reduction (%)	70.39
	P_{DG} (MW)/(Node)	2.0680 (29)
		2.3347 (11)
		2.8240 (106)

Source: Author's elaboration

Case 4 presents an improvement on power losses reduction while increasing the minimum voltage profile, 94.858 kW and 0.9819.p.u.

The simultaneous DFR and optimal DG placement and sizing was performed in Case 5, which presents better results than those previously analyzed. The total power losses and minimum voltage profile obtained in this case are 76.44 kW and 0.9836.p.u, respectively, resulting in a power reduction rate of 76.14%, as shown in Table 25.

Table 25 – Simulation results for Case 5, 136-bus system

Case	Item	SFS
5	Opened Switches	7-9-13-28-25-49-93-62-66-128-84-104-127-149-92-88-91-110-126-75-135
	P_{loss} (kW)	76.44
	V_{min} (p.u.)	0.9836
	Loss reduction (%)	76.14
	P_{DG} (MW)/(Node)	2.5115 (106)
		6.7112 (132)
		4.1480 (99)

Source: Author's elaboration

Furthermore, the total active power generation in Case 5 is 13.37 MW versus 7.23 MW in case 3. This confirms the ability of the SFS to efficiently perform the allocation and sizing of DGs when addressing the DFR problem. The optimal configuration of the tie-switches carried out by the SFS in Case 5 is represented by the interconnection 7-9-13-28-25-49-93-62-143-144-145-84-104-149-92-88-91-110-126-75-135.

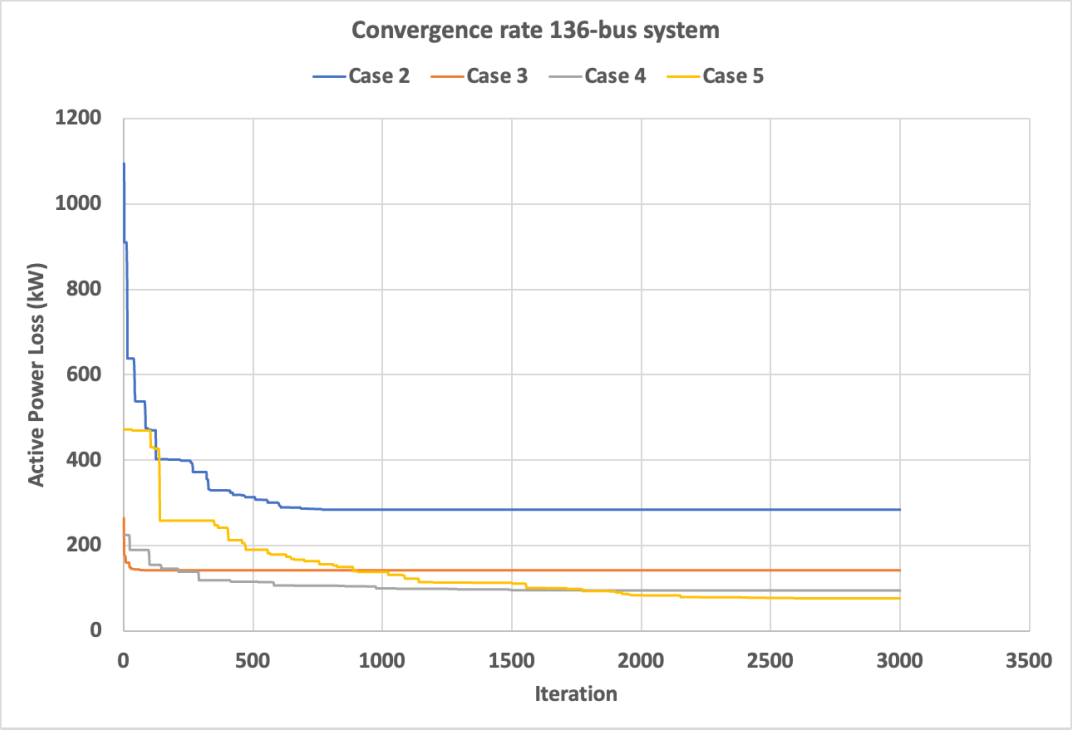

Figure 32 – Convergence characteristic of the 136-bus system.

Source: Author's elaboration.

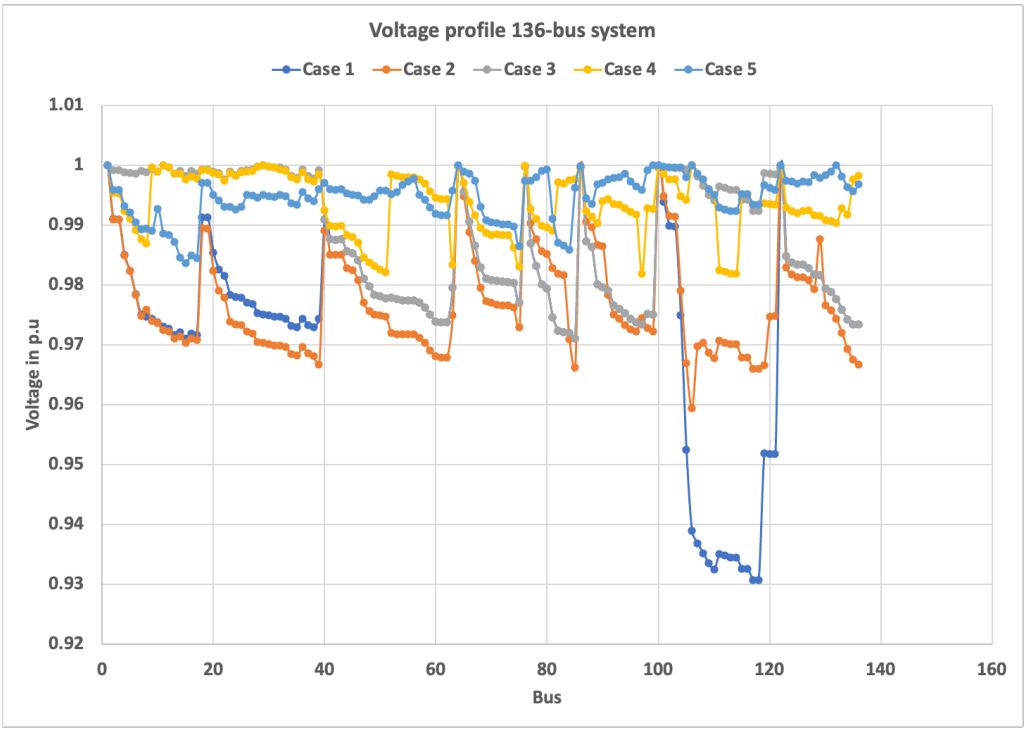

Figure 33 – Voltage profile for the 136-bus system.

Source: Author's elaboration

Figure 32 presents the convergence characteristic for the 136-bus system. The SFS converged around the 700th iteration in Case 2, while in Case 3 this occurred around the 100th iteration. Case 4 and Case 5 reached their convergence rate, respectively, around the 1500th and 2500th iteration. It is important to emphasize that when we are looking for a good local solution, the SFS can converge with a few iterations. In Cases 4 and 5, a good local solution can be achieved around the 100th iteration and the 1000th iteration with objective functions 155.13 kW and 138.34 kW respectively. These results show that the SFS can satisfy a wide range of accuracy rates, according to the customer's needs. The voltage profiles are presented in Figure 33 for the same feeder test, where the integration of DGs has significantly improved the overall voltage profile of the network, mainly in Case 5 where the DFR is performed simultaneously with DGs allocation.

Table 26 – Comparison of the results of Case 2 with others research

Methods	Opened Switches	Power loss (kW)	V_{min}(p.u)

Initial	136-137-138-139-140-141-142-143-144-145-146-147-148-149-150-151-152-153-154-155-156	320.36	0.9307
GA	7-35-51-90-96-106-118-126-135-137-138-141-142-144-145-146-147-148-150-151-155	280.19	0.9589
Heuristic	136-137-138-139-51-141-142-143-144145-146-147-148-149-150-151-152106-154-155-156	285.77	0.9631
SFS	7-137-83-38-51-141-53-119-144-145-84-147-148-150-90-151-96-106-128-154-156	284.13	0.9594

Source: Author's elaboration

The results presented in Table 26 show the optimal solution of SFS developed in this research with those found in GA (Carreno; Romero; Padilha-Feltrin, 2008) and Heuristic (Mantovani; Casari; Romero, 2000). The SFS performed with lower power losses than the heuristic method, but with an estimated gap of 1.4% compared to GA. However, the minimum voltage profile of the network with the SFS is better than that found with the basic GA.

4.2.2 LARGE-SCALE DISTRIBUTION FEEDER RECONFIGURATION WITH OPTIMAL PLACEMENT AND SIZING OF DISTRIBUTED GENERATION AND CAPACITOR BANKS USING STOCHASTIC FRACTAL SEARCH

In this section, we present simulation results carried out on the 119-bus and 136-bus systems for the simultaneous integration of DFR, DG and CB in large-scale distribution feeders. Three simulation cases were performed, and results were compared with those obtained in the previous section.

1) Case 6: Optimal placement and sizing of DG and CB.
2) Case 7: DFR is performed after optimal placement and sizing of the DGs and CBs using the results of Case 6.
3) Case 8: The DFR and optimal placement and sizing of DGs and CBs are performed simultaneously.

4.2.2.1 Simulation results with DGs and CBs integration for the 119-bus system

Table 27 – Simulation results of the 119-bus system

Case	Item	SFS
6	Opened Switches	118-119-120-121-122-123-124-125-126-127-128-129-130-131-132
	P_{loss} (kW)	283.66
	V_{min} (p.u.)	0.9678
	Loss reduction (%)	78.15
	P_{DG} (MW)/(Node)	2.9127 (110)
		2.8239 (72)
		2.8650 (50)
	CB (kVAr)/(Node)	1300 (80)
		1000 (96)
		1200 (41)
7	Opened Switches	42-26-21-43-33-46-39-125-76-70-127-129-85-105-36
	P_{loss} (kW)	246.80
	V_{min} (p.u.)	0.9728
	Loss reduction (%)	80.99
	P_{DG} (MW)/(Node)	2.9127 (110)
		2.8239 (72)
		2.8650 (50)
	CB (kVAr)/(Node)	1300 (80)
		1000 (96)
		1200 (41)
8	Opened Switches	41-26-21-43-46-36-38-125-69-80-97-87-103-116-33
	P_{loss} (kW)	191.25
	V_{min} (p.u.)	0.9828
	Loss reduction (%)	85.27
	P_{DG} (MW)/(Node)	3.4280 (50)
		3.6156 (73)
		4.1883 (109)
	CB (kVAr)/(Node)	900 (111)
		1300 (31)
		1300 (79)

Source: Author's elaboration

The active power losses and the minimum voltage profile in Case 6 are 283.66.73 kW, 0.9678.p.u, and DG locations are buses 110, 72, and 50. Capacitor

banks are located on buses 80, 96, and 41, with capacitor sizes 1300, 1000, and 1200 kVAr, respectively. These results are better than those of Case 3, Table 19 (344.73 kW, 0.9606). In addition, results present in Case 7 emphasize this improvement when the DFR is performed after DGs and CBs allocation (246.80 kW, 0.9728.p.u). The reduction in power losses in this case corresponds to 78%, compared to the base case. However, simulation carried out in Case 8, when the DFR, DG, and CB are simultaneously addressed have substantially improved the power losses and the minimum voltage profile (191.24 kW, 0.9828.p.u). The DGs are allocated on buses 50, 73 and 109, while the optimal placement of CBs gave buses 111, 31, and 79, with respective capacitance 900, 1300, and 1300 kVAr. These results demonstrate a positive impact of reactive power compensation of capacitor banks on the quality of the energy supplied to the load.

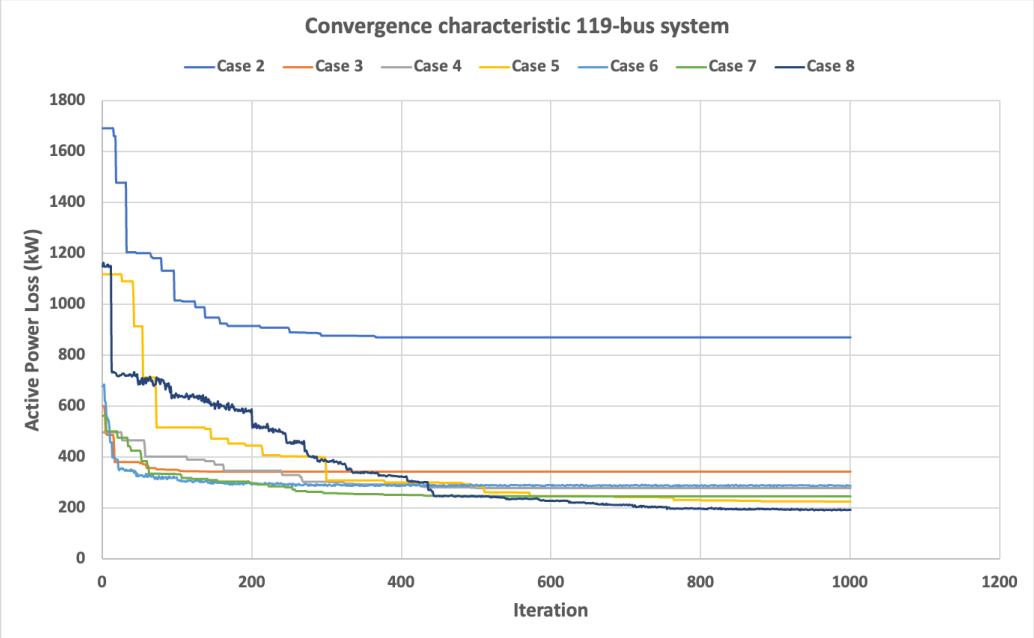

Figure 34 – Convergence characteristic of the 119-bus DFR with DG and CB

Source: Author's elaboration.

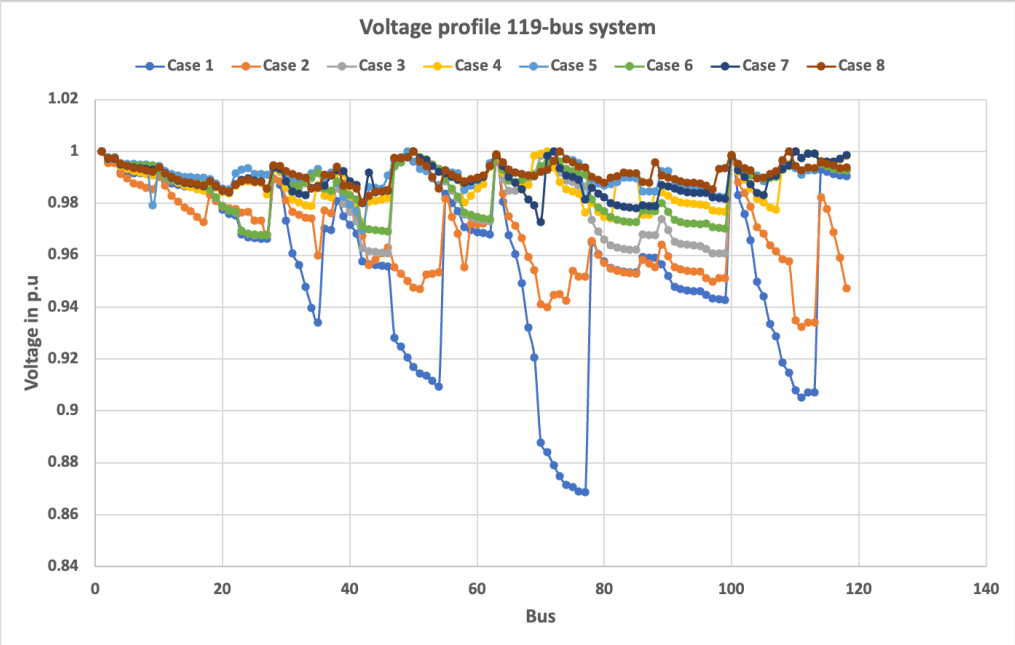

Figure 35 – Voltage profile of the 119-bus DFR with DG and CB.

Source: Author's elaboration.

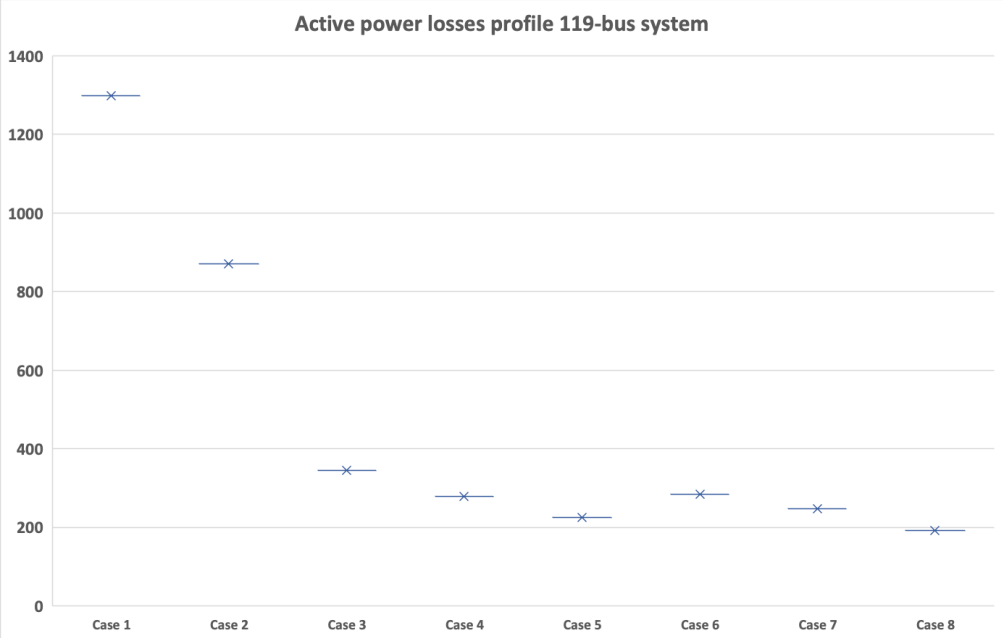

Figure 36 – Power losses profile of the 119-bus system

Source: Author's elaboration.

Figure 34 presents the convergence characteristic and Figure 35, the voltage profile of the 119-bus system. The voltage profiles have been improved at all buses of the system, during the optimization process, and especially in Case 8 (DFR+DG+CB). The power loss behavior is presented in Figure 36, where the minimum value was reached in Case 8 (191.25 kW).

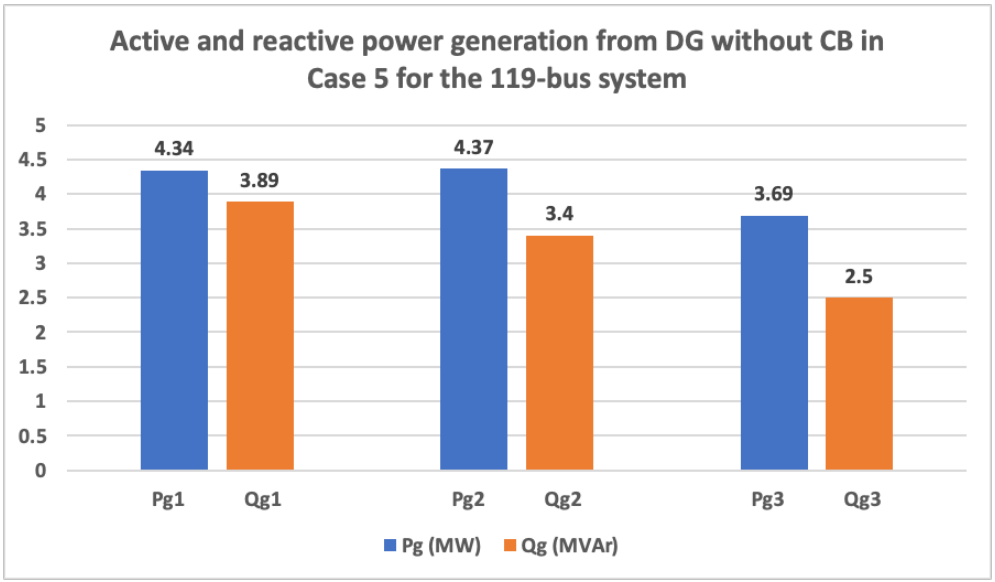

Figure 37 – Active and reactive power generation of DGs without CBs 119-bus

Source: Author's elaboration.

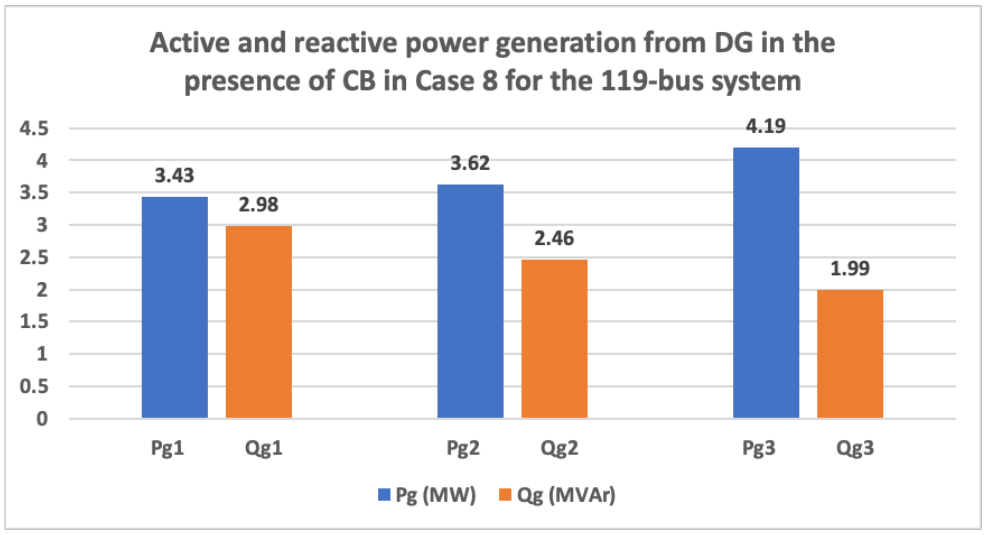

Figure 38 – Active and reactive power generation of DGs with CBs 119-bus

Source: Author's elaboration.

Figures 37 and 38 present the total active and reactive power generation from each DG in both cases, with and without CBs. We deduce that power generation decreases when the CBs are allocated in the network. This behavior is clearly illustrated in Figure 39, which shows the total active and reactive power outputs of DGs in both cases.

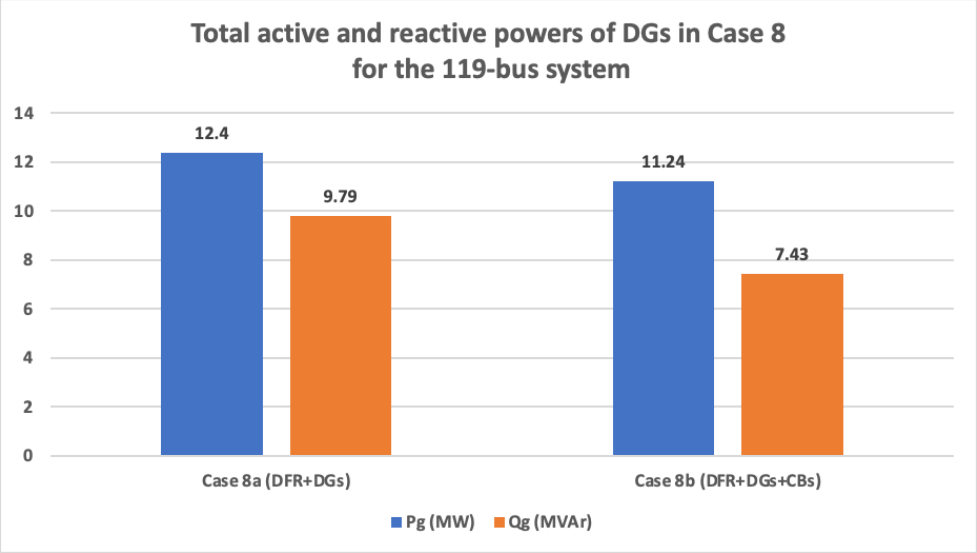

Figure 39 – Total active and reactive powers of DGs with and without CBs for the 119-bus system

Source: Author's elaboration.

4.2.2.2 Simulation results with DGs and CBs integration for the 136-bus system

Table 28 – Simulation results of the 136-bus system

Case	Item	SFS
6	Opened Switches	136-137-138-139-140-141-142-143-144-145-146-147-148-149-150-151-152-153-154-155-156
	P_{loss} (kW)	129.31
	V_{min} (p.u.)	0.9734
	Loss reduction (%)	59.64
	P_{DG} (MW)/(Node)	2.0946 (29)
		2.8850 (106)
		2.3476 (11)
	CB (kVAr)/(Node)	600 (52)
		600 (134)
		600 (82)
7	Opened Switches	73-137-8-26-51-141-55-143-144-145-134-147-148-89-150-151-96-153-126-128-156
	P_{loss} (kW)	87.29
	V_{min} (p.u.)	0.9830
	Loss reduction (%)	72.75

	P_{DG} (MW)/(Node)	2.0946 (29)
		2.8850 (106)
		2.3476 (11)
	CB (kVAr)/(Node)	600 (52)
		600 (134)
		600 (82)
8	Opened Switches	73-8-81-24-140-50-53-46-144-145-155-13-148-88-104-92-94-110-129-154-133
	P_{loss} (kW)	72.65
	V_{min} (p.u.)	0.9884
	Loss reduction (%)	77.32
	P_{DG} (MW)/(Node)	3.3397 (121)
		2.8878 (106)
		5.5494 (136)
	CB (kVAr)/(Node)	500 (74)
		400 (11)
		600 (84)

Source: Author's elaboration

The integration of the capacitor banks in the network has positive impacts on previous results presented in Tables 23 – 25. The active power losses decreased from 142.12 kW (Table 23, Case 3) to 129.31 kW (Case 6, Table 28). In the same way, the minimum voltage profile has been improved from 0.9711.p.u to 0.9734.p.u. These results were improved from 76.44 kW, 0.9836.p.u. (Table 25, Case 5) to 72.65 kW, 0.9884.p.u. (Table, 28, Case 8). The capacitor banks are allocated at bus 74 (500 kVAr), 11 (400 kVAr), and 84 (600 kVAr).

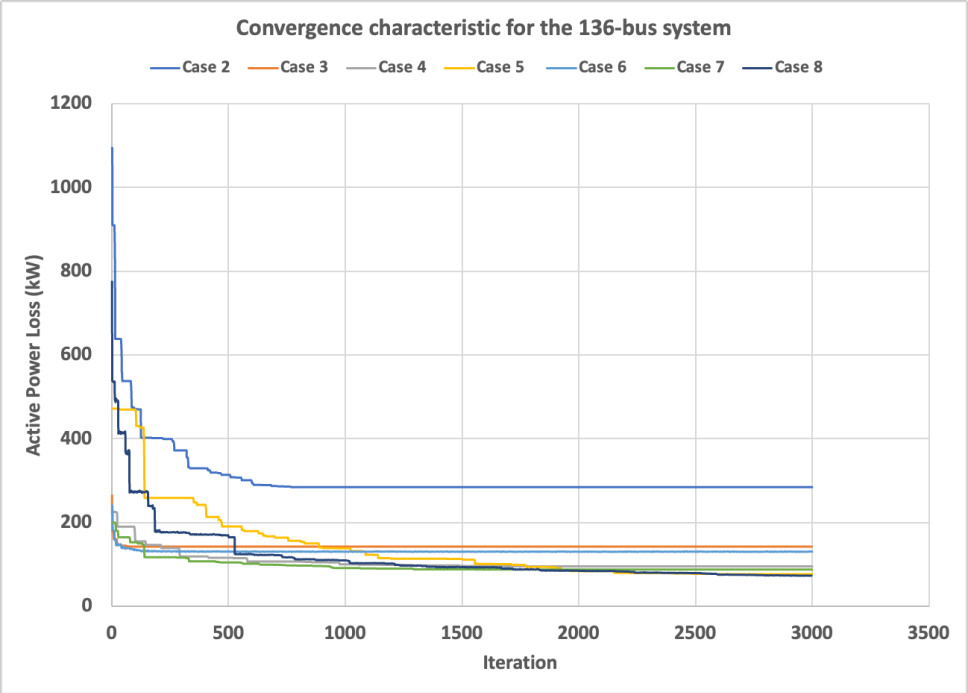

Figure 40 – Convergence characteristic of the 136-bus DFR with DG and CB

Source: Author's elaboration.

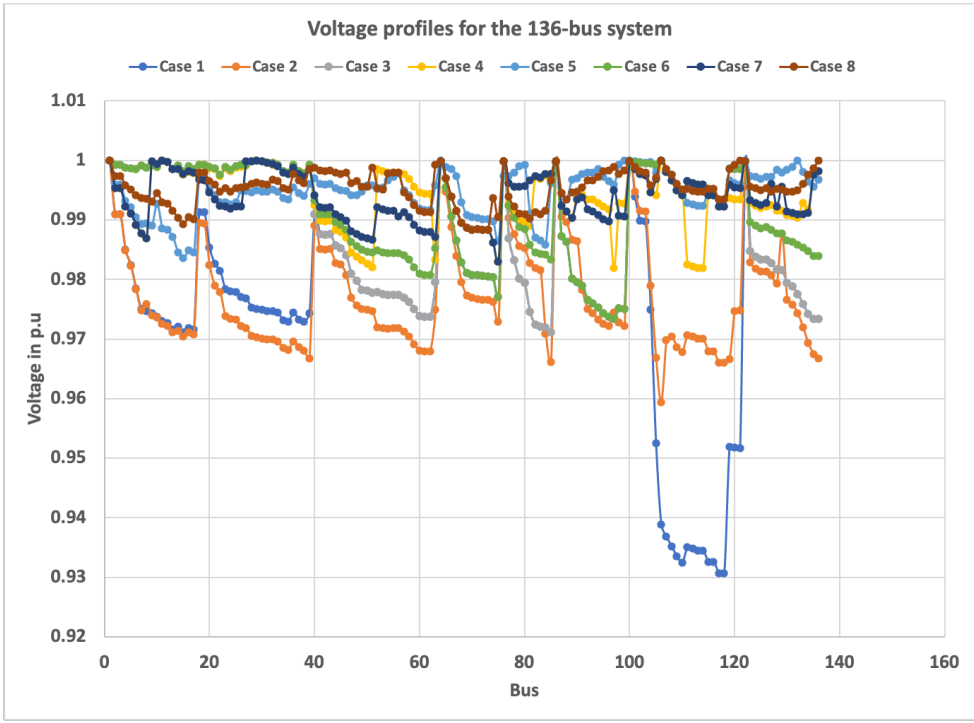

Figure 41 – Voltage profile of the 136-bus DFR with DG and CB

Source: Author's elaboration.

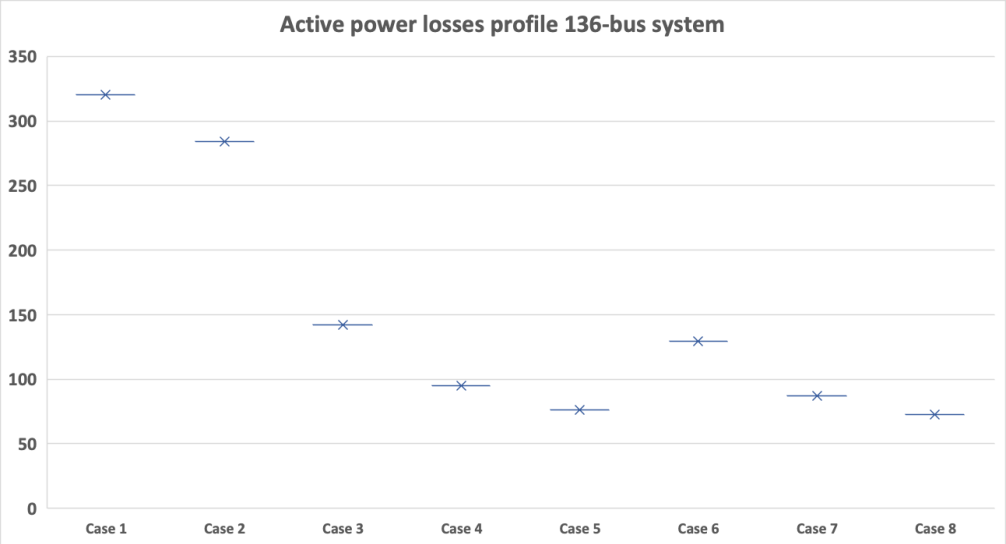

Figure 42 – Power losses profile of the 136-bus system

Source: Author's elaboration.

Figures 40 and 41 present the convergence characteristic and the voltage profile of the 136-bus system, respectively. In Case 8, the integration of DG and CB significantly reduced active power losses while improving the grid voltage profile. Figure 42 shows the power loss behavior, where the minimum value was reached in Case 8 (72.65 kW).

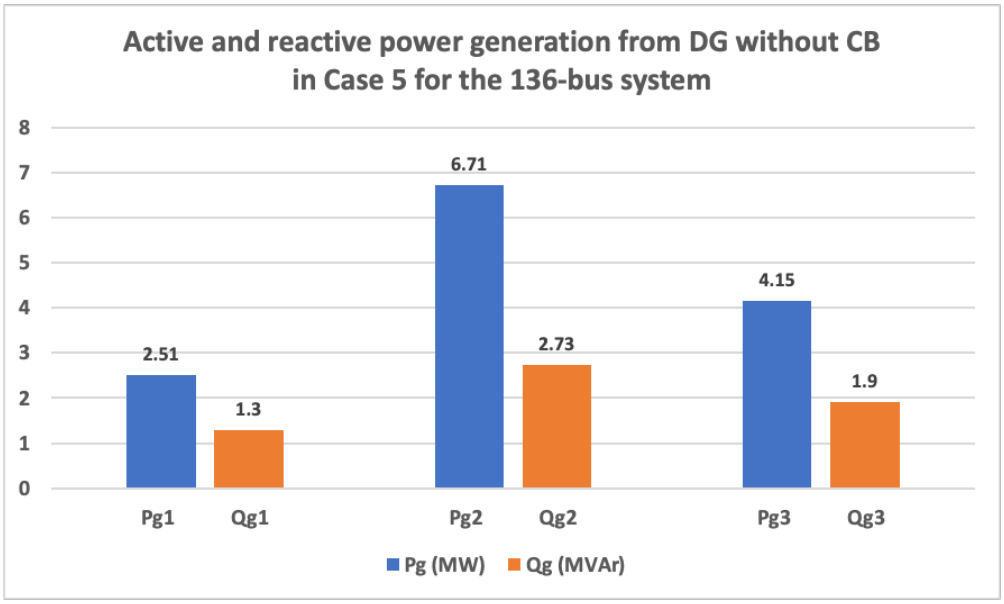

Figure 43 – Active and reactive power generation of DGs without CBs 136-bus

Source: Author's elaboration.

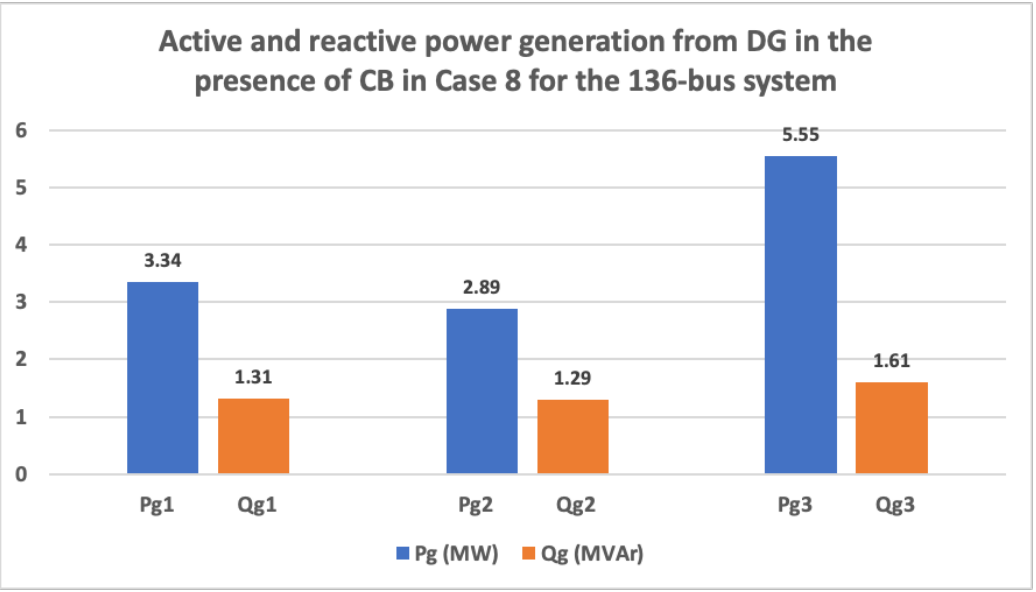

Figure 44 – Active and reactive power generation of DGs with CBs 136-bus

Source: Author's elaboration.

Figures 43 and 44 present the total real and reactive power generation of DGs with and without CBs. It can be inferred that power generations decrease when CBs are integrated into the grid. Figure 45 highlights this aspect, showing the total active and reactive power generated by DGs in both cases. This is a good behavior that we can expect from DGs and the grid when seeking techno-economic impacts.

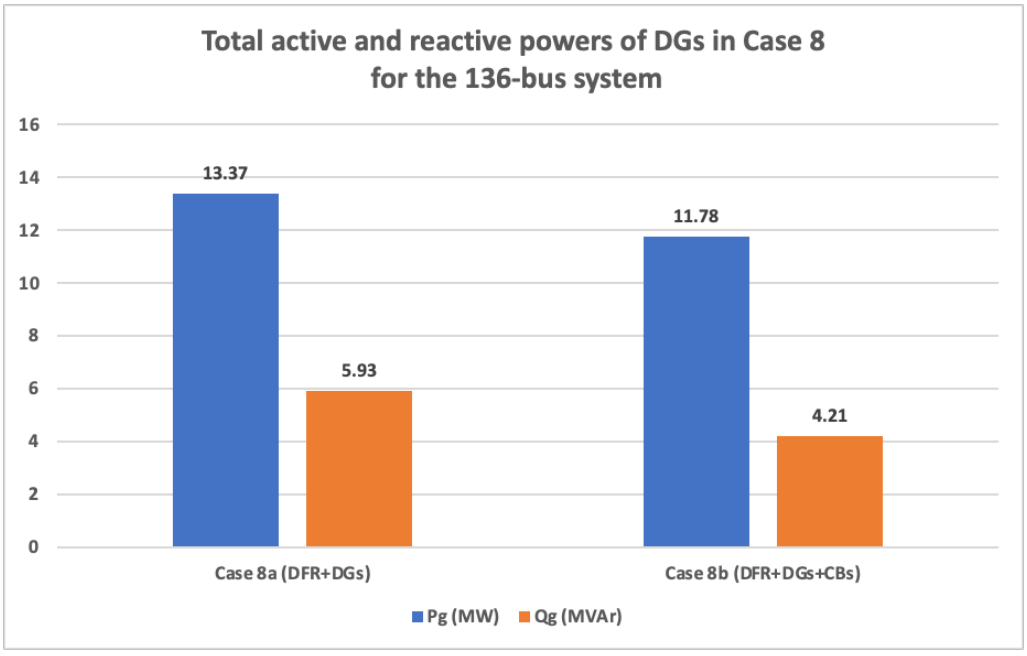

Figure 45 – Total active and reactive power of DGs in Case 5 with and without CBs for the 136-bus system

5 CONCLUSIONS

This work presented optimal power flow algorithms applied to distribution networks to mitigate voltage unbalance and power losses. The developed algorithms were successfully tested on large-scale distribution systems. In the first formulation we proposed an AC three-phase optimal power flow to mitigate voltage unbalance across all buses for unbalanced distribution systems, with voltage regulator taps adjustment and reactive power control of PV inverters. Small- and large-scale penetration of PV plants into large-scale distribution networks were addressed to study their impacts on the network performance. The simulation results showed that when the size of the PV plant is larger, the inverters must be able to perform both active and reactive power control especially during peak PV generation periods, to improve the power quality of the network. However, when small single-phase PV plants are well distributed along the grid, voltage unbalance and power losses are substantially reduced. Depending on the size of the grid, the size and locations of PV plants must be well defined to improve the power quality in the grid. In previous research carried out, we solved the voltage drop problem in which the voltage amplitude on three-phase is different from 1.0, while maintaining the 120° phase shift between phases, in small- and medium-scale unbalanced distribution networks, by injecting constant active power of PV plants while controlling the reactive power injection from inverters. This work is the extension of the previous research to large-scale distribution systems, which in practice presents some challenges to find an optimal operation point.

In the second formulation we develop an optimal power flow based on distribution feeder reconfiguration with the integration of distributed generations and capacitor banks, to reduce power losses. The OPF formulated was solved using the stochastic fractal search (SFS) algorithm combined with mathematical models to control and correct the violation of tie-switches bounds at the diffusion and updating stages of the SFS, and to define CBs size for better integration of them into the grid. The simulation results have shown the robustness of the SFS in solving this problem and provide a high-quality solution. The integration of DGs and CBs into the grid had a significant impact on reducing power losses and improving the minimum voltage profile of networks. Furthermore, DGs can provide reactive power to the grid, contributing to voltage control and loss reduction in the network. By allocating capacitor banks, the

grid reduces its dependence on power generation from DGs and therefore, can save money for the network owner.

For future works, we propose:

- The modeling of active power control capability of smart inverters in the formulation of the three-phase optimal power flow.
- The integration of other renewable sources in the formulation of the mathematical model of the TOPF, to analyze their impacts on the voltage unbalance.
- To address the optimal integration of PV plants in large-scale unbalanced distribution networks using an appropriate metaheuristic algorithm.
- To conduct techno-economic analyses of integrating PV systems into the distribution system.
- To address the distribution network reconfiguration for unbalanced networks with optimal integration of PV plants and capacitor banks.

REFERENCES

ALI, E. S.; ABD ELAZIM, S. M.; ABDELAZIZ, A. Y. Improved Harmony Algorithm for optimal locations and sizing of capacitors in radial distribution systems. **International Journal of Electrical Power & Energy Systems**, v. 79, p. 275–284, jul. 2016.

ARAUJO, L. R. *et al.* A Three-Phase Optimal Power-Flow Algorithm to Mitigate Voltage Unbalance. **IEEE Transactions on Power Delivery**, v. 28, n. 4, p. 2394–2402, out. 2013.

AYIKPA, Malinwo Estone. An Efficient Tool for Mitigating Voltage Unbalance with Reactive Power Control of Distributed Grid-Connected Photovoltaic Systems. **International Journal of Energy and Power Engineering**, v. 11, n. 2, 2017.

AYIKPA, Malinwo Estone. Optimal Placement and Sizing of Distributed Generations and Capacitor Banks in Large-Scale Distribution Network Using Feeder Reconfiguration. *In*: 2025 IEEE TEXAS POWER AND ENERGY CONFERENCE (TPEC). **2025 IEEE Texas Power and Energy Conference (TPEC)**. fev. 2025a. Disponível em: <https://ieeexplore.ieee.org/document/10906970/?arnumber=10906970>. Acesso em: 7 mar. 2025

AYIKPA, Malinwo Estone. **Voltage Unbalance Mitigation in Large-scale Distribution Networks with reactive power control of Grid-connected PV Plants using Three-phase Optimal Power Flow**. Preprints, , 30 out. 2025b. Disponível em: <https://www.techrxiv.org/users/983718/articles/1350669-voltage-unbalance-mitigation-in-large-scale-distribution-networks-with-reactive-power-control-of-grid-connected-pv-plants-using-three-phase-optimal-power-flow?commit=2213c371f7e97dc65d0d8cf8f9a922ecc268ed9c>. Acesso em: 20 jan. 2026

AYODELE, T. R.; OGUNJUYIGBE, A. S. O.; AKINOLA, O. O. Optimal Location, Sizing, and Appropriate Technology Selection of Distributed Generators for Minimizing Power Loss Using Genetic Algorithm. **Journal of Renewable Energy**, v. 2015, p. 1–9, 2015.

BAGGINI, Angelo. Handbook of Power Quality. **John Wiley & Sons Ltd**, p. 645, 2008.

BARAN, Antonio R.; FERNANDES, Thelma S. P. A three-phase optimal power flow applied to the planning of unbalanced distribution networks. **International Journal of Electrical Power & Energy Systems**, v. 74, p. 301–309, 1 jan. 2016.

BARAN, M. E.; WU, F. F. Optimal capacitor placement on radial distribution systems. **IEEE Transactions on Power Delivery**, v. 4, n. 1, p. 725–734, jan. 1989a.

BARAN, M. E.; WU, F. F. Network reconfiguration in distribution systems for loss reduction and load balancing. **IEEE Transactions on Power Delivery**, v. 4, n. 2, p. 1401–1407, abr. 1989b.

BENNY, Aneetta *et al.* Grid-integrated Photovoltaic System with Reactive and Active Power Capability. *In*: 2024 IEEE INTERNATIONAL CONFERENCE ON SIGNAL PROCESSING, INFORMATICS, COMMUNICATION AND ENERGY SYSTEMS

(SPICES). **2024 IEEE International Conference on Signal Processing, Informatics, Communication and Energy Systems (SPICES)**. set. 2024. Disponível em: <https://ieeexplore.ieee.org/document/10779663/>. Acesso em: 22 jul. 2025

BISWAS, Partha P. *et al.* A multiobjective approach for optimal placement and sizing of distributed generators and capacitors in distribution network. **Applied Soft Computing**, v. 60, p. 268–280, nov. 2017.

BONNETT, A. H.; SOUKUP, G. C. Understanding the NEMA motor-generator standards of section MG-1-1993, revision 3, three-phase induction motors. *In*: RECORD OF CONFERENCE PAPERS. IEEE INDUSTRY APPLICATIONS SOCIETY 44TH ANNUAL PETROLEUM AND CHEMICAL INDUSTRY CONFERENCE. **Record of Conference Papers. IEEE Industry Applications Society 44th Annual Petroleum and Chemical Industry Conference**. set. 1997. Disponível em: <https://ieeexplore.ieee.org/document/648188/>. Acesso em: 7 ago. 2025

BRUNO, Sergio *et al.* Unbalanced Three-Phase Optimal Power Flow for Smart Grids. **IEEE Transactions on Industrial Electronics**, v. 58, n. 10, p. 4504–4513, out. 2011.

CARPANETO, E.; CHICCO, G. Performance of the simulated annealing-based algorithms for the optimal reconfiguration of distribution systems. *In*: 2001 POWER TECH. **2001 IEEE Porto Power Tech Proceedings (Cat. No.01EX502)**. Porto, Portugal: IEEE, 2001. Disponível em: <http://ieeexplore.ieee.org/document/964953/>. Acesso em: 16 abr. 2024

CARRENO, Edgar Manuel; ROMERO, RubÉn; PADILHA-FELTRIN, Antonio. An Efficient Codification to Solve Distribution Network Reconfiguration for Loss Reduction Problem. **IEEE Transactions on Power Systems**, v. 23, n. 4, p. 1542–1551, nov. 2008.

CHENG, C. S.; SHIRMOHAMMADI, D. A three-phase power flow method for real-time distribution system analysis. **IEEE Transactions on Power Systems**, v. 10, n. 2, p. 671–679, maio 1995.

DALL'ANESE, Emiliano; ZHU, Hao; GIANNAKIS, Georgios B. Distributed Optimal Power Flow for Smart Microgrids. **IEEE Transactions on Smart Grid**, v. 4, n. 3, p. 1464–1475, set. 2013.

DE OLIVEIRA, L. W.; SETA, F. D. S.; DE OLIVEIRA, E. J. Optimal reconfiguration of distribution systems with representation of uncertainties through interval analysis. **International Journal of Electrical Power and Energy Systems**, v. 83, p. 382–391, 2016.

DEVABALAJI, K. R.; RAVI, K.; KOTHARI, D. P. Optimal location and sizing of capacitor placement in radial distribution system using Bacterial Foraging Optimization Algorithm. **International Journal of Electrical Power & Energy Systems**, v. 71, p. 383–390, out. 2015.

DIXIT, Mukul; KUNDU, Prasanta; JARIWALA, Hitesh R. Optimal placement of PV array in distribution system for power loss minimization considering feeder reconfiguration. *In*: 2016 IEEE 16TH INTERNATIONAL CONFERENCE ON ENVIRONMENT AND ELECTRICAL ENGINEERING (EEEIC). **2016 IEEE 16th**

International Conference on Environment and Electrical Engineering (EEEIC). jun. 2016.

DONDARIYA, Chandrakant; SAKRAVDIA, D. K. Voltage Stability Assessment and Improvement in Power Systems with Solar Photovoltaic Penetration. *In*: 2021 IEEE 2ND INTERNATIONAL CONFERENCE ON ELECTRICAL POWER AND ENERGY SYSTEMS (ICEPES). **2021 IEEE 2nd International Conference On Electrical Power and Energy Systems (ICEPES)**. dez. 2021. Disponível em: <https://ieeexplore.ieee.org/document/9699827/>. Acesso em: 22 jul. 2025

DRUS, Syed Muhammad Fadli Syed *et al.* Distribution Feeder Reconfiguration with Distributed Generation Using Backward/Forward Sweep Power Flow – Grey Wolf Optimizer. *In*: 2023 19TH IEEE INTERNATIONAL COLLOQUIUM ON SIGNAL PROCESSING & ITS APPLICATIONS (CSPA). **2023 19th IEEE International Colloquium on Signal Processing & Its Applications (CSPA)**. mar. 2023. Disponível em: <https://ieeexplore.ieee.org/document/10087738/?arnumber=10087738>. Acesso em: 2 ago. 2024

FORTESCUE, C. L. Method of Symmetrical Co-Ordinates Applied to the Solution of Polyphase Networks. **Transactions of the American Institute of Electrical Engineers**, v. XXXVII, n. 2, p. 1027–1140, jul. 1918.

GANGULY, S.; SAMAJPATI, D. Distributed generation allocation on radial distribution networks under uncertainties of load and generation using genetic algorithm. **IEEE Transactions on Sustainable Energy**, v. 6, n. 3, p. 688–697, 2015.

GARCIA, P. A. N. *et al.* Three-phase power flow calculations using the current injection method. **IEEE Transactions on Power Systems**, v. 15, n. 2, p. 508–514, maio 2000.

GIL MENA, Antonio José; MARTÍN GARCÍA, Juan Andrés. An efficient approach for the siting and sizing problem of distributed generation. **International Journal of Electrical Power & Energy Systems**, v. 69, p. 167–172, jul. 2015.

GUO, Yongqiang *et al.* Study on the Impact of Large-Scale Photovoltaic Integration on Grid Voltage. *In*: 2024 4TH INTERNATIONAL CONFERENCE ON NEW ENERGY AND POWER ENGINEERING (ICNEPE). **2024 4th International Conference on New Energy and Power Engineering (ICNEPE)**. nov. 2024. Disponível em: <https://ieeexplore.ieee.org/document/10860563/>. Acesso em: 22 jul. 2025

HONG, Ying-Yi; LIN, Faa-Jeng; HSU, Fu-Yuan. Enhanced Particle Swarm Optimization-Based Feeder Reconfiguration Considering Uncertain Large Photovoltaic Powers and Demands. **International Journal of Photoenergy**, v. 2014, n. 1, p. 704839, 2014.

K., Muthukumar; S., Jayalalitha. Integrated approach of network reconfiguration with distributed generation and shunt capacitors placement for power loss minimization in radial distribution networks. **Applied Soft Computing**, v. 52, p. 1262–1284, mar. 2017.

KERSTING, William H. **Distribution system modeling and analysis**. Boca Raton: CRC Press, 2002.

LEGHARI, Zohaib Hussain *et al.* A Critical Review of Optimization Strategies for Simultaneous Integration of Distributed Generation and Capacitor Banks in Power Distribution Networks. **Energies**, v. 15, n. 21, p. 8258, jan. 2022.

LI, Chao *et al.* A Two-stage Reactive Power Optimization Strategy for AC/DC Hybrid Distribution Network. *In*: 2020 5TH ASIA CONFERENCE ON POWER AND ELECTRICAL ENGINEERING (ACPEE). **2020 5th Asia Conference on Power and Electrical Engineering (ACPEE)**. jun. 2020. Disponível em: <https://ieeexplore.ieee.org/document/9136203/?arnumber=9136203>. Acesso em: 31 jul. 2024

LIU, Rundong *et al.* Voltage Stability Analysis Considering the Impact of Distributed Photovoltaic Generation. *In*: 2022 IEEE 6TH CONFERENCE ON ENERGY INTERNET AND ENERGY SYSTEM INTEGRATION (EI2). **2022 IEEE 6th Conference on Energy Internet and Energy System Integration (EI2)**. nov. 2022. Disponível em: <https://ieeexplore.ieee.org/document/10116303/>. Acesso em: 22 jul. 2025

LIU, Yafeng; ZHANG, Bo. Reactive Power Optimization Control Strategy in Photovoltaic Power Station Considering the Reliability of Photovoltaic Inverter. *In*: 2025 4TH INTERNATIONAL CONFERENCE ON ENERGY, POWER AND ELECTRICAL TECHNOLOGY (ICEPET). **2025 4th International Conference on Energy, Power and Electrical Technology (ICEPET)**. abr. 2025. Disponível em: <https://ieeexplore.ieee.org/document/11047399/>. Acesso em: 22 jul. 2025

MADEIRO, Salomão *et al.* Simultaneous capacitor placement and reconfiguration for loss reduction in distribution networks by a hybrid genetic algorithm. *In*: 2011 IEEE CONGRESS OF EVOLUTIONARY COMPUTATION (CEC). **2011 IEEE Congress of Evolutionary Computation (CEC)**. jun. 2011. Disponível em: <https://ieeexplore.ieee.org/document/5949884/?arnumber=5949884>. Acesso em: 14 ago. 2024

MAHDAVI, Elham *et al.* Reconfiguration of Distribution Networks with Simultaneous Allocation of Distributed Generation Using the Whale Optimization Algorithm. **Energies**, v. 16, n. 12, p. 4560, jan. 2023a.

MAHDAVI, Meisam *et al.* Coordinated Feeder Reconfiguration, Capacitor Placement and Allocation of Distributed Energy Resources for Loss Reduction Under Variable Loading Conditions. *In*: 2023 IEEE KANSAS POWER AND ENERGY CONFERENCE (KPEC). **2023 IEEE Kansas Power and Energy Conference (KPEC)**. abr. 2023b. Disponível em: <https://ieeexplore.ieee.org/document/10215466/?arnumber=10215466>. Acesso em: 14 ago. 2024

MALINWO E. AYIKPA; KATIA C. DE ALMEIDA; GUILHERME C. DANIELSKI. Three-Phase Optimal Power Flow for Study of PV Plant Distributed Impact on Distribution Systems. **J. of Electrical Engineering**, v. 5, n. 1, 28 jan. 2017.

MANTOVANI, José R. S.; CASARI, Fernando; ROMERO, Rubén A. RECONFIGURAÇÃO DE SISTEMAS DE DISTRIBUIÇÃO RADIAIS UTILIZANDO O CRITÉRIO DE QUEDA DE TENSÃO. *[S.d.]*.

MARQUSEE, Jeffrey; STRINGER, Andrew. **Distributed Energy Resource (DER) Reliability for Backup Electric Power Systems**. *[S.l.: S.n.]*. Disponível em: <https://www.osti.gov/servlets/purl/1964053/>. Acesso em: 15 out. 2025.

MOHAMED IMRAN A; KOWSALYA M. Optimal Distributed Generation and capacitor placement in power distribution networks for power loss minimization. *In*: 2014 INTERNATIONAL CONFERENCE ON ADVANCES IN ELECTRICAL ENGINEERING (ICAEE). **2014 International Conference on Advances in Electrical Engineering (ICAEE)**. Vellore, India: IEEE, jan. 2014. Disponível em: <http://ieeexplore.ieee.org/document/6838519/>. Acesso em: 27 mar. 2024

MOMOH, James A. **Electric power system applications of optimization**. New York, NY Basel: Dekker, 2001.

MUTHUKUMAR, K.; JAYALALITHA, S. Optimal placement and sizing of distributed generators and shunt capacitors for power loss minimization in radial distribution networks using hybrid heuristic search optimization technique. **International Journal of Electrical Power & Energy Systems**, v. 78, p. 299–319, jun. 2016.

NARA, K. *et al.* Implementation of genetic algorithm for distribution systems loss minimum re-configuration. **IEEE Transactions on Power Systems**, v. 7, n. 3, p. 1044–1051, ago. 1992.

NGUYEN, Thuan Thanh; TRUONG, Anh Viet; PHUNG, Tuan Anh. A novel method based on adaptive cuckoo search for optimal network reconfiguration and distributed generation allocation in distribution network. **International Journal of Electrical Power & Energy Systems**, v. 78, p. 801–815, jun. 2016.

NZIMANDE, Nomvelo; NORO, Yasuhiro. Study on Integration of Large-Scale Photovoltaic and Wind Power Generation into a Grid. *In*: 2022 IEEE PES/IAS POWERAFRICA. **2022 IEEE PES/IAS PowerAfrica**. ago. 2022. Disponível em: <https://ieeexplore.ieee.org/document/9905302/>. Acesso em: 22 jul. 2025

PAN, Xin *et al.* Reactive Power Optimization In Distribution Networks With High Penetration Of Renewable Energy Based On Second-Order Cone Programming. *In*: 2021 IEEE 5TH CONFERENCE ON ENERGY INTERNET AND ENERGY SYSTEM INTEGRATION (EI2). **2021 IEEE 5th Conference on Energy Internet and Energy System Integration (EI2)**. out. 2021. Disponível em: <https://ieeexplore.ieee.org/document/9713529/?arnumber=9713529>. Acesso em: 31 jul. 2024

PAUDYAL, Sumit; CANIZARES, Claudio A.; BHATTACHARYA, Kankar. Optimal Operation of Distribution Feeders in Smart Grids. **IEEE Transactions on Industrial Electronics**, v. 58, n. 10, p. 4495–4503, out. 2011.

PRAKASH, K.; SYDULU, M. Particle Swarm Optimization Based Capacitor Placement on Radial Distribution Systems. *In*: 2007 IEEE POWER ENGINEERING SOCIETY GENERAL MEETING. **2007 IEEE Power Engineering Society General Meeting**. Tampa, FL, USA: IEEE, jun. 2007. Disponível em: <http://ieeexplore.ieee.org/document/4275915/>. Acesso em: 11 mar. 2024

RAMA PRABHA, D. *et al.* Optimal location and sizing of distributed generation unit using intelligent water drop algorithm. **Sustainable Energy Technologies and Assessments**, v. 11, p. 106–113, set. 2015.

RAO, R. Srinivasa *et al.* Power Loss Minimization in Distribution System Using Network Reconfiguration in the Presence of Distributed Generation. **IEEE Transactions on Power Systems**, v. 28, n. 1, p. 317–325, fev. 2013.

Relatório Final_BEN 2025. , *[S.d.]*.

Resources – IEEE PES Test Feeder. , *[S.d.]*. Disponível em: <https://cmte.ieee.org/pes-testfeeders/resources/>. Acesso em: 26 jul. 2025

SALIMI, Hamid. Stochastic Fractal Search: A powerful metaheuristic algorithm. **Knowledge-Based Systems**, v. 75, p. 1–18, 1 fev. 2015.

SAW, Shubham Kumar; NAVADA, H. Girisha; SHUBHANGA, K. N. Power Flow Analysis of Power Distribution System Integrated with Solar Photovoltaic Based Distributed Generation. *In*: 2022 INTERNATIONAL CONFERENCE ON INTELLIGENT CONTROLLER AND COMPUTING FOR SMART POWER (ICICCSP). **2022 International Conference on Intelligent Controller and Computing for Smart Power (ICICCSP)**. jul. 2022. Disponível em: <https://ieeexplore.ieee.org/document/9862485/>. Acesso em: 22 jul. 2025

SEIPHETLHO, T. E.; RENS, A. P. J. On the assessment of voltage unbalance. *In*: 14TH INTERNATIONAL CONFERENCE ON HARMONICS AND QUALITY OF POWER - ICHQP 2010. **Proceedings of 14th International Conference on Harmonics and Quality of Power - ICHQP 2010**. set. 2010. Disponível em: <https://ieeexplore.ieee.org/document/5625366/>. Acesso em: 6 ago. 2025

SHIRMOHAMMADI, D.; HONG, H. W. Reconfiguration of electric distribution networks for resistive line losses reduction. **IEEE Transactions on Power Delivery**, v. 4, n. 2, p. 1492–1498, abr. 1989.

SOUZA, Simone S. F.; ROMERO, Ruben; FRANCO, John F. Artificial immune networks Copt-aiNet and Opt-aiNet applied to the reconfiguration problem of radial electrical distribution systems. **Electric Power Systems Research**, v. 119, p. 304–312, fev. 2015.

TIWARI, V.; DUBEY, H. M.; PANDIT, M. Assessment of Optimal Size and Location of DG/CB in Distribution Systems using Coulomb–Franklin's Algorithm. **Journal of The Institution of Engineers (India): Series B**, v. 103, n. 6, p. 1885–1908, 2022.

TORRES, J. *et al.* A genetic algorithm based on the edge window decoder technique to optimize power distribution systems reconfiguration. **International Journal of Electrical Power & Energy Systems**, v. 45, n. 1, p. 28–34, fev. 2013.

TRAN THE, Tung; VO NGOC, Dieu; TRAN ANH, Nguyen. Distribution Network Reconfiguration for Power Loss Reduction and Voltage Profile Improvement Using Chaotic Stochastic Fractal Search Algorithm. **Complexity**, v. 2020, p. 1–15, 21 mar. 2020.

TRAN, Tung The; TRUONG, Khoa Hoang; VO, Dieu Ngoc. Stochastic fractal search algorithm for reconfiguration of distribution networks with distributed generations. **Ain Shams Engineering Journal**, v. 11, n. 2, p. 389–407, 1 jun. 2020.

VARMA, Rajiv K. *et al.* Grid Support Benefits of Solar PV Systems as STATCOM (PV-STATCOM) Through Converter Control: Grid Integration Challenges of Solar PV Power Systems. **IEEE Electrification Magazine**, v. 9, n. 2, p. 50–61, jun. 2021.

VON JOUANNE, A.; BANERJEE, B. Assessment of voltage unbalance. **IEEE Transactions on Power Delivery**, v. 16, n. 4, p. 782–790, out. 2001.

YOUNG-JAE JEON; JAE-CHUL KIM. Network reconfiguration in radial distribution system using simulated annealing and Tabu search. *In*: 2000 IEEE POWER ENGINEERING SOCIETY WINTER MEETING. CONFERENCE PROCEEDINGS. **2000 IEEE Power Engineering Society Winter Meeting. Conference Proceedings (Cat. No.00CH37077)**. Singapore: IEEE, 2000. Disponível em: <http://ieeexplore.ieee.org/document/847169/>. Acesso em: 16 abr. 2024

YU, Kai *et al.* Reactive Voltage Control in Photovoltaic Power Stations Considering Source-Load Uncertainty. *In*: 2024 IEEE 6TH ADVANCED INFORMATION MANAGEMENT, COMMUNICATES, ELECTRONIC AND AUTOMATION CONTROL CONFERENCE (IMCEC). **2024 IEEE 6th Advanced Information Management, Communicates, Electronic and Automation Control Conference (IMCEC)**. maio 2024. Disponível em: <https://ieeexplore.ieee.org/document/10575119/>. Acesso em: 22 jul. 2025

APPENDIX A – PUBLICATIONS ASSOCIATED TO THIS WORK

This appendix presents publications associated to this thesis.

- **Papers presented at international conferences.**

1. M. E. Ayikpa, "Optimal Placement and Sizing of Distributed Generations and Capacitor Banks in Large-Scale Distribution Network Using Feeder Reconfiguration," **2025 IEEE Texas Power and Energy Conference (TPEC)**, College Station, TX, USA, 09–11 February 2025, pp. 1–6, DOI**:** 10.1109/TPEC63981.2025.10906970

2. M. E. Ayikpa, "Voltage Unbalance Mitigation in Large-scale Distribution Networks with High Penetration of Photovoltaic Generations using Three-phase Optimal Power Flow ", **International Conference on Electrical and Computer Engineering Researches (ICECER 2025)** 6–8 December 2025, Antananarivo – *Madagascar*.

3. M. E. Ayikpa, "Genetic Algorithm Based on Advanced Evolutionary Computation for the Generalized Assignment Problem", **International Conference on Artificial Intelligence, Computer, Data Sciences and Applications (ACDSA 2026),** 5–7 February 2026 in Boracay Island, Philippines.

- **Papers presented at national conferences.**

1. M. E. Ayikpa, Katia C. D., Danielski Guilherme C., "Estudo do impacto da geração fotovoltaica distribuída via fluxo de potência ótimo trifásico", **XXI Brazilian Congress of Automatic (CBA2016),** 3–7 October 2016 in Vitória – ES, Brasil, v.1, p. 2665–2670.

2. M. E. Ayikpa. "Algoritmo Genético Heurístico para o Problema de Atribuição Generalizada", **VIII ERMAC – Encontro Regional de Matemática aplicada e Computacional** – Região 9, Ilha Solteira, São Paulo, Brasil, 2024. v.1. p. 1-7.

- **Papers published in international peer-reviewed journals.**

1. M. E. Ayikpa “An Efficient Tool for Mitigating Voltage Unbalance with Reactive Power Control of Distributed Grid-Connected Photovoltaic Systems”, **International Journal of Energy and Power Engineering** Vol: 11, N°2, 2017, p. 187–195. https://doi.org/10.5281/zenodo.1128827

2. M. E. Ayikpa “Unbalanced Distribution Optimal Power Flow to Minimize Losses with Distributed Photovoltaic Plants”, **International Journal of Energy and Power Engineering** Vol:11, N°2, 2017, p. 207–212. https://doi.org/10.5281/zenodo.1129161

3. M. E. Ayikpa , Katia C. de Almeida and Guilherme C. Danielski, “Three-Phase Optimal Power Flow for Study of PV Plant Distributed Impact on Distribution Systems” **Journal of Electrical Engineering** Vol 5 N°1, 2017, p. 47–56. DOI:10.17265/2328-2223/2017.01.006

- **Paper submitted to an international peer-reviewed journal for publication.**

1. M. E. Ayikpa, "Large-scale Distribution Feeder Reconfiguration with Optimal Placement and Sizing of Distributed Generations and Capacitor Banks using Mathematical Models Applied to the Stochastic Fractal Search," **IEEE Transactions on Industry Applications** < under review >

APPENDIX B - BACKWARD-FORWARD POWER SUMMATION EQUATIONS

$$S_{i,ac} = S_i + \sum_{k \in D_i} S_k + \sum_{k \in D_i} Z_k \left(\frac{S_{k,ac}}{V_k} \right)^2$$

The real and imaginary parts of this equation are known as the first law of Kirchhoff and are expressed by:

$$P_{i,ac} = P_i - \sum_{i=1}^{N_{DG}} P_{i,DG} + \left[\sum_{d \in D_i} P_{d,ac} + x_d \left(\frac{P_{d,ac}^2 + Q_{d,ac}^2}{V_d^2} \right) \right]$$

$$Q_{i,ac} = Q_i - \sum_{i=1}^{N_{DG}} Q_{i,DG} - \sum_{i=1}^{N_{CB}} Q_{i,CB} + \left[\sum_{d \in D_i} Q_{d.ac} + x_d \left(\frac{P_{d,ac}^2 + Q_{d,ac}^2}{V_d^2} \right) \right]$$

The voltage drop in branch i of the generic network can be expressed as follows.

$$E_{u_i} - E_i = z_i \left(\frac{S_{i,ac}^*}{E_i^*} \right)$$

By manipulating (5), we get:

$$\begin{aligned} E_i^* E_{u_i} &= E_i^* E_i + z_i S_{i,ac}^* \\ &= V_i^2 + z_i S_{i,ac}^* \\ &= V_i^2 + (r_i + jx_i)\left(P_{i,ac} - jQ_{i,ac}\right) \end{aligned}$$

By applying the module operator and squaring the two sides of the expression, we obtain the following.

$$\begin{aligned} V_i^2 V_{u_i}^2 &= \left(V_i^2 + r_i P_{i,ac} + x_i Q_{i,ac}\right)^2 + \left(x_i P_{i,ac} - r_i Q_{i,ac}\right)^2 \\ &= \left(x_i P_{i,ac} + x_i Q_{i,ac}\right)^2 + 2\left(r_i P_{i,ac} + x_i Q_{i,ac}\right) V_i^2 + V_i^4 \\ &+ \left(x_i P_{i,ac} - r_i Q_{i,ac}\right)^2 \\ &= 2\left(r_i P_{i,ac} + x_i Q_{i,ac}\right) V_i^2 + V_i^4 + \left(P_{i,ac}^2 + Q_{i,ac}^2\right)\left(r_i^2 + x_i^2\right) \end{aligned}$$

From the above expression, we represent the second law of Kirchhoff by:

$$\left|V_{u_i}\right|^2 = |V_i|^2 + 2\left(r_i P_{i,ac} + x_i Q_{i,ac}\right) + \left(r_i^2 + x_i^2\right) \frac{\left(P_{i,ac}^2 + Q_{i,ac}^2\right)}{|V_i|^2}$$

APPENDIX C – FORMATION OF FUNDAMENTAL LOOPS FOR THE 14-BUS SYSTEM

The formation of fundamental loops is carried out after determining the bus incidence matrix A. The process begins by adding a normal open branch to the system to form a new loop; then if the sum of the absolute values of the branches connected to each node of matrix A in the corresponding column is equal to 1, these branches are removed from the network. This process is repeated until this type of node no longer remains in the system. At the end of the process, the number of remaining branches represents a fundamental loop. The figure and table below show, respectively, the topology of the 14-bus system and the first fundamental loop of this system.

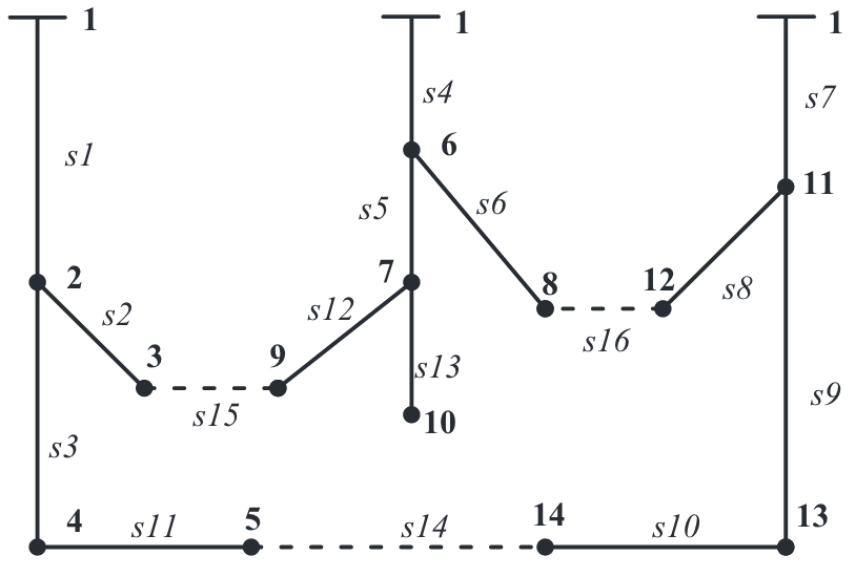

Topology of the 14-bus system (Nguyen; Truong; Phung, 2016)

Nodes

		1	2	3	4	5	6	7	8	9	10	11	12	13	14
	1	1	-1												
	2		1	-1											
	3		1		-1										
	4	1					-1								
	5						1	-1							
	6						1		-1						
	7	1										-1			
	8											1	-1		
	9											1		-1	
	10													1	-1
	11				1	-1									
	12							1		-1					
	13							1			-1				
Step 1	14					1									-1
Step 2		3	3	1	2	2	3	3	1	1	1	3	1	2	2
Step 3		3	2	0	2	2	2	1	0	0	0	2	0	2	2
Step 4		3	2	0	2	2	1	0	0	0	0	2	0	2	2
Step 5		2	2	0	2	2	0	0	0	0	0	2	0	2	2

Source: Author's elaboration

Step 1: Add branch 14 to matrix A

Step 2: Calculate the sum of the absolute values of the branches connected to each node of matrix A in the corresponding column. The branches connected to the nodes that have sum result equal to 1 are removed. In this case, branches 2, 6, 12, 13 and 8 are removed.

Step 3: Repeat the same process as in step 2, branch 5 is removed.

Step 4: Repeat the same process as in step 2, branch 4 is removed.

Step 5: All the sums of the absolute values of each element in a corresponding column in matrix A are different from 1. Therefore, the first fundamental loop gives the set of branches 1,3, 7, 9, 10, 11 and 14.

APPENDIX D – PRIMAL- DUAL INTERIOR POINT METHOD

The interior point method has been widely used to solve large-scale linear and nonlinear programming problems. The optimal power flow is an application of this method in electric power systems. Mathematically, the optimal power flow problem can be formulated as follows.

$$\begin{aligned} &Minimize\ f(\mathrm{x}) \\ s.a \quad &\mathrm{g}(\mathrm{x}) = 0 \\ &\mathrm{h}_{\min} \le \mathrm{h}(\mathrm{x}) \le \mathrm{h}_{\max} \end{aligned} \qquad \text{(C.1)}$$

where, f(x) is the objective function to be optimized; x are the optimization variables; g(x) is an *m*-dimensional vector, whose components are the equations $\mathrm{g_i(x)}$ that represent the equality constraints; h(x) is an *l*-dimensional vector of the equations $\mathrm{h_i(x)}$ that represent the inequality constraints.

Applying the primal dual interior point method to problem (C.1) requires the following steps:

- Transforming inequality constraints into equality constraints using slack variables.

$$\begin{aligned} &\mathrm{h}(\mathrm{x}) - s_l - \mathrm{h}_{\min} = 0 \\ &\mathrm{h}(\mathrm{x}) + s_u - \mathrm{h}_{\max} = 0 \\ &s_l, s_u > 0 \end{aligned} \qquad \text{(C.2)}$$

- where, s_l and s_u are vectors whose components (s_{l_i}, s_{u_i}) are corresponding slack variables.

- Adding the logarithmic barrier function to the objective function gives.

$$f(\mathrm{x}) - \mu\left[\sum_i lns_{l_i} + \sum_i lns_{u_i}\right] \qquad \text{(C.3)}$$

- The resulting problem is expressed as follows.

$$
\begin{aligned}
&Minimize\ f(\mathrm{x}) - \mu\left[\sum_i lns_{l_i} + \sum_i lns_{u_i}\right] \\
&s.a \qquad \mathrm{g}(\mathrm{x}) = 0 \\
&\qquad\quad \mathrm{h}(\mathrm{x}) - s_l - \mathrm{h}_{\min} = 0 \\
&\qquad\quad \mathrm{h}(\mathrm{x}) + s_u - \mathrm{h}_{\max} = 0 \\
&\qquad\quad s_l, s_u > 0
\end{aligned}
\qquad \text{(C.4)}
$$

❖ Formation of the Lagrangian function

$$
\begin{aligned}
\pounds(\mathrm{x}, s_l, s_u, \lambda, \pi_l, \pi_u) = f(\mathrm{x}) - \mu\left[\sum_i lns_{l_i} + \sum_i lns_{u_i}\right] - \lambda^t \mathrm{g}(\mathrm{x}) \\
- \pi_{h_l}^t \left[\mathrm{h}(\mathrm{x}) - s_l - \mathrm{h}_{\min}\right] - \pi_{h_u}^t \left[\mathrm{h}(\mathrm{x}) + s_u - \mathrm{h}_{\max}\right]
\end{aligned}
\qquad \text{(C.5)}
$$

where λ_i is the Lagrange multiplier corresponding to the i-th equality constraint, and π_i is the Lagrange multiplier corresponding to the i-th inequality constraint.

❖ Derivation of the first-order optimality conditions of Karush-Kuhn-Tucker

$$
\begin{aligned}
&\nabla_x \pounds\left(\mathrm{x}, s_l, s_u, \lambda, \pi_l, \pi_u\right) = 0 = \nabla_x f(\mathrm{x}) - \nabla_x \mathrm{g}(\mathrm{x})^t \lambda - \nabla_x \mathrm{h}(\mathrm{x})^t \left(\pi_l + \pi_u\right) \\
&\nabla_{sl} \pounds\left(\mathrm{x}, s_l, s_u, \lambda, \pi_l, \pi_u\right) = 0 = \mu \mathrm{e} - \mathrm{S}_l \pi_l \\
&\nabla_{su} \pounds\left(\mathrm{x}, s_l, s_u, \lambda, \pi_l, \pi_u\right) = 0 = \mu \mathrm{e} + \mathrm{S}_u \pi_u \\
&\nabla_\lambda \pounds\left(\mathrm{x}, s_l, s_u, \lambda, \pi_l, \pi_u\right) = 0 = -\mathrm{g}(\mathrm{x}) \\
&\nabla_{\pi_l} \pounds\left(\mathrm{x}, s_l, s_u, \lambda, \pi_l, \pi_u\right) = 0 = -\left[\mathrm{h}(\mathrm{x}) - s_l - \mathrm{h}_{\min}\right] \\
&\nabla_{\pi_u} \pounds\left(\mathrm{x}, s_l, s_u, \lambda, \pi_l, \pi_u\right) = 0 = -\left[\mathrm{h}(\mathrm{x}) + s_u - \mathrm{h}_{\max}\right]
\end{aligned}
\qquad \text{(C.6)}
$$

where $\nabla_x f(\mathrm{x})$ and $\nabla_x \mathrm{h}(\mathrm{x})$ are the gradient vectors of $f(\mathrm{x})$ and $\mathrm{h}(\mathrm{x})$, respectively; $\nabla_x \mathrm{g}(\mathrm{x}) = \mathbf{J}(\mathrm{x})$ is the Jacobian matrix of $\mathrm{g}(\mathrm{x})$; $\mathbf{e}$ is a unit vector; S_l and S_u are diagonal matrices formed by the elements of the vectors s_l and s_u, respectively.

The conditions expressed by (C.6) are complemented by the non-negativity constraints, corresponding to the slack variables, and the sign constraints, relating to the dual multipliers.

$$s_l \geq 0, \quad s_u \geq 0, \quad \pi_l \geq 0, \quad \pi_u \leq 0$$

The stationary point of the problem represented by (C.4) is obtained by solving (C.6). Using the Newton-Raphson method, the following system of nonlinear equations must be solved at each iteration as presented in (C.7).

$$\begin{aligned}
\mathbf{H}(\mathrm{x},\lambda,\pi_l,\pi_u)\Delta\mathrm{x} - \mathbf{J}(\mathrm{x})^t\Delta\lambda - \nabla_x \mathrm{h}(\mathrm{x})^t\left(\Delta\pi_l + \Delta\pi_u\right) &= -t \\
-\Pi_l\Delta\mathrm{S}_l - \mathrm{S}\Delta_l &= -\left(\mu\mathrm{e} - \mathrm{S}_l\pi_l\right) \\
\Pi_u\Delta\mathrm{S}_u + \mathrm{S}\Delta_u &= -\left(\mu\mathrm{e} + \mathrm{S}_u\pi_u\right) \\
-\mathrm{J}(\mathrm{x})^t\Delta\mathrm{x} + \Delta\mathrm{S}_l &= \mathrm{h}(\mathrm{x}) - \mathrm{S}_l - \mathrm{h}_{\min} \\
-\mathrm{J}(\mathrm{x})^t\Delta\mathrm{x} + \Delta\mathrm{S}_u &= \mathrm{h}(\mathrm{x}) + \mathrm{S}_u - \mathrm{h}_{\max}
\end{aligned} \qquad \text{(C.7)}$$

where,

$$\mathbf{H}(\mathrm{x},\lambda,\pi_l,\pi_u) = \nabla_x^2 f(\mathrm{x}) - \sum_i \lambda_i \nabla_x^2 \mathrm{g}_i(\mathrm{x}) - \sum_j \left(\pi_l + \pi_u\right)\nabla_x^2 \mathrm{h}_j(\mathrm{x})$$

is the matrix of second derivatives of the Lagrangian function with respect to the optimization variables.

$\nabla_x^2 f(\mathrm{x})$, $\nabla_x^2 \mathrm{g}_i(\mathrm{x})$ and $\nabla_x^2 \mathrm{h}_j(\mathrm{x})$ are the second-derivative matrices of $f(\mathrm{x})$, $\mathrm{g}_i(\mathrm{x})$ e $\mathrm{h}_j(\mathrm{x})$, respectively.

$$t = \nabla_x \mathfrak{L}\left(\mathrm{x}, \mathrm{s}_l, \mathrm{s}_u, \lambda, \pi_l, \pi_u\right) = \nabla_x f(\mathrm{x}) - \mathrm{J}(\mathrm{x})^t \lambda - \nabla_x \mathrm{h}(\mathrm{x})^t \left(\pi_l + \pi_u\right)$$

Π_l and Π_u are diagonal matrices formed by the elements of the vectors π_l and π_u, respectively. Equation (C.7) can be rewritten in matrix form as follows.

$$\mathrm{W}\left(\mathrm{x}, \mathrm{s}_l, \mathrm{s}_u, \lambda, \pi_l, \pi_u\right) . \begin{bmatrix} \Delta\mathrm{x} \\ \Delta\mathrm{s}_l \\ \Delta\mathrm{s}_u \\ \lambda \\ \Delta\pi_l \\ \Delta\pi_u \end{bmatrix} = \begin{bmatrix} -t \\ -\left(\mu\mathrm{e} - \mathrm{S}_l\pi_l\right) \\ -\left(\mu\mathrm{e} + \mathrm{S}_u\pi_u\right) \\ \mathrm{g}\left(\mathrm{x}\right) \\ \mathrm{h}\left(\mathrm{x}\right) - \mathrm{s}_l - \mathrm{h}_{\min} \\ \mathrm{h}\left(\mathrm{x}\right) + \mathrm{s}_u - \mathrm{h}_{\max} \end{bmatrix} \qquad \text{(C.8)}$$

where, the matrix $\mathbf{W}(\mathrm{x}, \mathrm{S}_l, \mathrm{S}_u, \lambda, \pi_l, \pi_u)$ is given by (C.9).

$$\begin{bmatrix} \mathbf{H}(\mathrm{x},\lambda,\pi_l,\pi_u) & 0 & 0 & -\mathbf{J}(\mathrm{x})^t & -\nabla_x \mathrm{h}(\mathrm{x})^t & -\nabla_x \mathrm{h}(\mathrm{x})^t \\ 0 & -\mathbf{\Pi}_l & 0 & 0 & -\mathbf{S}_l & 0 \\ 0 & 0 & \mathbf{\Pi}_u & 0 & 0 & \mathbf{S}_u \\ -\mathbf{J}(\mathrm{x}) & 0 & 0 & 0 & 0 & 0 \\ -\nabla_x \mathrm{h}(\mathrm{x}) & \mathbf{I} & 0 & 0 & 0 & 0 \\ -\nabla_x \mathrm{h}(\mathrm{x}) & 0 & -\mathbf{I} & 0 & 0 & 0 \end{bmatrix} \quad \text{(C.9)}$$

Where, I, is the identity matrix. Note that this matrix, originally not symmetric, can be made symmetric by multiplying the second row by $-\mathbf{S}_l^{-1}$ and the third row by $\mathbf{S}_u^{-1}$. The solution to equation (C.8) provides the increments in the primal and dual variables of the optimization problem. The non-violation of the non-negativity constraints of the slack variables and the signs constraints of the dual multipliers is ensured by calculating the step length in the primal and dual spaces as described in (C10).

$$\begin{aligned} \gamma_p &= min\left[\min_{\Delta s_{li}<0} \frac{s_{li}}{|\Delta s_{li}|} \quad \min_{\Delta s_{ui}<0} \frac{s_{ui}}{|\Delta s_{ui}|} \quad 1.0\right] \\ \gamma_d &= min\left[\min_{\Delta \pi_{lj}<0} \frac{\pi_{lj}}{|\Delta \pi_{lj}|} \quad \min_{\Delta \pi_{uj}>0} \frac{-\pi_{uj}}{|\Delta \pi_{uj}|} \quad 1.0\right] \end{aligned} \quad \text{(C.10)}$$

The updating of primal and dual variables is given by (C.11).

$$\begin{aligned} x^{k+1} &= x^k + \sigma\gamma_p \Delta x^k & \lambda^{k+1} &= \lambda^k + \sigma\gamma_d \Delta\lambda^k \\ \mathrm{s}_l^{k+1} &= \mathrm{s}_l^k + \sigma\gamma_p \Delta \mathrm{s}^k & \pi_l^{k+1} &= \pi_l^k + \sigma\gamma_d \Delta\pi_l^k \\ \mathrm{s}_u^{k+1} &= \mathrm{s}_u^k + \sigma\gamma_p \Delta \mathrm{s}^k & \pi_u^{k+1} &= \pi_u^k + \sigma\gamma_d \Delta\pi_u^k \end{aligned} \quad \text{(C.11)}$$

Where σ is a constant whose purpose is to ensure that the variables s and π do not cancel each other out, with a recommended value of 0.9995.

Therefore, the purpose of the step factors $\sigma\gamma_p$ and $\sigma\gamma_d$ is to guarantee the non-negativity of slack variables and ensure a sufficient reduction in merit represented by the Lagrangian function. The value of the barrier parameter is computed at the end of each iteration using (C.12).

$$\mu = \frac{s^l \pi^l - s^\mu \pi^\mu}{2l\beta} \qquad \text{(C.12)}$$

Where l is the number of inequality constraints.

The algorithm for solving an optimization problem via the Primal-Dual Interior Point method is summarized in the following steps.

1. Initialization of primal and dual variables.
2. Calculation of the gradient vector of the augmented Lagrangian function, equation (C.6).
3. Convergence test: comparison of the Euclidean norm of the gradient vector and the value of the barrier parameter with their respective tolerances. If the convergence criteria are met, the iterative process is complete (the optimal solution has been found); otherwise, proceed to the next step.
4. Calculation and factorization of matrix W, from (C.8).
5. Solution of the linear system, (C.7).
6. Determination of step lengths in primal and dual spaces, (C.10).
7. Update of optimization variables, (C.11).
8. Calculation of the new value of the barrier parameter μ, (C.12) and return to step 2.

ANNEX A – DATA USED IN THIS WORK

- **IEEE 123 bus system**

The IEEE 123 node data were modified for the TOPF studies. The data used to perform simulations are presented below.

Line segment data

Node A	Node B	Length (ft)	Config.
1	2	1750	10
1	3	250	11
1	7	300	1
3	4	200	11
3	5	325	11
5	6	250	11
7	8	200	1
8	12	225	10
8	9	225	9
8	13	300	1
9	127	0	Regu
127	14	425	9
13	34	150	11
13	18	825	2
14	11	250	9
14	10	250	9
15	16	375	11
15	17	350	11
18	19	250	9
18	21	300	2
19	20	325	9
21	22	525	10
21	23	250	2
23	24	550	11
23	25	275	2
25	129	0	Regu
129	26	350	7
25	28	200	2
26	27	275	7
26	31	225	11
27	33	500	9

28	29	300	2
29	30	350	2
30	123	200	2
31	32	300	11
34	15	100	11
35	36	650	8
35	40	250	1
36	37	300	9
36	38	250	10
38	39	325	10
40	41	325	11
40	42	250	1
42	43	500	10
42	44	200	1
44	45	200	9
44	47	250	1
45	46	300	9
47	48	150	4
47	49	250	4
49	50	250	4
50	51	250	4
52	53	200	1
53	54	125	1
54	55	275	1
54	57	350	3
55	56	275	1
57	58	250	10
57	60	750	3
58	59	250	10
60	61	550	5
60	62	250	12
62	63	175	12
63	64	350	12
64	65	425	12
65	66	325	12
67	68	200	9
67	72	275	3
67	97	250	3
68	69	275	9
69	70	325	9
70	71	275	9

72	73	275	11
72	76	200	3
73	74	350	11
74	75	400	11
76	77	400	6
76	86	700	3
77	78	100	6
78	79	225	6
78	80	475	6
80	81	475	6
81	82	250	6
81	84	675	11
82	83	250	6
84	85	475	11
86	87	450	5
87	88	175	9
87	89	275	6
89	90	225	10
89	91	225	6
91	92	300	11
91	93	225	6
93	94	275	9
93	95	300	6
95	96	200	10
97	98	275	3
98	99	550	3
99	100	300	3
100	122	800	3
101	102	225	11
101	105	275	3
102	103	325	11
103	104	700	11
105	106	225	10
105	108	325	3
106	107	575	10
108	109	450	9
108	121	1000	3
109	110	300	9
110	111	575	9
110	112	125	9
112	113	525	9

113	114	325	9
115	35	375	4
116	1	400	1
51	128	500	4
118	52	400	1
119	130	0	Regu.
131	67	350	6
120	101	250	3
117	125	0	Substat.
125	126	0	Regu.
126	116	0	switch
13	118	0	switch
18	115	0	switch
60	119	0	switch
61	126	0	switch
126	124	0	XFM-1
97	120	0	switch

Overhead Lines Configurations

Config.	Phasing	Phase Cond.	Neutral Cond.	Spacing
		ACSR	ACSR	ID
1	A B C N	336,400 26/7	4/0 6/1	500
2	C A B N	336,400 26/7	4/0 6/1	500
3	B C A N	336,400 26/7	4/0 6/1	500
4	C B A N	336,400 26/7	4/0 6/1	500
5	B A C N	336,400 26/7	4/0 6/1	500
6	A C B N	336,400 26/7	4/0 6/1	500
7	A C N	336,400 26/7	4/0 6/1	505
8	A B N	336,400 26/7	4/0 6/1	505
9	A N	1/0	1/0	510
10	B N	1/0	1/0	510
11	C N	1/0	1/0	510

Underground Line Configuration

Config.	Phasing	Cable	Spacing ID
12	A B C	1/0 AA, CN	515

Transformer Data

	kVA	kV – low		R – %	X – %
Substation		115 – D	4.16 – Gr-W	1	8
XFM – 1	150	4.16 – D	.480 – D	1.27	2.72

Shunt Capacitors

Node	Ph-A	Ph-B	Ph-C
	kVAr	kVAr	kVAr
83	200	200	200
88	50		
90		50	
92			50
Total	250	250	250

Regulator Data

Regulator ID:	1		
Line Segment:	150 - 149		
Location:	150		
Phases:	A-B-C		
Connection:	3-Ph, Wye		
Monitoring Phase:	A		
Bandwidth:	2.0 volts		
PT Ratio:	20		
Primary CT Rating:	700		
Compensator:	Ph-A		
R - Setting:	3		
X - Setting:	7.5		
Voltage Level:	120		
Regulator ID:	2		
Line Segment:	9 - 14		
Location:	9		
Phases:	A		
Connection:	1-Ph, L-G		
Monitoring Phase:	A		
Bandwidth:	2.0 volts		
PT Ratio:	20		
Primary CT Rating:	50		
Compensator:	Ph-A		
R - Setting:	0.4		
X - Setting:	0.4		
Voltage Level:	120		

Regulator ID:	3		
Line Segment:	25 - 26		
Location:	25		
Phases:	A-C		
Connection:	2-Ph,L-G		
Monitoring Phase:	A & C		
Bandwidth:	1		
PT Ratio:	20		
Primary CT Rating:	50		
Compenator:	Ph-A	Ph-C	
R - Setting:	0.4	0.4	
X - Setting:	0.4	0.4	
Voltage Level:	120	120	
Regulator ID:	4		
Line Segment:	160 - 67		
Location:	160		
Phases:	A-B-C		
Connection:	3-Ph, LG		
Monitoring Phase:	A-B-C		
Bandwidth:	2		
PT Ratio:	20		
Primary CT Rating:	300		
Compensator:	Ph-A	Ph-B	Ph-C
R - Setting:	0.6	1.4	0.2
X - Setting:	1.3	2.6	1.4
Voltage Level:	124	124	124

Spot Loads

Node	Load	Ph-1	Ph-1	Ph-2	Ph-2	Ph-3	Ph-4
	Model	kW	kVAr	kW	kVAr	kW	kVAr
1	Y-PQ	40	20	0	0	0	0
2	Y-PQ	0	0	20	10	0	0
4	Y-PQ	0	0	0	0	40	20
5	Y-I	0	0	0	0	20	10
6	Y-Z	0	0	0	0	40	20
7	Y-PQ	20	10	0	0	0	0
9	Y-PQ	40	20	0	0	0	0
10	Y-I	20	10	0	0	0	0
11	Y-Z	40	20	0	0	0	0
12	Y-PQ	0	0	20	10	0	0
16	Y-PQ	0	0	0	0	40	20
17	Y-PQ	0	0	0	0	20	10
19	Y-PQ	40	20	0	0	0	0
20	Y-I	40	20	0	0	0	0
22	Y-Z	0	0	40	20	0	0
24	Y-PQ	0	0	0	0	40	20
28	Y-I	40	20	0	0	0	0
29	Y-Z	40	20	0	0	0	0
30	Y-PQ	0	0	0	0	40	20
31	Y-PQ	0	0	0	0	20	10
32	Y-PQ	0	0	0	0	20	10
33	Y-I	40	20	0	0	0	0
34	Y-Z	0	0	0	0	40	20
35	D-PQ	40	20	0	0	0	0
37	Y-Z	40	20	0	0	0	0
38	Y-I	0	0	20	10	0	0
39	Y-PQ	0	0	20	10	0	0
41	Y-PQ	0	0	0	0	20	10
42	Y-PQ	20	10	0	0	0	0
43	Y-Z	0	0	40	20	0	0
45	Y-I	20	10	0	0	0	0
46	Y-PQ	20	10	0	0	0	0
47	Y-I	35	25	35	25	35	25
48	Y-Z	70	50	70	50	70	50
49	Y-PQ	35	25	70	50	35	20
50	Y-PQ	0	0	0	0	40	20
51	Y-PQ	20	10	0	0	0	0
52	Y-PQ	40	20	0	0	0	0
53	Y-PQ	40	20	0	0	0	0
55	Y-Z	20	10	0	0	0	0
56	Y-PQ	0	0	20	10	0	0
58	Y-I	0	0	20	10	0	0
59	Y-PQ	0	0	20	10	0	0
60	Y-PQ	20	10	0	0	0	0
62	Y-Z	0	0	0	0	40	20
63	Y-PQ	40	20	0	0	0	0
64	Y-I	0	0	75	35	0	0
65	D-Z	35	25	35	25	70	50
66	Y-PQ	0	0	0	0	75	35
68	Y-PQ	20	10	0	0	0	0
69	Y-PQ	40	20	0	0	0	0
70	Y-PQ	20	10	0	0	0	0
71	Y-PQ	40	20	0	0	0	0
73	Y-PQ	0	0	0	0	40	20
74	Y-Z	0	0	0	0	40	20
75	Y-PQ	0	0	0	0	40	20
76	D-I	105	80	70	50	70	50
77	Y-PQ	0	0	40	20	0	0
79	Y-Z	40	20	0	0	0	0
80	Y-PQ	0	0	40	20	0	0
82	Y-PQ	40	20	0	0	0	0
83	Y-PQ	0	0	0	0	20	10
84	Y-PQ	0	0	0	0	20	10
85	Y-PQ	0	0	0	0	40	20
86	Y-PQ	0	0	20	10	0	0
87	Y-PQ	0	0	40	20	0	0
88	Y-PQ	40	20	0	0	0	0
90	Y-I	0	0	40	20	0	0
92	Y-PQ	0	0	0	0	40	20
94	Y-PQ	40	20	0	0	0	0
95	Y-PQ	0	0	20	10	0	0
96	Y-PQ	0	0	20	10	0	0
98	Y-PQ	40	20	0	0	0	0
99	Y-PQ	0	0	40	20	0	0
100	Y-Z	0	0	0	0	40	20
102	Y-PQ	0	0	0	0	20	10
103	Y-PQ	0	0	0	0	40	20
104	Y-PQ	0	0	0	0	40	20
106	Y-PQ	0	0	40	20	0	0
107	Y-PQ	0	0	40	20	0	0
109	Y-PQ	40	20	0	0	0	0
111	Y-PQ	20	10	0	0	0	0
112	Y-I	20	10	0	0	0	0
113	Y-Z	40	20	0	0	0	0
114	Y-PQ	20	10	0	0	0	0
Total		1420	775	915	515	1155	635

Configuration 1:

```
            Z (R +jX) in ohms per mile
 0.4576  1.0780   0.1560  0.5017   0.1535  0.3849
                  0.4666  1.0482   0.1580  0.4236
                                   0.4615  1.0651
```

B in micro Siemens per mile

5.6765 -1.8319 -0.6982

5.9809 -1.1645

5.3971

Configuration 2:

Z (R +jX) in ohms per mile

0.4666 1.0482 0.1580 0.4236 0.1560 0.5017

0.4615 1.0651 0.1535 0.3849

0.4576 1.0780

B in micro Siemens per mile

5.9809 -1.1645 -1.8319

5.3971 -0.6982

5.6765

Configuration 3:

Z (R +jX) in ohms per mile

0.4615 1.0651 0.1535 0.3849 0.1580 0.4236

0.4576 1.0780 0.1560 0.5017

0.4666 1.0482

B in micro Siemens per mile

5.3971 -0.6982 -1.1645

5.6765 -1.8319

5.9809

Configuration 4:

Z (R +jX) in ohms per mile

0.4615 1.0651 0.1580 0.4236 0.1535 0.3849

0.4666 1.0482 0.1560 0.5017

0.4576 1.0780

B in micro Siemens per mile

5.3971 -1.1645 -0.6982

5.9809 -1.8319

5.6765

Configuration 5:

Z (R +jX) in ohms per mile

0.4666 1.0482 0.1560 0.5017 0.1580 0.4236

0.4576 1.0780 0.1535 0.3849

0.4615 1.0651

B in micro Siemens per mile

5.9809 -1.8319 -1.1645

5.6765 -0.6982

5.3971

Configuration 6:

Z (R +jX) in ohms per mile

0.4576 1.0780 0.1535 0.3849 0.1560 0.5017

0.4615 1.0651 0.1580 0.4236

0.4666 1.0482

B in micro Siemens per mile

5.6765 -0.6982 -1.8319

5.3971 -1.1645

5.9809

Configuration 7:

Z (R +jX) in ohms per mile

0.4576 1.0780 0.0000 0.0000 0.1535 0.3849

0.0000 0.0000 0.0000 0.0000

0.4615 1.0651

B in micro Siemens per mile

5.1154 0.0000 -1.0549

0.0000 0.0000

5.1704

Configuration 8:

Z (R +jX) in ohms per mile

0.4576 1.0780 0.1535 0.3849 0.0000 0.0000

0.4615 1.0651 0.0000 0.0000

0.0000 0.0000

B in micro Siemens per mile

5.1154 -1.0549 0.0000

5.1704 0.0000

0.0000

Configuration 9:

Z (R +jX) in ohms per mile

1.3292 1.3475 0.0000 0.0000 0.0000 0.0000

0.0000 0.0000 0.0000 0.0000

0.0000 0.0000

```
          B in micro Siemens per mile
            4.5193    0.0000    0.0000
                      0.0000    0.0000
                                0.0000
```

Configuration 10:

```
           Z (R +jX) in ohms per mile
 0.0000   0.0000   0.0000   0.0000   0.0000   0.0000
                   1.3292   1.3475   0.0000   0.0000
                                     0.0000   0.0000
          B in micro Siemens per mile
            0.0000    0.0000    0.0000
                      4.5193    0.0000
                                0.0000
```

Configuration 11:

```
           Z (R +jX) in ohms per mile
 0.0000   0.0000   0.0000   0.0000   0.0000   0.0000
                   0.0000   0.0000   0.0000   0.0000
                                     1.3292   1.3475
          B in micro Siemens per mile
            0.0000    0.0000    0.0000
                      0.0000    0.0000
                                4.5193
```

Configuration 12:

```
           Z (R +jX) in ohms per mile
 1.5209   0.7521   0.5198   0.2775   0.4924   0.2157
                   1.5329   0.7162   0.5198   0.2775
                                     1.5209   0.7521
          B in micro Siemens per mile
           67.2242    0.0000    0.0000
                     67.2242    0.0000
                               67.2242
```

- **Data used to solve the DFR problem**

The data used to solve the DFR cases are available in the Matpower 8.0b1 package and can be downloaded for free at https://matpower.org.